ARL-TR-10483 ● Nov 2026

On Simulating the Deflagration of Ethyl Nitrate with a Quasi-One-Dimensional Two-Phase (Liquid-Gas) Model Having Detailed Finite-Rate Chemical Kinetics Mechanisms for Both Phases

by Michael J. McQuaid, Chiung-Chu Chen, Jeffrey D. Veals, Christopher Stone, and Rodger Cornell

DISTRIBUTION STATEMENT A. Approved for public release: distribution unlimited.

NOTICES

Disclaimers

The findings in this report are not to be construed as an official Department of the Army position unless so designated by other authorized documents.

Citation of manufacturer's or trade names does not constitute an official endorsement or approval of the use thereof.

Destroy this report when it is no longer needed. Do not return it to the originator.

ARL-TR-10483 ● Nov 2026





On Simulating the Deflagration of Ethyl Nitrate with a Quasi-One-Dimensional Two-Phase (Liquid-Gas) Model Having Detailed Finite-Rate Chemical Kinetics Mechanisms for Both Phases

Michael J. McQuaid, Chiung-Chu Chen, Jeffrey D. Veals, Christopher Stone, and Rodger Cornell
DEVCOM Army Research Laboratory

DISTRIBUTION STATEMENT A. Approved for public release: distribution unlimited.

REPORT DOCUMENTATION PAGE

1. REPORT DATE	2. REPORT TYPE	3. DATES COVERED	
		START DATE	END DATE
November 2026	Technical Report	6 January 2025	12 June 2026

4. TITLE AND SUBTITLE
On Simulating the Deflagration of Ethyl Nitrate with a Quasi-One-Dimensional Two-Phase (Liquid–Gas) Model Having Detailed Finite-Rate Chemical Kinetics Mechanisms for Both Phases

5a. CONTRACT NUMBER	5b. GRANT NUMBER	5c. PROGRAM ELEMENT NUMBER
5d. PROJECT NUMBER	**5e. TASK NUMBER**	**5f. WORK UNIT NUMBER**

6. AUTHOR(S)
Michael J. McQuaid, Chiung-Chu Chen, Jeffrey D. Veals, Christopher Stone, and Rodger Cornell

7. PERFORMING ORGANIZATION NAME(S) AND ADDRESS(ES)
DEVCOM Army Research Laboratory
ATTN: FCDD-RLA-WC
Aberdeen Proving Ground, MD 21005

8. PERFORMING ORGANIZATION REPORT NUMBER
ARL-TR-10483

9. SPONSORING/MONITORING AGENCY NAME(S) AND ADDRESS(ES)	10. SPONSOR/MONITOR'S ACRONYM(S)	11. SPONSOR/MONITOR'S REPORT NUMBER(S)

12. DISTRIBUTION/AVAILABILITY STATEMENT
DISTRIBUTION STATEMENT A. Approved for public release: distribution unlimited.

13. SUPPLEMENTARY NOTES
Michael J. McQuaid retired from ARL in April 2025 but returned as an emeritus volunteer to complete the research outlined in this report.

14. ABSTRACT
Toward developing and applying multiphase physics-based deflagration models with better potential to computationally design and screen min-smoke" propellant (MSP) formulations, a quasi-1D, two-phase model of ethyl nitrate's deflagration that included detailed finite-rate chemical kinetics mechanisms for both phases was formulated and applied. Several hypotheses that have been proposed to explain the discrepancy between measured and model-predicted burning rate values were investigated. We concluded the discrepancy is likely due to a missing or poorly represented chemical kinetics submechanism(s). Providing insight into the relative importance of various mechanisms that determine the rate at which MSPs deflagrate, this study constitutes a step toward establishing models with better potential to design and screen MSP formulations for tactical rocket motor applications.

15. SUBJECT TERMS
Weapons Sciences, thermochemical kinetics, burning rates, propellants, nitrate esters, computational fluid dynamics

16. SECURITY CLASSIFICATION OF:			17. LIMITATION OF ABSTRACT	18. NUMBER OF PAGES
a. REPORT	b. ABSTRACT	C. THIS PAGE		
UNCLASSIFIED	UNCLASSIFIED	UNCLASSIFIED	UU	86

19a. NAME OF RESPONSIBLE PERSON	19b. PHONE NUMBER *(Include area code)*
Michael J. McQuaid	(520) 691-577

STANDARD FORM 298 (REV. 5/2020)
Prescribed by ANSI Std. Z39.18

Contents

List of Figures v

List of Tables vi

1. Introduction 1

2. The Models 8

2.1 The Detailed Finite-Rate Chemical Kinetics Mechanism 8

2.2 The Homogenous Reactor Model 9

2.3 The Deflagration Model 10

2.3.1 The Gas-Phase Domain: $x \geq +0$ 10

2.3.2 The Liquid–Gas Interface: $x = 0$ 11

2.3.3 The Liquid-Phase Domain: $-d \leq x \leq -0$ 12

2.3.4 Solution Search Protocol 14

3. Summary of Validating Measurement-Based Data 17

3.1 Gas-Phase Decomposition: Levy (1952, 1954a) 17

3.2 Burning Rate and *l*-Phase Temperature Profile Data 18

3.2.1 Steinberger et al. (1955) 18

3.2.2 Hildenbrand and Whittaker (1955) and Hildenbrand et al. (1954) 19

3.2.3 Faeth (1972) 19

4. Results 20

4.1 Gas-Phase Decomposition 20

4.1.1 $P_k(t)/P_0$ Predictions: Baseline $\dot{\omega}_{k,g}$ Estimates 20

4.1.2 $P_k(t)/P_0$ Predictions: Globally Scaled $\dot{\omega}_{k,g}$ Estimates 22

4.2 Burning Rate Predictions 25

4.3 Temperature at the Liquid–Gas Interface 28

4.4 *l*-Phase Temperature Profiles 30

4.5 Differences between the Deflagrations of EthN and d_5-EthN 32

5. Discussion **37**

6. Summary and Conclusion **41**

7. References **43**

Appendix A. The Skeletal Chemical Kinetics Mechanism for the Deflagration Model **47**

A.1 chem.out 49

A.2 therm.dat 61

A.3 tran.dat 66

Appendix B. Representative Input File for Closed-System, Constant-Volume, Constant-Temperature (CNVT) Calculations **68**

Appendix C. Representative Input Files for Gas- and Liquid-Phase PREMIX Problems **70**

C.1 premix.inp 71

C.2 premix_lq.inp 73

List of Symbols, Abbreviations, and Acronyms **75**

Distribution List **78**

List of Figures

Figure 1. Comparisons of CNVT-predicted and measurement-based $P_k(t)/P_0$ values for EthN and selected species produced by EthN(g)'s decomposition at 434 K: baseline $\dot{\omega}_{k,g}$ estimates. 21

Figure 2. Comparisons of CNVT-predicted and measurement-based $P_k(t)/P_0$ values for EthN and selected species produced by EthN(g)'s decomposition at 454 K: baseline $\dot{\omega}_{k,g}$ estimates. 22

Figure 3. Comparisons of CNVT-predicted and measurement-based $P_k(t)/P_0$ values for EthN and selected species produced by EthN(g)'s decomposition at 474 K: baseline $\dot{\omega}_{k,g}$ estimates. 22

Figure 4. Comparisons of CNVT-predicted and measurement-based $P_k(t)/P_0$ values for EthN and selected species produced by EthN(g)'s decomposition at 434 K: globally scaled $\dot{\omega}_{k,g}$ estimates. 23

Figure 5. Comparisons of CNVT-predicted and measurement-based $P_k(t)/P_0$ values for EthN and selected species produced by EthN(g)'s decomposition at 454 K: globally scaled $\dot{\omega}_{k,g}$ estimates. 24

Figure 6. Comparisons of CNVT-predicted and measurement-based $P_k(t)/P_0$ values for EthN and selected species produced by EthN(g)'s decomposition at 474 K: globally scaled $\dot{\omega}_{k,g}$ estimates. 24

Figure 7. Comparison of CNVT-predicted $P_{EthN}(t)/P_0$ values as a function of P_0: T_{exp} = 454 K; globally scaled $\dot{\omega}_{k,g}$ estimates. 25

Figure 8. Comparison of measured and model-predicted $r(P)$ values. 26

Figure 9. Comparison of measured and predicted temperatures at the liquid–gas interface (T^0). 29

Figure 10. Comparison of measured and predicted l-phase $T(x)$ profiles for EthN burning at 13.6 atm. 31

Figure 11. Comparison of measured and predicted l-phase $T(x)$ profiles for EthN burning at 7.8 atm. 31

Figure 12. Comparison of $r(P)$ predictions for EthN and d_5-EthN: Case A. 32

Figure 13. Comparison of $X_H(x)$ and $X_D(x)$ predictions: Case A; P = 30.6 atm. 34

Figure 14. Comparison of $V_H(x)$ and $V_D(x)$ predictions: Case A; P = 30.6 atm. 35

Figure 15. Comparison of $Y_H(x)V_H(x)$ and $Y_D(x)V_D(x)$ predictions: Case A; P = 30.6 atm. 35

Figure 16. Comparison of $\lambda_{EthN\ sys}(x)$ and $\lambda_{d_5-EthN\ sys}(x)$ predictions: P = 30.6 atm. 37

List of Tables

Table 1. Case distinguishing specifications for $f_g(T)$, $f_l(T)$, and T^{-d}. 26
Table 2. Species' mole fraction predictions at $x = -0$: Case B..... 277
Table 3. Species' mole fraction predictions at $x = -0$: Case F. 28
Table 4. Comparison of $\dot{M}_g$ and $\dot{M}_l$ predictions as a function of T^0. 30
Table 5. $X^{+0}_{H/D,g}$ predictions: Case A..... 33
Table 6. Comparison of $\{X_{k,g}\}^{+0}$ predictions for Cases A and E. 40

1. Introduction

For tactical missiles designed for missions in which the rocket motor's exhaust plume can degrade situational awareness or be exploited to reveal the position of their launch platform, the motors are typically fueled with "min-smoke" propellants (MSPs). On a weight-percent basis, MSPs mainly comprise organic compounds functionalized with nitroxy (-ONO_2) groups. Referred to as nitrate esters, standard ingredients within this class of energetic materials (EMs) include nitrocellulose (NC) and nitroglycerine (NG).

In addition to nitrate esters, MSP formulations also include a catalyst to minimize (in a pressure range of interest) the exponent (n') in the Vielle's burning-rate law:

$$r = aP^{n'} \ , \tag{1}$$

where r is an "effective linear regression rate," P is the pressure, and a is a constant. Desirable because it facilitates the optimization of a motor's performance, the burning rate behavior in the range of P in which n' is minimized is referred to as a "plateau." "Super-rate" burning at lower pressures is a concomitant feature of MSP $r(P)$ plots. Recently reviewed by Warren et al. (2021), various theories have been proposed to explain how catalysts produce plateaus and super rates. However, Warren et al. note potential shortcomings of those they reviewed, and we are not aware of any (beyond mere intuition) that have served to advance an MSP development effort.

Hoping to gain additional insight into the phenomena, we formulated a framework for creating multiphase, physics-based deflagration models with detailed representations for the thermochemical kinetics in both liquid and gas phases. Results produced by a model for simulating the deflagration of solid (s) ozone ($O_{3,s}$) indicated that its expansion for applicability in simulating the deflagration of nitrate esters might produce insights that could accelerate MSP development efforts (McQuaid 2025). The study summarized herein was undertaken as the next step toward that objective.

The relationship between Equation 1 and propulsion system performance derives from the relationship between $r(P)$ and the mass flux ($\dot{m}_{c\to g}$) at the interface between condensed (c) and gas (g) phases. That is,

$$\dot{m}_{c\to g}(P) = r(P) * \rho_c \ , \tag{2}$$

where ρ_c is the MSP's density. Coupled with a representation for computing the (surface) area of the interface between the two phases (A^{c-g}), Equation 2 provides

a basis for computing the total gasification rate ($\dot{M}$) at any temporal instant (t) during an interior ballistic cycle. That is,

$$\dot{M}(P,t) = \dot{m}_{c\to g}(P) * A^{c-g}(t) = r(P) * \rho_c * A^{c-g}(t). \qquad (3)$$

Integrating Equation 3 with a representation for the combustion process through which the condensed phase is converted into g-phase products provides a basic framework for computing the rate at which chemical energy stored in an MSP is converted into kinetic energy, and therefrom propulsion system performance.*

In the (re)investigation into the deflagration of $O_{3,s}$ (McQuaid 2025), a steady, isobaric, quasi-1D three-phase (solid–liquid–gas) deflagration model with detailed finite-rate representations for the thermochemical kinetics in the liquid (l) and gas (g) phases was developed and employed to simulate the process. Although the thermochemical kinetic details of $O_{3,s}$'s deflagration have little in common with those of nitrate esters, $O_{3,s}$'s deflagration had previously been modeled and analyzed by Miller (1995, 1997). As such, Miller's results offered a convenient benchmark for developing and debugging the basic framework for a three-phase deflagration model. The simplicity of the O_3 system's reaction chemistry compared with that of deflagrating nitrate esters also offered a relatively inexpensive basis for testing various theories for the mechanism(s) by which catalysts produce super-rate and plateau regions in an MSP's $r(P)$ plot. Furthermore, that simplicity facilitated the analysis of the impact on the $r(P)$ predictions produced by changes to the liquid phase's thermochemical kinetics.

Starting with a case that corresponded to one presented and discussed by Miller (1997), a series of cases whose parameterizations were based on lessons learned from the case that preceded it evolved. That evolution ultimately led to a case in which an $r(P)$ plot with both super-rate and plateau regions was produced. It predicated 1) limiting chemical reactivity to a reversible one-step path between liquid ozone ($O_{3,l}$) and O_l and $O_{2,l}$ and 2) lowering the enthalpy of O_l from a best guess. In addition, the capacity of those predicates to produce both super-rate and plateau regions in the same plot was further enhanced by decreasing the liquid-to-gas volatilization rate in proportion to $O_{3,l}$'s decomposition. The correspondence between those predicates and a chelation/complex-formation theory proposed to explain the super-rate burning of catalyzed MSPs (Dauerman and Tajima 1968; Suh et al. 1974; Fifer and Lannon 1975; Farber and Srivastava 1978; Warren et al. 2021)

* In our deflagration model, $\dot{M}(P)$ is a state variable and $r(P)$ is derived from it. As such, for model validation, we had the choice of converting measurement-based $r(P)$ data into $\dot{M}(P)$ data or $\dot{M}(P)$ predictions into $r(P)$ predictions. Since $r(P)$ values are more familiar to experimentalists and interior ballisticians, we chose the latter option.

was apparent. Moreover, the model provided additional support for the theory by demonstrating it could concomitantly produce a plateau.

Based on those findings, the effort to develop and apply an analogous model to simulate the deflagration of a molecularly small organic nitrate ester was considered warranted. With the availability of measurement-based $r(P)$ data for model validation being the primary criterion, several candidates were identified and considered. They included methyl nitrate (MeN), ethyl nitrate (EthN), 2-nitroxy propane, and NG. Of them, all of whose deflagrations had previously been simulated by coauthors of this report, the EthN system had several attributes that made it preferable and was selected.

Our group's effort to model the deflagration of EthN began in 2012 (Chen and McQuaid 2013). At that time, Nusca (2014a) was developing a 2D model for simulating the deflagration of MSP grains embedded with thermally conductive wires. Tasked with developing a detailed mechanism to represent the *g*-phase thermochemical kinetics in that model, McQuaid and Chen (2013) did not like readily available options. In particular, the state-of-the-art in representing the *g*-phase thermochemical kinetics of the combustion of MSPs and their ingredients was the dark-zone (DZ) mechanism developed and validated by Anderson and coworkers (Miller and Anderson 2004; Anderson et al. 2011). Its status notwithstanding, it comprised a set of elementary reactions in which no molecule had more than four multielectron atoms. (The multielectron atoms were C, N, and O.) Therefore, semi-empirical formulae would have had to be developed and utilized to represent the rate of mass transfer at the liquid–gas interface and the (nascent) *g*-phase products in Nusca's (2014a) model.

Although the efficacy of that paradigm for 1D scenarios (called CYCLOPS) had been demonstrated by Miller and Anderson (2004), Chen and McQuaid (2007) were uncertain that it would produce reliable results in the application of interest and therefore sought an alternative. Having demonstrated a capability for developing finite-rate thermochemical kinetic mechanisms for relatively large organic EMs (Chen and McQuaid 2007), they anticipated that high-fidelity physics-based representations for the earliest stages of the decomposition of MSPs could be developed. However, it was also obvious that suitable representations for molecules as large as NG and NC would not be completed for many years. Therefore, to bridge that gap, they developed a mechanism that included steps to represent the decomposition of the simplest closed-shell organic nitrates, namely, MeN and EthN, hoping it would prove to be an adequate surrogate for higher-fidelity representations in Nusca's (2014a) model.

Recommending that approach, MeN's and EthN's decomposition and combustion had been studied relatively well, often with the objective being to better understand the decomposition and combustion of MSPs and their ingredients. (See references in Chen and McQuaid [2013] and McQuaid and Chen [2016].) In particular, the prior corpus pertaining to the decomposition of MeN and EthN indicated that their rate-determining step was

$$\text{HRO-NO}_2 \leftrightarrow \text{HRO}\cdot + \text{NO}_2 \tag{4}$$

or

$$\text{HRO-NO}_2 \leftrightarrow \text{RO} + \text{HONO}, \tag{5}$$

where R was -CH_2- or -CH_2CH_2-. Moreover, it was considered likely that the rate-determining step for the decomposition of larger nitrate esters was analogous. Therefore, by adding these reactions (as well as reactions for decomposing their products) to the DZ mechanism, it seemed likely that the reaction chemistry near the burning surface would be better represented and make the 2D model's predictions more reliable and instructive.

As part of the effort to validate the MeN–EthN mechanism, Chen and McQuaid (2013) integrated it with a (basic) quasi-1D two-phase CYCLOPS model and used it to predict $r(P)$ values for EthN. They observed that the predictions were approximately a factor of three lower than values measured by Steinberger et al. (1955).

Attempting to rationalize the discrepancy, Chen and McQuaid (2013) noted that the CYCLOPS model represented the liquid–gas interface as a plane. As such, the A^{l-g} value computed for the system was equal to the system's cross-sectional area (A^0). Since this was the minimum value that A^{l-g} could have been in the experiments, and it seemed likely that the discrepancy between measured and model-predicted $r(P)$ values would scale in proportion to the discrepancy between A^{l-g} and A^0, a factor-of-three difference between the two could be imagined on that basis alone. In addition, although the model was formulated based on the assumption that *c*-phase reaction chemistry need not be represented to obtain reasonable $r(P)$ predictions, Chen and McQuaid (2013) could imagine that including such chemistry might generate higher $r(P)$ predictions. Therefore, the level of agreement observed was judged to be "reasonable." (What is reasonable, of course, depends on one's objectives.)

Simulations performed with Nusca's 2D model using a skeletal version of the MeN–EthN(*g*) mechanism subsequently corroborated this judgment (Nusca 2104a). Specifying an MeN–EthN mixture with an CHNO stoichiometry similar to

that of an MSP as the nascent product of the mass transfer process at the solid–gas interface, the combination produced results that were in reasonable agreement with measurement-based findings. Even more gratifying, insights into the mechanisms by which higher effective linear burning rates are achieved by embedding wires in propellant grains were obtained and provided a basis for screening wire-embedded MSP-grain designs.

Since Chen and McQuaid's (2013) study, both the CYCLOPS framework and the thermochemical kinetics mechanism for modeling EthN's decomposition and deflagration have evolved. Additions to the CYCLOPS framework with the potential to impact $r(P)$ predictions include 1) a submodel to calculate the area of the liquid–gas interface if it is "fizzy" (McQuaid and Chen 2016b) and 2) a physics-based Hertz–Langmuir–Knudsen (HLK) submodel for calculating the mass transfer rate at the liquid–gas interface (McQuaid and Chen 2016a). Refinements and additions to the EthN mechanism accrued from efforts to build mechanisms for a variety of larger organic nitrate esters, including NG (Chen and McQuaid 2022), NC (Chen et al. 2021), and nitroguanidine (NQ) (Chen and McQuaid 2024). However, in the course of those efforts, we found (but did not publish) that $r(P)$ predictions for EthN produced by models that included an HLK representation and the most recent version of the EthN(g) mechanism available at the time were not much different from those produced by the model–mechanism combination developed and employed for the 2013 study.

The inclusion of a submodel to calculate the area of the liquid–gas interface if it is fizzy was motivated in part by studies of the deflagration of ammonium perchlorate (AP) (McQuaid and Chen 2014; Nusca 2014b). Finding that the basic CYCLOPS framework could not reproduce the "exponent break" in the $r(P)$ plots of AP-based propellants, McQuaid and Chen (2014) concluded that further investigation of Irwin et al.'s (1963) hypothesis that exponent breaks were due to increased A^{c-g} values produced by thermomechanically induced particle breakup was warranted. Following up on this conjecture, Nusca (2014b) developed and applied a 2D model that corroborated that mechanism's potential to produce exponent breaks. Likewise, McQuaid and Chen (2014) developed an empirically based submodel for the CYCLOPS framework to represent the creation of a fizz zone and quantify its potential to increase $r(P)$ values.

Implementing the fizz-zone submodel in a study of MeN's deflagration, McQuaid and Chen (2016b) found its inclusion could increase $r(P)$ predictions by as much as 25% above baseline ($A^{l-g} = A^0$) rates. In addition, based on the study of $O_{3,l}$'s deflagration, we thought the characteristics of the fizz zone could be manipulated to produce plateau burning rate behavior as well. However, we have not seen any theories or measurement-based evidence which suggests that catalysts promote

surface breakup and the formation of a fizz zone. In addition, in the case of MeN, the magnitude of the increase in the $r(P)$ predictions produced by fizz zones fell far short of those observed for catalyzed MSPs. Moreover, we were skeptical of our ability to find or establish a physics-based representation for the formation of a fizz zone (or any other spallation process for that matter). Lacking such a representation, the model would have little potential for producing predictions that could inform the design of MSP formulations. Therefore, that possibility was not investigated.

Our prior lack of motivation to develop and apply deflagration models that included representations for the *c*-phase's thermochemical kinetics and transport stemmed from analogous considerations. Although we suspected that the inclusion of such representations might produce higher $r(P)$ predictions, until 2020 there were no practical means to develop them from first principles. Therefore, the submodel would have had to have been empirical, and we doubted a deflagration model so equipped would produce information that could be leveraged to tailor burning rate behavior.

Leading to the current study, investigations into a theory proposed by McQuaid and coworkers (Veals et al. 2018; McQuaid et al. 2020) changed those expectations. That theory posits that for molecules in a liquid to (irreversibly) react, they need to be adjacent to a free-volume hole whose volume (V_{hfv}) is large enough for it to occur as if they were in a gas. For example,

$$\mathrm{CH_3CH_2ONO_2}(l) \rightarrow [\mathrm{CH_3CH_2O}\cdot(g) \rightarrow \mathrm{NO_2}(g)]_{V_{hfv}} \rightarrow$$

$$\mathrm{CH_3CH_2O}(l) + \mathrm{NO_2}(l). \qquad (6)$$

Following from that premise, the magnitudes of *l*-phase reaction-rate coefficients $\left(k_l^i\right)$ for such reactions are related to their *g*-phase analog $\left(k_g^i\right)$ by a probability factor (Pr) related to the condensed-phase's T-dependent hole-free volume $\left[\hat{V}_{hfv}(T)\right]$,

$$k_l^i = Pr\left(\hat{V}_{hfv}\right) * k_g^i = Pr(T) * k_g^i = \exp\left(\frac{-B}{T-T_0}\right) * k_g^i \,, \qquad (7)$$

where B and T_0 are constants for a given *l*-phase chemical composition. Compared with the basic CYCLOPS framework, the effort to develop and apply such a submodel could be expected to be costly. However, the results of the study of $O_{3,s}$ deflagration indicated the extra cost might be warranted.

Building on lessons learned in the study of $O_{3,s}$'s deflagration, for studying EthN we developed a quasi-1D two-phase (liquid–gas) model into which we integrated a recently developed mechanism for modeling NQ(*g*)'s decomposition and

combustion (Chen et al. 2024). Containing a submechanism we thought would be suitable for the application, the NQ(g) mechanism was also the basis for modeling the l-phase's reaction chemistry.

Assuming that only a small fraction (e.g., <10%) of the parent molecules in the liquid phase would decompose before reaching the liquid–gas interface, we further assumed that the change in $\hat{V}_{hfv}(T)$ would be similarly small. If so, it would be reasonable to assume that B and T_0 were constant throughout the liquid. Beyond that assumption, we used some relatively rudimentary approximations to compute the l-phase's equation of state and its enthalpy as a function of T. Results produced by the model are presented and discussed.

In addition to investigating if the introduction of l-phase reaction chemistry would produce $r(P)$ predictions for EthN that were in better agreement with measured values, we also created a model with the potential to identify the source of differences between the $r(P)$ values of (normal) EthN and perdeutero-EthN (d_5-EthN) that were measured by Steinberger et al. (1955). Steinberger et al. conducted the experiments that generated the comparisons because they suspected that liquid–gas interface temperatures were too low for a then prevailing "thermal mechanism" to account for the $r(P)$ values observed for nitrate esters. Rather, they hypothesized that the diffusion of atomic hydrogen (H) might be an important mechanism of energy feedback in the flame and opined that the difference between the $r(P)$ values they measured for the two systems corroborated their hypothesis.

The d_5-EthN model was derived from the EthN model by changing the atomic weights of all the system's H atoms (W_H) from 1.00794 to 2.0141 atomic mass units (amu) (i.e., the value for deuterium [D]). The $r(P)$ predictions it produced for d_5-EthN proved to be approximately 10% lower than their EthN counterpart. However, rather than being attributable to differences between the diffusion velocities of H and D, our analysis suggested that a reduction in the g-phase's thermal conductivity (λ_g) produced by the change in molecular weights of H-containing species (alone) could account for the differences in the predictions.

Finally, we integrated the thermochemical kinetics mechanism with a canonical homogeneous reactor (HR) model to simulate experiments in which the temporal evolutions of the concentrations of EthN and three products of its g-phase decomposition were measured (Levy 1952, 1954a). Finding that the model's predictions for the global rates of those evolutions were significantly less than those measured, we reran the simulations with all the k_g^i in the mechanism multiplied by a T-dependent scaling factor. We found that reasonable agreement between the model's predictions and the measurement-based results could be obtained with a scaling factor that lowered the activation energies of all the reactions in the

mechanism by 2 kcal/mol. Moreover, we subsequently found that by refining the thermochemical properties of a small subset of species in the NQ mechanism, good agreement between the HR model's predictions and the measurement-based values were obtained.

Modified to include those refinements, the EthN deflagration model produced $r(P)$ predictions that were negligibly higher than those produced by the original mechanism. Nonetheless, the study's weight of evidence suggests that the discrepancies between measured and model-predicted $r(P)$ values for EthN were largely due to shortcomings of the chemical kinetics mechanism and that the modifications needed to address them will likely be relatively minor. In addition, to the extent we expect such modifications will be applicable to mechanisms for MSP ingredients such as NC and NG, they will improve the predictive capability of models for designing and screening MSP formulations.

2. The Models

2.1 The Detailed Finite-Rate Chemical Kinetics Mechanism

A detailed finite-rate chemical kinetics mechanism that Chen et al. (2024) developed to represent the decomposition and combustion of NQ(g) was the basis for all the mechanisms used for this study. Comprising formulae for computing the rates of 1889 elementary reactions and thermophysical and transport properties for 305 species, it was our group's most recently developed mechanism that included a submechanism suitable for modeling the decomposition and combustion of EthN(g).

Appreciating that many of the reactions and species in the NQ(g) mechanism would be superfluous with respect to modeling EthN(g)'s decomposition and combustion, we assessed the possibility that a suitable mechanism with far fewer irrelevant reactions and species could be extracted from it by inspection. However, even though the NQ(g) mechanism's origin traced to the 2013 version of the EthN(g) mechanism, the EthN(g) mechanism had evolved and become thoroughly intertwined with submechanisms developed for other systems. Therefore, we were not confident that we could reliably extract a skeletal mechanism that was suitable for the parameter spaces of interest by inspection alone. Thus, we settled for integrating the full NQ(g) mechanism with the HR model described in Section 2.2.

We also integrated the full NQ(g) mechanism with the deflagration model described in Section 2.3. However, we found that the computational cost of the sum of the calculations required to complete the study we envisioned would be too costly with that mechanism–model combination. Therefore, we used the trial mechanism

method to reduce it (Kotlar 2010; McQuaid 2013). The bases for eliminating reactions and the resulting skeletal mechanism (248 reactions and 82 species) are presented in Appendix A.

To create a mechanism for the variation of the model for simulating the deflagration of d_5-EthN, we only needed to change the values of W_H from 1.00794 to 2.0141 amu (W_D) in one subroutine (CKATOM) of the CHEMKIN subroutine library. That change was then promulgated by 1) recompiling the mechanism (*chem.inp* + *therm.dat* → *chem.bin*) using the interpreter (*ckinterp.exe*) created with the revised library and 2) recompiling the transport library (*tran.dat* → *tran.bin*) with that *chem.bin* as input.

2.2 The Homogenous Reactor Model

Rereading Levy's (1954a) paper in the course of conducting this study, we appreciated (for the first time) that a canonical closed-system, constant-volume, constant-temperature, *g*-phase (CNVT) HR model that we had developed and applied to simulate the decomposition of NG in a bulb held at a constant T should reasonably represent his experiments (McQuaid et al. 2021). The species' conservation equations in the CNVT model were formulated in terms of mass fractions (Y_k) for a set (K) of atomic and molecular species k,

$$\frac{dY_{k,g}}{dt} = f_g(T)\left[\dot{\omega}_{k,g} W_k/\rho_g\right], \tag{8}$$

where $\dot{\omega}_k$ is the molar production rate per unit volume of the k^{th} species due to chemical reactions, ρ_g is the *g*-phase's density, and $f_g(T)$ is a scaling factor

$$f_g(T) = A' \exp(B'/RT), \tag{9}$$

where A' and B' are heuristically specified constants and R is the universal gas constant. As discussed by McQuaid et al. (2021), $f_g(T)$'s form was chosen so that its constants were relatable to the frequency factors (A^i) and activation energies (E_a^i) in the chemical kinetics mechanism's modified Arrhenius expressions for computing k_g^i.

The relationship between ρ_g, P, and T was based on the ideal gas law. The system of equations was solved with DASPK (Li and Petzold 1999). An input file that is representative of those used to parameterize the CNVT model for the study is provided in Appendix B.

2.3 The Deflagration Model

The formulation of the steady, isobaric, quasi-1D two-phase deflagration model formulated for the study followed from lessons learned in developing and applying a three-phase model for simulating $O_{3,s}$'s deflagration (McQuaid 2025). For EthN, a third phase was not needed because its freezing point is reported to be 171 K (Timmermans and Mattaar 1921), and the three sets of measurement-based $r(P)$ values that we found in the open literature were (presumably) obtained from experiments in which the strands were at "room temperature" when deflagration was initiated. (Faeth [1972] did not report what the starting temperatures of the strands in his experiments were. We assume they were approximately 298 K.) This section outlines the formulation and parameterization of the two-phase model. The solution search protocol implemented for the study is also summarized.

2.3.1 The Gas-Phase Domain: $x \geq +0$

The g-phase's dynamics were modeled with a customized precommercial CHEMKIN-III version of PREMIX. (The commercial version is summarized by Kee et al. [2000].) The governing equations it implements to conserve mass, energy, and species in a steady, isobaric, quasi-1D flame are presented and discussed by Kee et al. (1989). (Momentum conservation is implicitly satisfied if the governing equations for mass, energy, and species conservation are satisfied.) To facilitate the (global) scaling of $\dot{\omega}_{k,g}$, the (standard) governing equations for modeling the continuity of each chemical species and the energy flux were modified to introduce $f_g(T)$. That is,

$$\dot{M}_g \frac{dY_{k,g}}{dx} + \frac{d[\rho_g A_g Y_{k,g} V_{k,g}]}{dx} - f_g(T) A_g \dot{\omega}_{k,g} W_k = 0 \qquad (10)$$

and

$$\dot{M}_g \frac{dT}{dx} - \frac{1}{c_{p,g}} \frac{d}{dx}\left(\lambda_g A_g \frac{dT}{dx}\right) + \frac{A_g}{c_{p,g}} \sum_{k=1}^{K} \rho_g Y_{k,g} V_{k,g} c_{p,k,g} \frac{dT}{dx} +$$

$$\frac{A_g}{c_{p,g}} \sum_{k=1}^{K} f_g(T) \dot{\omega}_{k,g} h_{k,g} W_k = 0, \qquad (11)$$

where A_g is the (x-dependent) cross-sectional area of the gas, $c_{p,g}$ is the gas's (x-dependent) constant-pressure heat capacity, $V_{k,g}$ is k's (x-dependent) diffusion velocity, and $h_{k,g}$ is its (x-dependent) mass-specific enthalpy.

All the thermophysical parameters and reaction-rate expressions that were needed to compute $\dot{\omega}_{k,g}$ were calculated based on the g-phase chemical kinetics mechanism and its associated thermochemical and transport property database. The

system of equations was solved with TWOPNT (Grcar 1992). An input file that is representative of those employed to parameterize the model in this domain is provided in Appendix C.

2.3.2 The Liquid–Gas Interface: $x = 0$

As in the three-phase model of $O_{3,s}$'s deflagration, predictions for the energy flux and temperature at the liquid–gas interface (T^0) in the current model were produced by the basic CYCLOPS framework. As discussed in detail by McQuaid and Stone (2024), that framework directs the search for a (r, T^0) solution that results in the boundary condition at the interface

$$\left[\lambda_g \frac{dT}{dx}\right]^{+0} = r\rho_l^{-\infty}\left(\sum_k^K (Y_{k,g})^{-0}(h_{k,g})^{+0} - h_l^{-\infty}\right) \quad (12)$$

being satisfied. The left side of Equation 12 corresponds to the energy flux incident on the interface due to the thermal conductivity (λ_g) and the temperature gradient (dT/dx) of the gas at the interface ($x = +0$). The right side corresponds to the energy flux needed to raise the enthalpy of a mass flux with density ($\rho_l^{-\infty}$) from the value for the liquid phase at $x = -\infty$ ($h_l^{-\infty}$) to that of the K gas-phase species with mass fractions $Y_{k,g}$ and mass-specific enthalpies $h_{k,g}$. The parameters λ_g, dT/dx, and $h_{k,g}$ are functions of T^0. The parameters λ_g and dT/dx are also functions of P.

Because the *l*-phase's dynamics were explicitly simulated in the current model, its spatial extent was bounded, with the value for $h_l^{-\infty}$ corresponding to a value at a finite distance (d) from the interface $\left(h_l^{-d}\right)$. Nonetheless, the formulation of the energy conservation equation at $x = 0$ remained completely independent of the properties of the liquid phase. That dependence was included via the representation of the *l*-phase's dynamics. That representation is summarized in Section 2.3.3.

A Google search found that EthN(l)'s ρ_c at 293 K had been reported to be 1.1084 g/cm^3. However, we were unable to establish that value's origin and therefore had some concern about its reliability. Nonetheless, it was difficult for us to imagine that this value differed by more than 5% from its actual value. Coupled with the fact that the dependence of the model's $r(P)$ predictions with respect to ρ_c's specification was linear, this uncertainty was insignificant from the standpoint of model validation. Therefore, it was not further considered.

EthN(g)'s $h_{k,g}^{+0}$ and λ_g^{+0} values were calculated based on formulae prescribed by the *g*-phase chemical kinetics mechanism's thermochemical and transport property databases. Values for h_l^x were computed per

$$h_{EthN,l} = \frac{R}{W_{EthN}}\left(1.04189870x10^{1}T + \frac{1.99914874x10^{-2}T^{2}}{2} - \frac{8.53432965x10^{-6}T^{3}}{3} + \frac{1.65402632x10^{-9}T^{4}}{4} - \frac{1.20272355x10^{-13}T^{5}}{5} - 2.73746409x10^{4}\right). \quad (13)$$

This formula was derived from a fit of the given functional form to $h_{EthN,l}(T)$ values calculated per

$$h_{EthN,l}(T) = h_{EthN,g}(T) - h_{v,EthN}(T),$$

where $h_{EthN,g}(T)$ values were computed with formulae prescribed by the *g*-phase mechanism's thermochemical property database, and $h_{v,EthN}(T)$ values were derived from vapor pressure data published by Gray et al. (1956). At 298.15 K, this expression produces an $h_{EthN,l}$ value equal to −51.2 cal/g (−46.6 kcal/mol). This value is approximately 1 kcal/mol more negative than values derived from data measured by Fairbrother et al. (1957) and Gray and Smith (1954).

For the d_5-EthN deflagration model, we assumed that d_5-EthN(*l*)'s density (ρ_{l,d_5-EthN}) would be related to EthN(*l*)'s in proportion to the ratio of their molecular weights—namely, $\rho_{l,d_5-EthN} = \left(W_{d_5-EthN}/W_{EthN}\right) * \rho_{l,EthN}$, where W_{EthN} was 91.06705 amu and W_{d_5-EthN} was 96.09770 amu—and had the model compute it accordingly.

2.3.3 The Liquid-Phase Domain: $-d \le x \le -0$

As in the three-phase $O_{3,s}$ deflagration model, governing equations and boundary conditions for the *l*-phase domain were formulated that were analogous those of the *g*-phase domain. Likewise, an in-house precommercial CHEMKIN-III version of PREMIX was modified to numerically represent and solve them.

The *l*-phase's equation of state was based on the $\rho_{l,EthN}(293)$ value mentioned in Section 2.3.2 and a T-dependence for EthN's density that was produced by molecular dynamics simulations (Veals et al. 2025). Combined, they yielded

$$\frac{\rho_{l,EthN}(T)}{1\ g/cm^3} = 1.7145 - 3.6728\text{x}10^{-3}T + 7.8601x10^{-6}T^{2} - 8.2807x10^{-9}T^{3}, \quad (15)$$

where T is in Kelvin.

For the energy conservation equation, we assumed diffusion's contribution to the dynamics would be negligibly small and zeroed the term included to represent it.*

* Because PREMIX's subroutines for computing diffusion coefficients were specifically formulated and parameterized for *g*-phase systems, we were also concerned that they might produce compromisingly poor estimates for a liquid phase. Therefore, we considered it prudent to eliminate that possibility.

That left

$$\dot{M}_l \frac{dT}{dx} - \frac{1}{c_{p,l}} \frac{d}{dx}\left(\lambda_l A_l \frac{dT}{dx}\right) + \frac{A_l}{c_{p,l}} \sum_{k'=1}^{K'} f_l(T) \dot{\omega}_{k',l} h_{k',l} W_{k'} = 0\,, \quad (16)$$

where $c_{p,l}$ was the l-phase's constant-pressure heat capacity, λ_l was its thermal conductivity, $\dot{\omega}_{k',l}$ was the molar rate of production of k' per unit volume, and $h_{k',l}$ was its mass-specific enthalpy.

For the computation of $\dot{\omega}_{k',l}$, the relationship between $\dot{\omega}_{k',l}$ and $\dot{\omega}_{k,g}$ that derives from Equation 7

$$\dot{\omega}_{k',l} = Pr(T) \dot{\omega}_{k,g} \quad (17)$$

was substituted into the governing equations. To compute the rates of reactions that were a function of the concentration(s) of third bodies, the model converted $\rho_{l,EthN}(T)$ into an effective pressure $[P_l(T)]$ based on the ideal gas law,

$$P_l(T) = \frac{\rho_{l,EthN}(T) RT}{W_{EthN}}. \quad (18)$$

We also assumed that the concentrations of the products of EthN(l)'s decomposition would be small and that the magnitudes of the products' intermolecular interactions with EthN molecules would not differ significantly from the magnitude of an EthN molecule's interaction with other EthN molecules. Therefore, we programmed the model to compute $h_{k',l}$ values by subtracting $h_{v,EthN} W_{EthN}$ values from g-phase mechanism-based $h_{k,g} W_k$ values,

$$h_{k',l} W_k = h_{k,g} W_k - h_{v,EthN} W_{EthN}\,, \quad (19)$$

where $h_{v,EthN} W_{EthN}$ values were computed with a formula derived from an Antoine equation representation of vapor pressure data measured by Gray et al. (1956). That formula was

$$h_{v,EthN} W_{EthN} = 2.302 R \frac{1337.035 T^2}{(T+48.37)^2}\,, \quad (20)$$

where T is in Kelvin. We note that the value of $h_{k',l} W_k$ at 298.15 K produced by Equation 19 (−46.6 kcal/mol) is approximately 1 kcal/mol more negative than values derived from measurement-based data that were reported by Fairbrother et al. (1957) (−45.5 kcal/mol) and Gray et al. (1956) (−45.7 kcal/mol).

For the d_5-EthN deflagration model, we assumed that on a molar basis, d_5-EthN's enthalpy of vaporization ($h_{v,d_5-EthN}W_{d_5-EthN}$) would be approximately equal to EthN's. Therefore, $h_{v,d_5-EthN}W_{d_5-EthN}$ was set equal to $h_{v,EthN}W_{EthN}$ in it. *

Based on the relationship

$$c_{p,l} = \frac{dh_l}{dT} \tag{21}$$

the expression

$$\frac{c_{p,l}}{1\ erg/g-K} = \frac{R}{W_{EthN}} * (1.04189870x10^{1} + 1.99914874x10^{-2}T$$
$$-8.53432965x10^{-6}T^2 + 1.65402632x10^{-9}T^3 - 1.20272355x10^{-13}T^4) \tag{22}$$

was derived from Equation 13 and employed to compute the $c_{p,l}$ values.

Based on λ_l values for EthN that were measured by Hildenbrand and Happe (1957), $\lambda_l(T)$ values were computed per

$$\frac{\lambda_l}{1\ cal/(cm-s-K)} = 5.007x10^{-4} - 7.500x10^{-8}T. \tag{23}$$

Similar to the formulation of Equation 16, the term representing diffusion was zeroed in the species conservation equations, leaving

$$\dot{M}_l \frac{dY_{k',l}}{dx} - A_l f_l(T)\dot{\omega}_{k',l}W_{k'} = 0\ , \tag{24}$$

where $Y_{k',l}$ was the mass fraction of k'.

2.3.4 Solution Search Protocol

As in the application of the three-phase model of $O_{3,s}$'s deflagration, the first step of the solution-search protocol implemented for this study was a basic CYCLOPS framework calculation. For this calculation, the mole fraction of the parent molecule on the liquid side of the liquid–gas interface (i.e., $X^{-0}_{EthN,l}$) was set equal to 1. Producing estimates for $\dot{M}$ and T^0, this calculation was the basis for establishing three boundary conditions for an l-phase domain problem to follow.

* In addition to $h_{k,l}$ and h_v, other thermophysical properties of d_5-EthN(l) were expected to be different from EthN(l)'s, and we developed some scaling relationships to produce estimates for them based solely on the difference in the two molecules' molecular weights. However, finding that the introduction of l-phase reaction chemistry did not impact $r(P)$ predictions, and disinclined to defend those relationships, we chose not to include them (or the predictions produced by them) herein.

They were

$$T^{-0} = T^{+0}, \tag{25}$$

$$T^{-d} = T^{-\infty} \tag{26}$$

and a target value for $[dT/dx]^{-0}$

$$\left[\frac{dT}{dx}\right]_{target}^{-0} = \left(\left[\lambda_g \frac{dT}{dx}\right]^{+0} - \left[\dot{M}_g h_{v,EthN}/A_l W_{EthN}\right]^{-0}\right)/\lambda_l^{-0}. \tag{27}$$

In addition, unlike the $O_{3,s}$ deflagration model, where $-d$'s value was one of the eigenvalues sought, in the current model it was a fixed value that simply needed to make physical sense. Formalizing our intuition, its magnitude ($|-d|$) was specified by dividing the difference between T^{-0} and T^{-d} by the average of $[dT/dx]_{target}^{-0}$ and the minimum possible value for $[dT/dx]^{-d}$ (namely, 0). That is,

$$|-d| = \frac{T^{-0} - T^{-d}}{0.5\left(\left[\frac{dT}{dx}\right]_{target}^{-0} + \left[\frac{dT}{dx}\right]^{-d}\right)} + d' = \frac{T^{-0} - T^{-d}}{0.5\left[\frac{dT}{dx}\right]_{target}^{-0}} + d', \tag{28}$$

where d' was a constant that was to be set equal to a value that was large enough for $[dT/dx]^{-d}$ to approach zero, but (presumably) not larger than the lengths of the tubes in the experiments. (Neither Steinberger et al. [1955] nor Hildenbrand et al. [1954] reported the lengths of the tubes in their experiments.)

Believing that the distance from the location(s) at which the measurements were made and the bottom of the tube were likely to be at least 1 cm, we set d' equal to 1 cm for a preliminary set of calculations. So specified, we found that $[dT/dx]^{-d}$ values were less than 1 K/cm, and thus effectively zero. Moreover, we found that $r(P)$ predictions produced with d' set to values greater than 1 cm were negligibly different from their 1-cm-based counterpart. Therefore, we did not further consider this matter.

Needing to provide an initial estimate for the *l*-phase domain's temperature profile $\left[T\left(x_j\right)\right]$ at grid points (j), we attempted to establish an analytically based method. Unfortunately, none proved tenable. Therefore, we investigated various heuristic approaches that were based on our experience in specifying initial estimates for solutions to PREMIX problems from which PREMIX's solution-search protocol would (reliably) progress. The method we settled on specified an initial 12-point grid comprising

$$x_1 = -d \tag{29}$$

and

$$x_2 = x_1 + d' \tag{30}$$

followed by 10 equally spaced points (x_j),

$$x_{j+1} = x_j + \frac{d-d'}{10}. \tag{31}$$

Values for $T(x_1)$ and $T(x_2)$ were set equal to T^{-d}. The remaining $T(x_j)$ were specified based on $[dT/dx]^{-0}_{target}$ per

$$T(x_{j+1}) = T(x_j) + 0.5\left[\frac{dT}{dx}\right]^{-0}_{target}(x_{j+1} - x_j). \tag{32}$$

This profile and $\dot{M}_l$ (= $\dot{M}_g$) were then written into an input file (*premix_lq.inp*). That file also specified $X_{EthN}(x_j)$ equal to 1 for all j.

The resulting problem was first solved with $Pr(T)$ in Equation 17 set equal to 0. (We found that TWOPNT was unable to proceed from the starting estimate if $Pr(T)$ was greater than 0.) Once the solution to that (n = 1) problem was obtained, a search to find a value for $\dot{M}_l$ that would produce $[dT/dx]^{-0}_{target}$ was initiated. Noting that, with all else being equal, the prediction for $[dT/dx]^{-0}$ was inversely proportional to $\dot{M}_l$'s value, an $\dot{M}_l$ estimate for the next ($n + 1$) iteration was produced per

$$\dot{M}_{l,n+1} = \dot{M}_{l,n}\left[1 - \left[\left(\left[\frac{dT}{dx}\right]^{-0}_{n} - \left[\frac{dT}{dx}\right]^{-0}_{target}\right)\Big/\left[\frac{dT}{dx}\right]^{-0}_{target}\right]\right]. \tag{33}$$

All other state-variables for the $n + 1$ problem were initially set equal to their value in the solution to the previous problem (n), and the new problem was then solved. This procedure was repeated until

$$\left|\left(\left[\frac{dT}{dx}\right]^{-0}_{n+1} - \left[\frac{dT}{dx}\right]^{-0}_{target}\right)\Big/\left[\frac{dT}{dx}\right]^{-0}_{target}\right| \leq 0.01. \tag{34}$$

Once this criterion was met, the *l*-phase's reaction chemistry was turned on by specifying $Pr(T)$ in Equation 17 equal to 1, and the procedure to find an $\dot{M}_l$ value that generated a $[dT/dx]^{-0}$ prediction meeting the criterion specified by Equation 34 was repeated.

Once Equation 34 was satisfied with $Pr(T)$ set equal to 1, the chemical composition at the liquid–gas interface predicted by that solution $\left[\{X_{k,l}\}^{-0}\right]$ was used as the nascent product set $\left[\{X_{k,g}\}^{-0}\right]$ for a subsequent (m + 1) CYCLOPS calculation. The $\dot{M}_g$ value produced by that calculation was then compared to the $\dot{M}_g$ value

produced by the previous (m) CYCLOPS calculation. The procedure was stopped when

$$\left|\frac{\dot{M}_{g,m+1}-\dot{M}_{g,m}}{\dot{M}_{g,m}}\right| \leq 0.0005. \quad (35)$$

In addition, as discussed in Section 4.2, we found that $\dot{M}_{g,m}$ predictions were approximately 10% smaller than the $\dot{M}_{l,m}$ predictions. Therefore, we performed a set of calculations to determine if $\dot{M}_{g,m}$ and $\dot{M}_{l,m}$ predictions could be brought into better agreement by increasing or decreasing T^{-0} values from their HLK-based value. By trial and error, we found that better agreement between them could indeed be achieved in this manner. Therefore, we recommend that this step be automated in future versions of the model.

3. Summary of Validating Measurement-Based Data

As discussed in the Introduction, we modeled four different sets of experiments from which measurement-based data pertaining to EthN's and *d*$_5$-EthN's decomposition and deflagration were derived. This section reviews details of those experiments that were pertinent to parameterizing the models we implemented to represent them.

3.1 Gas-Phase Decomposition: Levy (1952, 1954a)*

To study EthN(g)'s decomposition, Levy (1952, 1954a) used IR spectroscopy to quantify the t-dependent concentrations of EthN, ethyl nitrite, NO_2, and NO in a "bulb" comprising a Pyrex tube with rock-salt faces. The bulb had a constant volume, and the decomposition process occurred while it was immersed in a bath held at a (thermostatically controlled) constant temperature (T_{exp}). Results were published for experiments in which T_{exp} was equal to 434, 454, or 474 K. At the moment of the bulb's immersion in the bath (t = 0), the samples were "pure" EthN(g) ($X_{EthN,g}$ = 1) at an initial pressure (P_0). According to Levy's 1952 publication, P_0 values ranged from 10 to 50 mmHg. However, experiment-specific P_0 values were not (generally) reported, only $P_k(t)/P_0$ values.

In support of his data reduction approach, Levy (1952) reported $P_{EthN}(t_f)$ values (where t_f was a fixed duration of time) for a set of experiments in which T_{exp} was equal the 454 K and P_0 values were varied (in the range mentioned). (Although Levy did not report t_f's value, it can be deduced from other data in the report to

* The two publications summarize the same set of experiments. The paper published in 1954 was essentially an abridged version of the report published in 1952. The report contains all the details of the experiments that were the bases for parameterizing the model.

have been ~40 min.) Finding the $P_{EthN}(t_f)/P_0$ values to be very similar, he concluded that EthN(g)'s decomposition under these conditions was first order. However, we observed that the $P_{EthN}(t_f)/P_0$ values he reported decreased (slightly) with an increase in P_0.* Model predictions relevant to this observation are presented in Section 4.1.

Also (potentially) relevant, Levy (1952) counted t from the moment the bulb was immersed in the thermostatically controlled bath until the moment it was subsequently immersed in a cold-water bath. Basing that methodology on the assumption that the length of time it took for the bulb and its contents to reach T_{exp} was negligible relative to the time scale of the experiments, he corroborated it by measuring the time it took for a bulb filled with air to reach 474 K. In addition, he expected that the time for the kinetics of the decomposition process to be quenched after the bulb's immersion in the cold-water bath (vs. the time necessary for the contents to reach that bath's temperature) would be much less than that. On those bases, Levy concluded that "this order of time was within the accuracy of the experiment, especially at 454 K and 434 K." Therefore, although we could have added to the CNVT model representations for the warm-up and cooling phases of the procedure Levy describes, we believed his conclusion to be reasonable and made no attempt to do so.

We also note that another concern that is often raised and addressed in such studies is the potential for wall-catalyzed reactions to impact the results. However, we saw no mention of this concern in either of Levy's publications. Therefore, this possibility was not considered in our analysis.

3.2 Burning Rate and *l*-Phase Temperature Profile Data

3.2.1 Steinberger et al. (1955)

Steinberger et al. (1955) measured EthN's and d_5-EthN's $r(P)$ values as part of a study to test their hypothesis that H-atom diffusion is an important mechanism of energy feedback in the deflagration of nitrate esters. Their description of the experimental apparatus and procedures is cursory. Strands were burned in a 3-mm ID Pyrex tube under a nitrogen blanket in a windowed bomb. The length of the tube was not reported. T^{-d} values were reported to be 298 ± 2 K. Two methods were employed to measure $r(P)$ values, and they produced "identical" results.

* In a subsequent paper in which results of the decomposition of EthN(g) in the presence of additives are presented and discussed, Levy (1954b) acknowledged that the decomposition of pure EthN(g) under the conditions of his experiments was not "truly" first order.

The results were presented in a figure. We digitized them using DataThief (Tummers 2006).

Of concern to Faeth (1972), but not mentioned or addressed by Steinberger et al. (1955), was the potential for dissolved gases to influence the results. While Steinberger et al. did not state it in their publication, we cannot imagine they would not have ignited strands as soon as reasonably possible after their bomb was pressurized. Therefore, we assumed the potential for dissolved gases to underlie differences between measured and model-based values for parameters of interest was negligible.

3.2.2 Hildenbrand and Whittaker (1955) and Hildenbrand et al. (1954)

As part of a study whose primary focus was the measurement of $T(x)$ profiles in deflagrating liquid strands, Hildenbrand and Whittaker (1955) measured $r(P)$ values for EthN burning in a 3.7-mm ID Pyrex tube within a nitrogen-pressurized bomb. (They did not report the length of the tube.) T^{-d} values were reported to be 298 ± 2 K. The deflagration process was filmed with a high-speed camera, and $r(P)$ values were derived from the recordings. However, Hildenbrand and Whittaker (1955) do not state what the camera's resolution was. They also did not comment on the nature of the liquid-gas interface other than to observe that "igniter effects"—presumably surface instabilities—were completely damped out by the time the deflagration wave reached the thermocouple. They listed their results in a table.

Regarding the $T(x)$ profiles they published, Hildenbrand et al. (1954) discussed in some detail aspects of the thermocouples and the device employed to record the signals produced by them. However, given the relatively low rates at which the EMs they were studying burned, they concluded it was not necessary to correct for the diameter of the thermocouple or the frequency response of the recording device. Therefore, they simply reported the raw data. Those data were presented in a graph. We digitized them using DataThief (Tummers 2006).

Like Steinberger et al. (1955), Hildenbrand et al. (1954) did not state a concern about the potential for dissolved gases to impact the results. However, (again) we could not imagine they would not ignite strands as soon as reasonably possible after their bomb was pressurized. Therefore, we considered the point moot.

3.2.3 Faeth (1972)

Faeth (1972) measured $r(P)$ values for EthN as part of a study whose primary focus was to gain insight into the role played by gases produced by the decomposition of a liquid EM's parent molecule dissolving in the liquid. In the experiments, he

burned EthN in a 4-mm-diameter Pyrex tube with a length we inferred from a schematic diagram of his apparatus to be approximately 8 cm. He did not explicitly state what the T^{-d} values were. We assumed they were room temperature (298 K). Faeth reported nominal measured $r(P)$ and $T^0(P)$ values in tables. In addition, he presented an *l*-phase $T(x)$ profile obtained from an experiment conducted at 13.6 atmosphere (atm). (He deemed it representative of those produced in his study.) We digitized the data points in the published profile using DataThief (Tummers 2006).

Relevant to the current study, Faeth observed that the curvature of the liquid surface due to wall surface tension effects was "not large." At the lowest pressure at which he conducted experiments, he observed that the surface's minimum radius of curvature was no less than 20 mm, and it was less curved at higher pressure. (He believed this was due to a reduction in the surface tension with increasing pressure.) In addition, as found by others, he observed that EthN's deflagration became unstable or turbulent at pressures above 61.2 atm. Therefore, he did not report $r(P)$ or $T^0(P)$ data produced by experiments conducted at pressures above this limit.

We also note that, because Faeth was interested in the influence of dissolved gases on the state of the liquid surface, he pressurized his apparatus "just prior" to igniting strands to ensure that the bulk of the strand "had the low concentration of dissolved gas characteristic of liquids at atmospheric pressure." We could not think of a reason to question this assertion.

4. Results

4.1 Gas-Phase Decomposition

In this section, CNVT-based $P_k(t)/P_0$ predictions for EthN, ethyl nitrite, NO_2, and NO are compared to values Levi (1952, 1954a) measured in the experiments that are summarized in Section 3.1. Two sets of modeling predictions are presented. One set was produced with "baseline" chemical production rate estimates, i.e., $f(T)\dot{\omega}_{k,g}$ with $f(T)$ set equal to 1. The other set was produced with $f(T)$ set equal to $\exp[1006.4/(T/1\text{ K})]$.

4.1.1 $P_k(t)/P_0$ Predictions: Baseline $\dot{\omega}_{k,g}$ Estimates

Figures 1–3 present CNVT-based $P_k(t)/P_0$ predictions for EthN, ethyl nitrite, NO_2, and NO that were produced with baseline $\dot{\omega}_{k,g}$ estimates and compares them to Levy's (1952, 1954a) measurement-based data. Simulations were performed for the three T_{exp} values at which the experiments were conducted: 434, 454, and 474 K. $P_{NO}(t)/P_0$ predictions are shown for all three cases, but Levy did not report their

measurement-based counterpart for the experiments he conducted at 434 and 474 K. Except where otherwise indicated, the simulation's P_0 was 30 mmHg.

As Figures 1–3 show, the general trends in the relative magnitudes of the CNVT model's $P_k(t)/P_0$ predictions were similar to those that Levy measured. However, the predictions' timescales were much longer.

As mentioned in Section 3.1, Levy (1954a) also reported $P_{EthN}(t_f)/P_0$ values for a set of experiments in which T_{exp} was 454 K and P_0 had a range of values. Observing that $P_{EthN}(t_f)/P_0$ decreased slightly with increase in P_0, we were curious whether the model would reproduce that finding. Therefore, we ran simulations with P_0 equal to 10, 30, and 50 mmHg. As shown in Figure 2, the model did not reproduce the trend, but the results were reasonably consistent with Levy's (initial) conclusion that the fraction of EthN consumed was (effectively) independent of P_0 in the P_0 range established in his experiments.

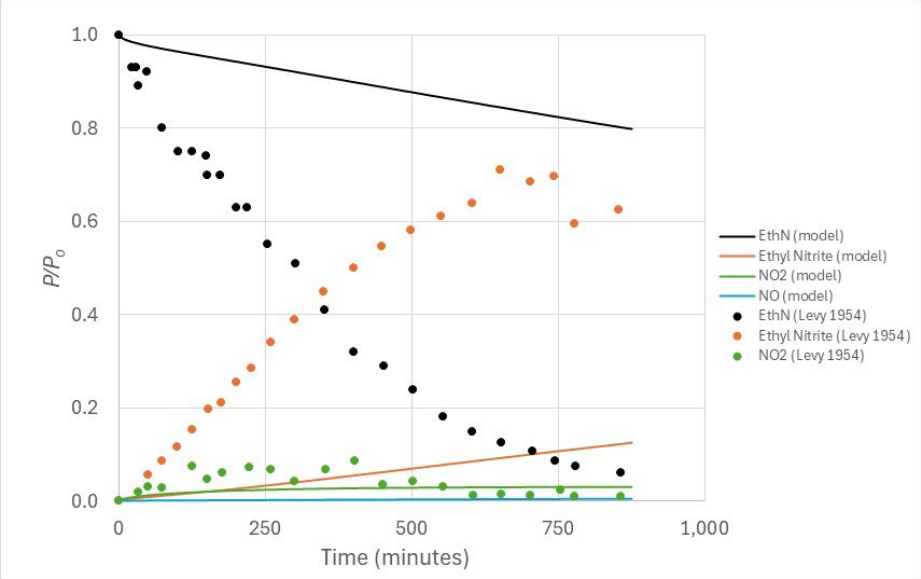


Figure 1. Comparisons of CNVT-predicted and measurement-based $P_k(t)/P_0$ values for EthN and selected species produced by EthN(*g*)'s decomposition at 434 K: baseline $\dot{\omega}_{k,g}$ estimates.

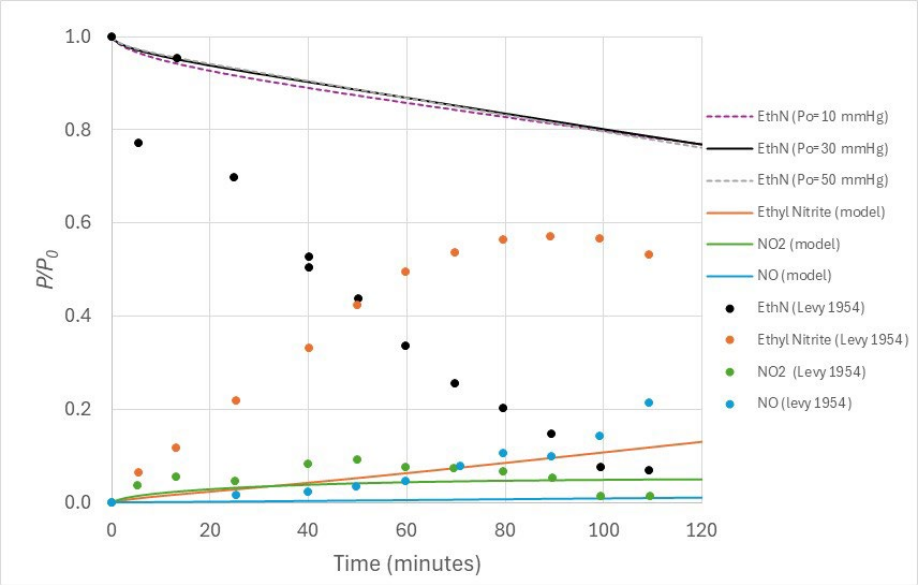


Figure 2. Comparisons of CNVT-predicted and measurement-based $P_k(t)/P_0$ values for EthN and selected species produced by EthN(g)'s decomposition at 454 K: baseline $\dot{\omega}_{k,g}$ estimates.

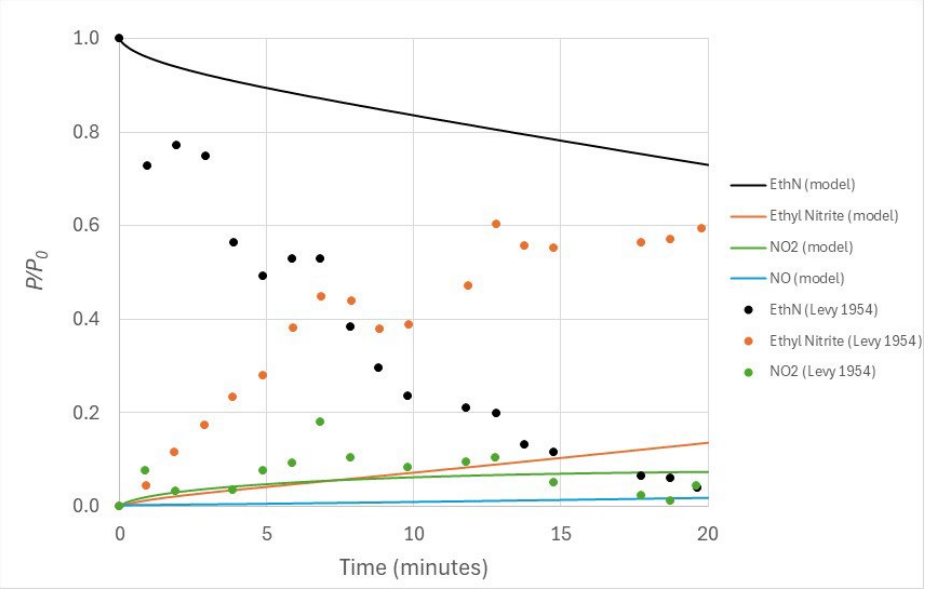


Figure 3. Comparisons of CNVT-predicted and measurement-based $P_k(t)/P_0$ values for EthN and selected species produced by EthN(g)'s decomposition at 474 K: baseline $\dot{\omega}_{k,g}$ estimates.

4.1.2 $P_k(t)/P_0$ Predictions: Globally Scaled $\dot{\omega}_{k,g}$ Estimates

Figures 4–6 present CNVT-based $P_k(t)/P_0$ predictions for EthN, ethyl nitrite, NO_2, and NO that were produced with globally scaled $\dot{\omega}_{k,g}$ estimates and compares them to Levy's (1952, 1954a) measurement-based data. Simulations were performed for the three T_{exp} values at which Levy conducted experiments: 434, 454, and 474 K.

In each case, $f_g(T)$ in Equation 8 was set equal to $\exp[1000/(T/1\ K))]$. In effect, this specification lowered the E_a^i of all the reactions in the mechanism 2 kcal/mol. Its value was 10.2 at 434 K, 9.2 at 454 K, and 8.4 at 474 K. As Figures 4–6 show, its inclusion yielded $P_k(t)/P_0$ predictions for EthN and ethyl nitrite that were in much better agreement with the measured values. In addition, as shown in Figure 7, it produced the slight increase in the rate of EthN(g)'s consumption with increase in P_0 that was observed in the data published by Levy (1952).

Based on those results, we searched for "suspect" parameterizations in the baseline mechanism's thermochemical kinetic database. Some were identified and updated. However, those updates (alone) did not produce $r(P)$ predictions that were significantly different from those produced by the baseline mechanism. Therefore, we did not further employ the updates in the study. We plan to present and discuss them in a future report.

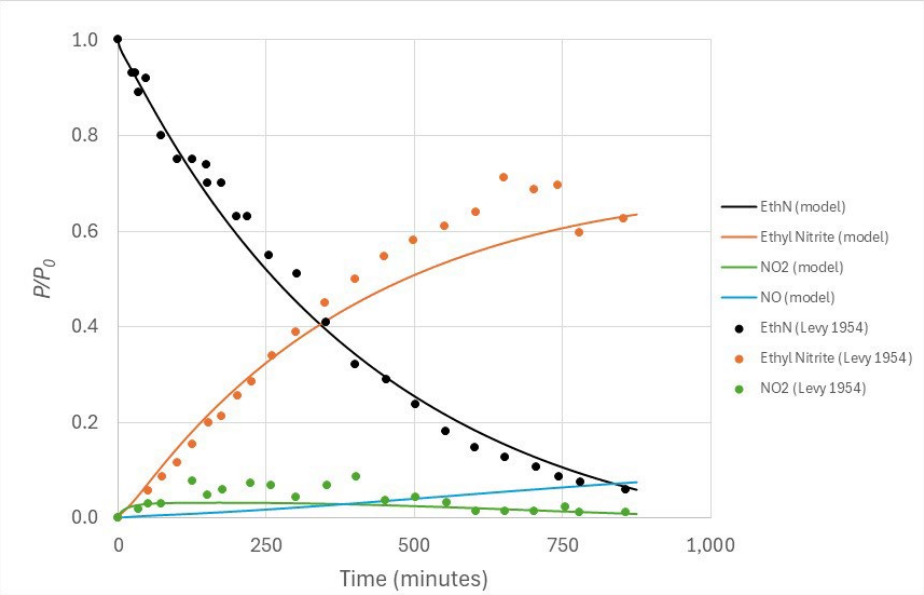


Figure 4. Comparisons of CNVT-predicted and measurement-based $P_k(t)/P_0$ values for EthN and selected species produced by EthN(g)'s decomposition at 434 K: globally scaled $\dot{\omega}_{k,g}$ estimates.

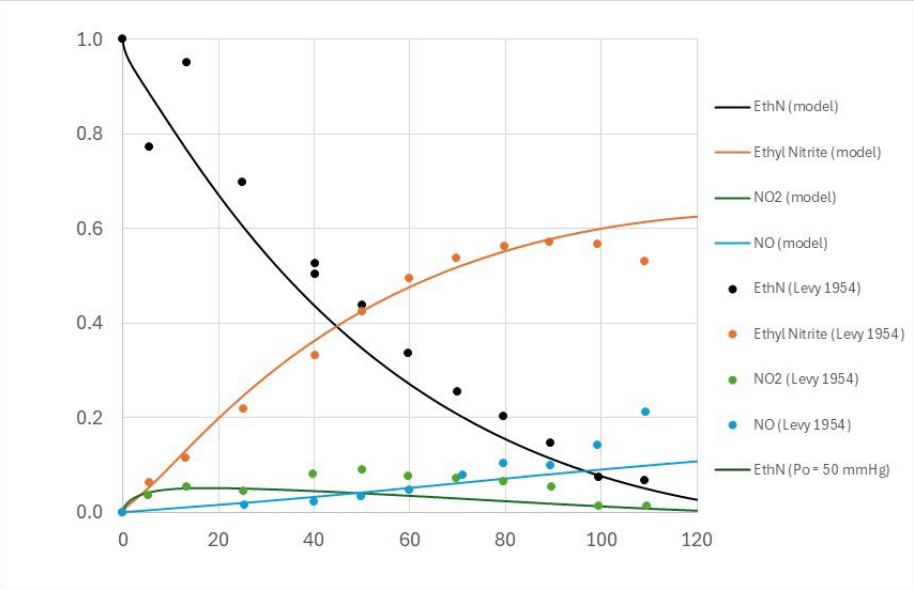


Figure 5. Comparisons of CNVT-predicted and measurement-based $P_k(t)/P_0$ values for EthN and selected species produced by EthN(g)'s decomposition at 454 K: globally scaled $\dot{\omega}_{k,g}$ estimates.

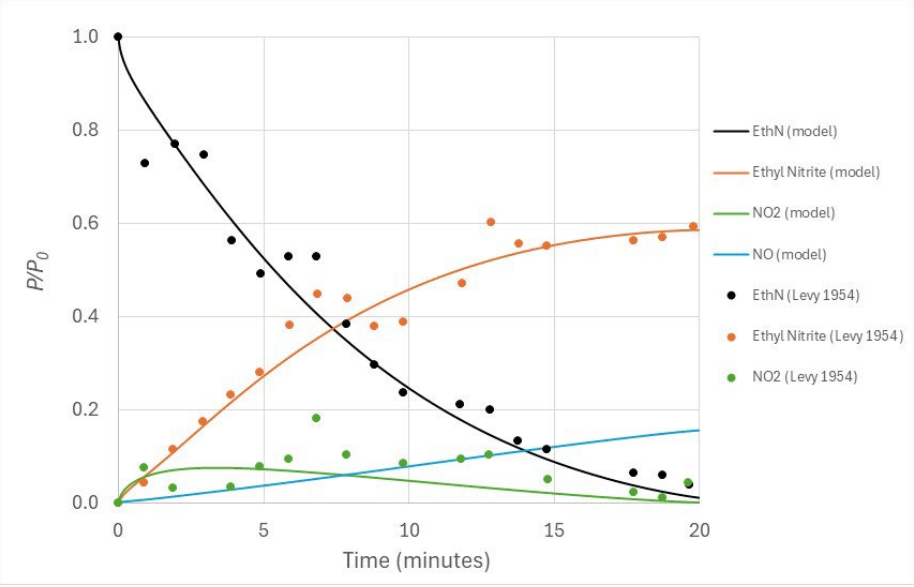


Figure 6. Comparisons of CNVT-predicted and measurement-based $P_k(t)/P_0$ values for EthN and selected species produced by EthN(g)'s decomposition at 474 K: globally scaled $\dot{\omega}_{k,g}$ estimates.

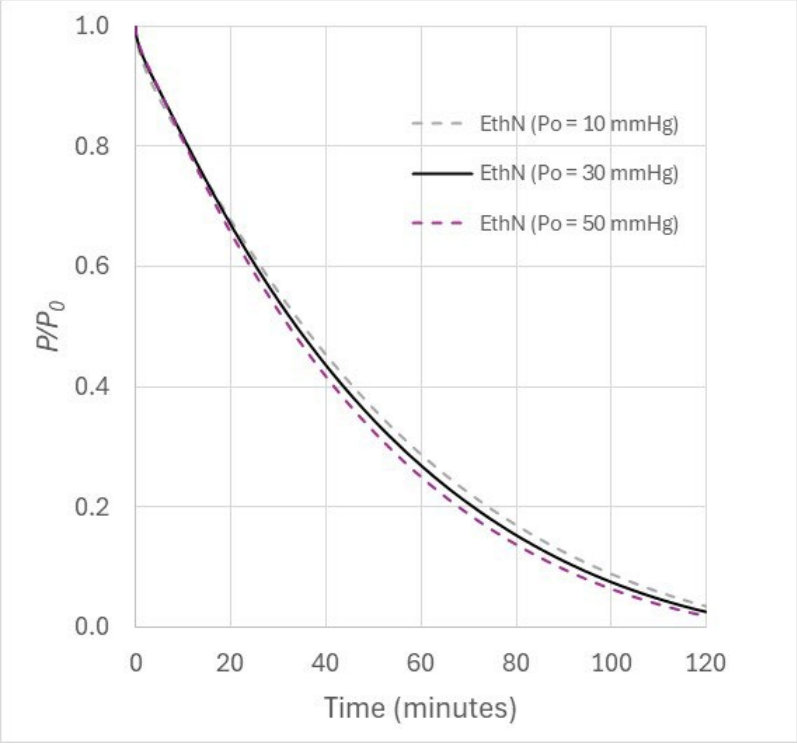


Figure 7. Comparison of CNVT-predicted $P_{EthN}(t)/P_0$ values as a function of P_0: T_{exp} = 454 K; globally scaled $\dot{\omega}_{k,g}$ estimates.

4.2 Burning Rate Predictions

Figure 8 presents $r(P)$ predictions produced by six different parameterizations of the deflagration model and compares them to values measured by Hildenbrand and Whittaker (1955), Steinberger et al. (1955), and Faeth (1972). The combination of parameter values that distinguish the six cases are summarized in Table 1. Compared to one another, these results quantified the impact of 1) including *l*-phase reaction chemistry and conductive processes and 2) globally scaling $\dot{\omega}_{k,g/l}$ estimates.

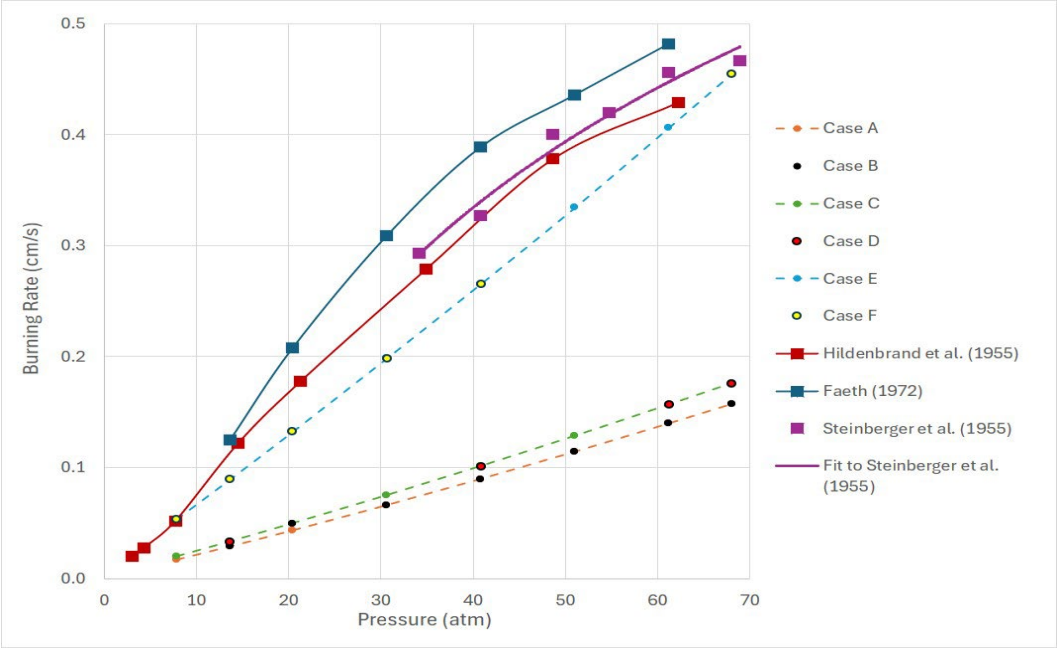


Figure 8. Comparison of measured and model-predicted $r(P)$ values.

Table 1. Case distinguishing specifications for $f_g(T)$, $f_l(T)$, and T^{-d}.

Case	$f_g(T)$	$Pr(T) * f_l(T)$	T^{-d} (K)
A	1	0	298.15
B	1	1	298.15
C	1	0	348.15
D	1	1	348.15
E	exp(2500/T)	0	298.15
F	exp(2500/T)	exp(2500/T)	298.15

Case A corresponds to the basic CYCLOPS framework. As already mentioned, that framework is predicated on the assumption that *c*-phase reaction chemistry does not play a meaningful role in the deflagration process. In the current model, *l*-phase reactions were turned off by setting $Pr(T) * f_l(T)$ equal to 0.

Case A's $r(P)$ predictions proved to be similar to those produced previously by us with the basic CYCLOPS framework. Since the 2013 study by Chen and McQuaid, the basic framework's $r(P)$ predictions have consistently been approximately a factor-of-three lower than measured values over the range of pressures considered. Consistent with those findings, the Case A results reaffirmed that the mechanism library relevant to modeling the deflagration of nitrate esters that has evolved since 2013 has not improved matters.

With *l*-phase reaction chemistry turned on (Case B), the $r(P)$ predictions proved to be negligibly different from their Case A counterparts. Pertaining to this finding, Table 2 shows $\{X_{k',l}(P)\}^{-0}$ values for species that in the 68-atm simulation had a value that exceeded 1×10^{-6}. (At lower pressures, $\{X_{k',l}\}^{-0}$ values for all species not listed in the table were lower than 1×10^{-6}.) At 68 atm, $X_{EthN,l}$ exceeded 0.99975. Moreover, since the $|\dot{\omega}_{k,l}|$ estimates were considered likely to be the largest they could be (relative to their $|\dot{\omega}_{k,g}|$ counterparts), the results were consistent with the assumption that EthN(*l*)'s decomposition was negligible and therefore need not be represented to produce reasonable $r(P)$ predictions.

Table 2. Species' mole fraction predictions at $x = -0$: Case B.

	Pressure (atm)						
Species	**13.6**	**20.4**	**30.6**	**40.8**	**51.0**	**61.2**	**68.0**
$ETONO_2$	0.999993	0.999981	0.999953	0.999913	0.999861	0.999800	0.999754
CH_2O	0.000003	0.000008	0.000021	0.000040	0.000064	0.000093	0.000114
CH_3NO_2	0.000003	0.000008	0.000019	0.000036	0.000058	0.000084	0.000103
NO_2	0.000000	0.000001	0.000002	0.000004	0.000005	0.000007	0.000009
C_2H_5ONO	0.000000	0.000000	0.000001	0.000002	0.000003	0.000004	0.000005
CH_3CHO	0.000000	0.000001	0.000001	0.000002	0.000003	0.000004	0.000004
CH_3ONO_2	0.000000	0.000000	0.000001	0.000001	0.000002	0.000003	0.000004
CH_4	0.000000	0.000001	0.000001	0.000002	0.000002	0.000003	0.000004
HONO	0.000000	0.000000	0.000000	0.000000	0.000001	0.000001	0.000001

Knowing that the $r(P)$ predictions would increase with a less negative specification of h_l^{-d} (Chen et al. 2019), and observing that the $h_{EthN,l}(298)$ value computed per Equation 13 was approximately 1 kcal/mol more negative than the average of measurement-based values, we knew that using the average of the measured values would improve the agreement between measured and predicted $r(P)$ values (at least somewhat). In addition, we thought that in the experiments heat transfer from the flame through the Pyrex tube to the liquid might have made the h_l^{-d} values in the experiments even more positive than the measured $h_{EthN,l}(298)$ values. Therefore, Cases C and D were formulated to quantify the impact of raising T^{-d} and (concomitantly) h_l^{-d}.

With T^{-d} specified to be 50 K higher than the nominal value reported by the experimentalists, the Equation 13-based $h_l(348)$ estimate was 1.6 kcal/mol less negative than the Equation 13-based $h_l(298)$ estimate. It was also 0.5 kcal/mol less negative than the nominal measurement-based $h_l(298)$ value. Specified for Cases C and D, this h_l^{-d} value resulted in $r(P)$ predictions for the two cases that, as shown in Figure 8, were approximately 10% higher than their Case A and B counterparts. Thus, we concluded that although discrepancies between actual and computed $h_l(T)$ values as well as unaccounted for heat transfer from the flame to the liquid via the Pyrex tube may have contributed to the 200% difference between the

baseline model's $r(P)$ predictions and those that were measured, we doubted the combination of those discrepancies could account for more than 20% of the difference.

Figure 8 also shows the $r(P)$ predictions produced by multiplying the baseline $\dot{\omega}_{k,g/l}$ estimates by exp[2500/(T/1 K)]. Implemented in Cases E and F, this artifice produced $r(P)$ predictions that were in much better agreement with the measured values. However, as found in comparing Case A predictions with Case B predictions, and Case C predictions with Case D predictions, the differences between the $r(P)$ predictions produced with l-phase reaction chemistry turned off (Case E) and on (Case F) were negligible.

Relevant to this finding, Table 3 shows $\{X_{k\prime,l}\}^{-0}$ predictions produced at selected pressures for species that in the 61.2 atm simulation had values that exceeded 1×10^{-6}.* (At lower pressures, the $\{X_{k\prime,l}\}^{-0}$ predictions for all species not listed in the table were lower.) In the 61.2 atm simulation, $X_{EthN,l}$ was greater than 0.9995. Moreover, the $|\dot{\omega}_{k,l}|$ estimates were considered likely to be largest they could be relative to their $|\dot{\omega}_{k,g}|$ counterparts. As such, the results corroborated our assumption that EthN's l-phase decomposition was negligible and therefore need not be represented to produce reasonable $r(P)$ predictions.

Table 3. Species' mole fraction predictions at $x = -0$: Case F.

	Pressure (atm)			
Species	**13.6**	**20.4**	**30.6**	**61.2**
$ETONO_2$	0.999963	0.999925	0.999842	0.999538
CH_2O	0.000017	0.000036	0.000075	0.000220
CH_3NO_2	0.000016	0.000033	0.000070	0.000204
C_2H_5ONO	0.000001	0.000001	0.000003	0.000010
NO_2	0.000001	0.000002	0.000003	0.000008
CH_3ONO_2	0.000001	0.000001	0.000003	0.000008
CH_3CHO	0.000000	0.000001	0.000002	0.000004
CH_4	0.000000	0.000001	0.000002	0.000004
HONO	0.000000	0.000000	0.000001	0.000002

4.3 Temperature at the Liquid–Gas Interface

Figure 9 presents the T^0 predictions produced by the six cases and compares them to values measured by Faeth (1972) and Hildenbrand and Whittaker (1955). Figure 9 also shows predictions for EthN's boiling point (T_b) as a function of P that

* Attempts to produce Case F predictions at other pressures were unsuccessful, failing because the solver was unable to produce solutions meeting specified convergence criteria for the l-phase domain. Given the results obtained by that point, we did not think the effort needed to find a remedy for this issue was warranted.

were computed based on vapor pressures measured at temperatures from 273 to 341 K. As shown, the differences between the T^0 predictions produced by the six cases were relatively small and the predictions were in reasonable agreement with the values measured by Faeth (1972). Not surprisingly, the inclusion of *l*-phase reaction chemistry had effectively no impact on the results.

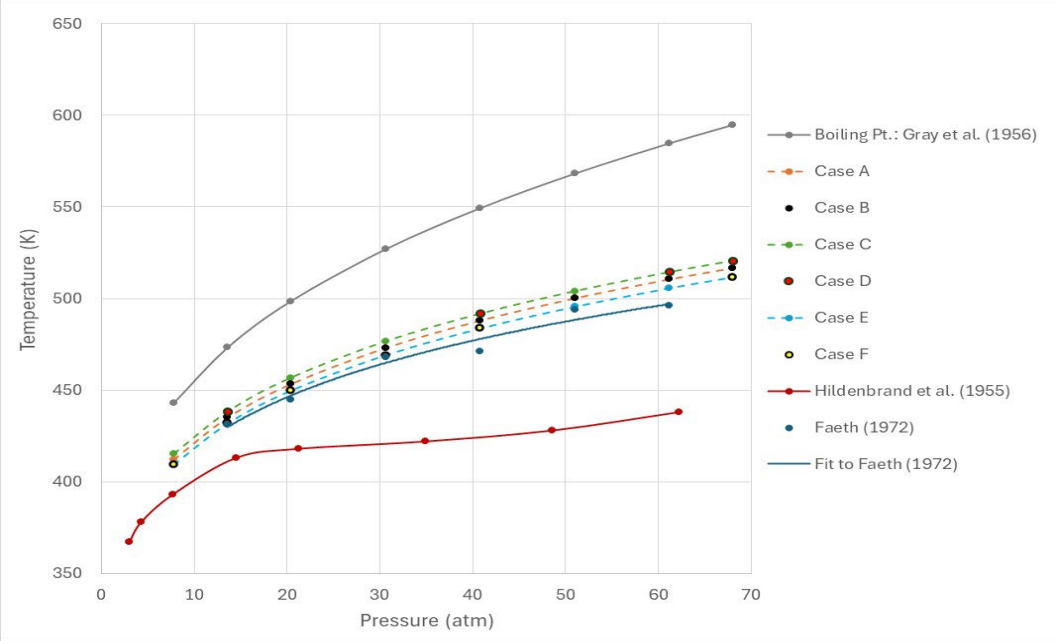


Figure 9. Comparison of measured and predicted temperatures at the liquid–gas interface (T^0).

The data in Figure 9 prompted our interest in establishing the sensitivity of the $r(P)$ predictions to variations in T^0. (That question did not occur to us in our study of $O_{3,s}$'s deflagration.) Pursuing it, we reran the Case B simulations with T^0 fixed at values that were 5 and 10 K below the HLK-based prediction. The results are presented in Table 4. As we have observed for other EMs, the CYCLOPS-based $\dot{M}_g$ predictions proved to be relatively insensitive to the value of T^0 (near its HLK-based value), rising little (if at all) with increase in T^0. The T^0 dependence of $\dot{M}_l$ predictions was also small but (percentagewise) somewhat greater than that of the $\dot{M}_g$ predictions. Moreover, the $\dot{M}_l(T^0_{HLK}\text{-}5)$ predictions were less than the $\dot{M}_l(T^0_{HLK})$ predictions and the $\dot{M}_l(T^0_{HLK}-5)$ predictions were less than the $\dot{M}_l(T^0_{HLK}-10)$ predictions. Combined, the trends led to better overall agreement between the $\dot{M}_g$ and $\dot{M}_l$ predictions when T^0 was 5 K less than the HLK-based prediction.* In

* Although a higher resolution search for the value of T^0 that minimized the difference between $\dot{M}_g$ and $\dot{M}_l$ might have produced predictions that differed from 5 K by several degrees K, given this study's objectives and the magnitude of the disagreement between measured and model-predicted $r(P)$ values, we did not deem the effort needed to the perform such a search warranted. For future studies, however, we recommend that an automated search for the value of T^0 that minimizes the difference between $\dot{M}_g$ and $\dot{M}_l$ (to the extent possible) be formulated and added to the protocol.

addition, those T^0 predictions were in better agreement with the values measured by Faeth.

Table 4. Comparison of $\dot{M}_g$ and $\dot{M}_l$ predictions as a function of T^0.

P (atm)	T^0 (K)	$\dot{M}_g$ (g/s)	$\dot{M}_l$ (g/s)	Difference[a] (%)
7.8	412[b]	1.868E-02	2.082E-02	11.5
	407	1.869E-02	2.006E-02	7.4
	402	1.869E-02	2.009E-02	7.5
13.6	435[b]	3.186E-02	3.527E-02	10.7
	430	3.187E-02	3.404E-02	6.8
	425	3.187E-02	3.408E-02	6.9
20.4	453[b]	4.781E-02	5.258E-02	10.0
	448	4.781E-02	5.098E-02	6.6
	443	4.781E-02	5.103E-02	6.7
30.6	473[b]	7.274E-02	7.973E-02	9.6
	468	7.277E-02	7.721E-02	6.1
	463	7.280E-02	7.730E-02	6.2
40.8	488[b]	9.871E-02	1.080E-01	9.4
	483	9.874E-02	1.048E-01	6.1
	478	9.874E-02	1.048E-01	6.1
51.0	500[b]	1.257E-01	1.375E-01	9.4
	495	1.257E-01	1.329E-01	5.7
	490	1.257E-01	1.330E-01	5.8
61.2	511[b]	1.537E-01	1.676E-01	9.1
	506	1.537E-01	1.622E-01	5.5
	501	1.537E-01	1.623E-01	5.6
68.0	517[b]	1.728E-01	1.885E-01	9.1
	512	1.728E-01	1.823E-01	5.5
	507	1.728E-01	1.824E-01	5.5

[a] $100*(\dot{M}_l - \dot{M}_g)/\dot{M}_g$.
[b] HLK-based prediction.

4.4 *l*-Phase Temperature Profiles

Figure 10 compares the measured and model-predicted *l*-phase $T(x)$ profiles for EthN burning at 13.6 atm. As shown, the Case F $T(x)$ profile, which corresponds to $r(P)$ predictions that are in better agreement with measured values, is in better agreement with the measured profile. Moreover, we suspect that even better agreement between measured and predicted $T(x)$ profiles would be produced by a simulation in which the $r(P)$ prediction was in even better agreement with the measured value.

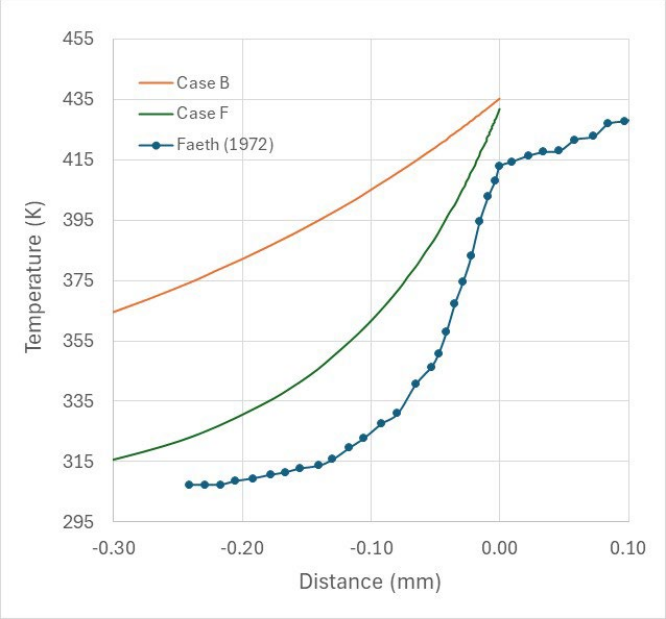


Figure 10. Comparison of measured and predicted *l*-phase $T(x)$ profiles for EthN burning at 13.6 atm.

Similarly, Figure 11 compares the model-predicted l-phase $T(x)$ profile for EthN burning at 7.8 atm to data published by Hildenbrand et al. (1954). (At this pressure, a solution that met the specified convergence criteria in the l-phase domain was not obtained for Case B.) Again, the $T(x)$ profile predicted by Case F, which corresponds to a $r(P)$ prediction that is in better agreement with the measured value, is in better agreement with the measured profile.

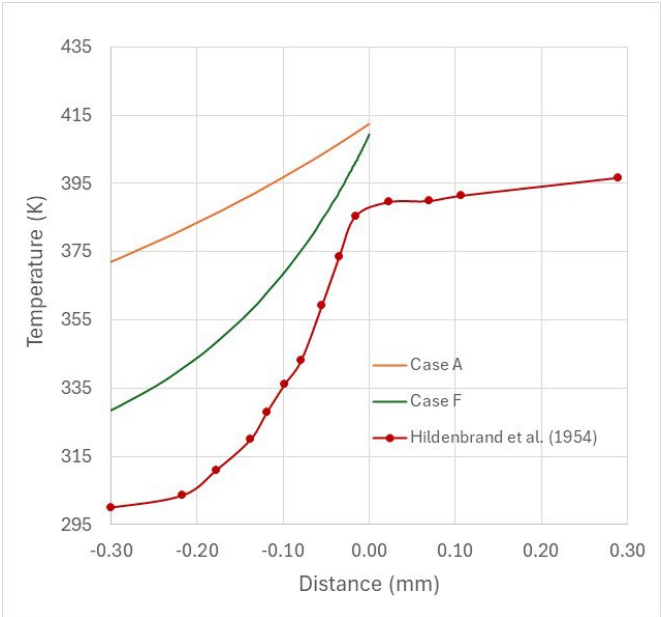


Figure 11. Comparison of measured and predicted *l*-phase $T(x)$ profiles for EthN burning at 7.8 atm.

4.5 Differences between the Deflagrations of EthN and d_5-EthN

Figure 12 compares the Case A $r(P)$ predictions produced for (normal) EthN and d_5-EthN. At each pressure, the prediction for d_5-EthN was approximately 9% slower than the prediction for EthN. Although that reduction was less than half of the approximately 25% reduction measured by Steinberger et al. (1955), we assumed it was larger than the numerical uncertainty in the calculations and sought an explanation.

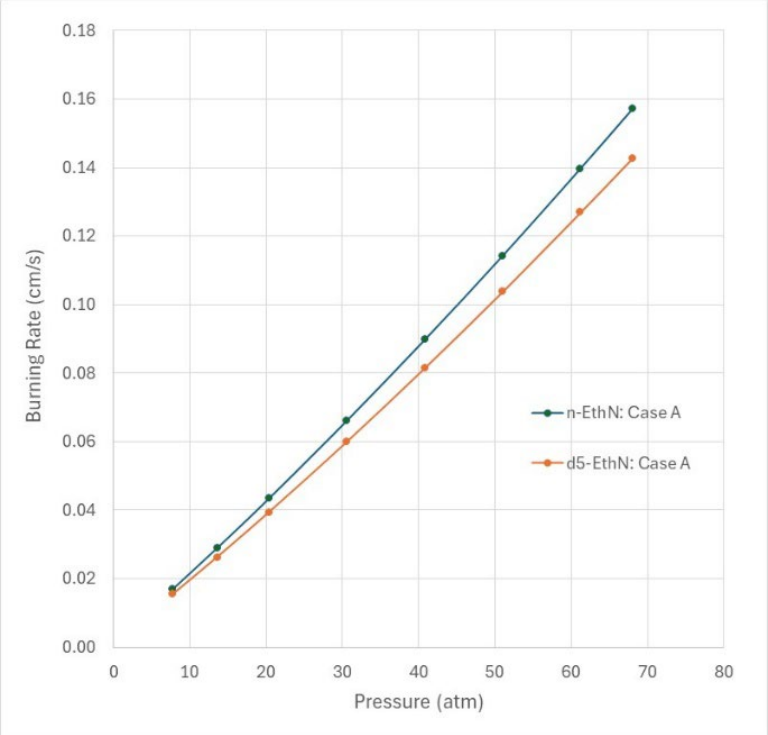


Figure 12. Comparison of $r(P)$ predictions for EthN and d_5-EthN: Case A.

Acknowledging Steinberger et al.'s (1955) hypothesis about the importance of the diffusion of H-atoms and their reaction with parent molecules near the liquid–gas interface, we started our analysis by comparing $X^{+0}_{H/D,g}$ predictions for the two cases. Results are presented in Table 5. Two aspects of them were notable. First, at each pressure the $X^{+0}_{D,g}$ prediction was from 20% to 30% *higher* than the $X^{+0}_{H,g}$ prediction. Second, and more importantly, all the values were less than the convergence criterion for the absolute values of state variables (ATOL = 1×10^{-10}) that was specified for the calculations. As such, the strongest conclusion we could

derive from the results was that predicted $X_{H/D,g}^{+0}$ values were less than 1×10^{-10}.* Because all $X_{H/D,g}^{+0}$ predictions in the two sets were less than this value, their value relative to one another remained an open question. Regardless, both observations suggested the role of H atoms in driving mass transfer at the interface, if any, is very limited.

Table 5. $X_{H/D,g}^{+0}$ predictions: Case A.

P (atm)	H	D	Difference[a]
7.8	1.01E-11	1.30E-11	29
13.6	1.30E-11	1.66E-11	28
20.4	1.61E-11	2.04E-11	27
30.6	2.07E-11	2.58E-11	25
40.8	2.54E-11	3.14E-11	23
51.0	3.02E-11	3.68E-11	22
61.2	3.43E-11	4.13E-11	21
68.0	3.70E-11	4.43E-11	20

[a] $100*(X_{D,g} - X_{H,g})/X_{H,g}$

Seeking additional support for this conclusion, we found that further downstream, where the $X_{H/D,g}(x)$ values were numerically significant, the $X_{H/D,g}(x)$ profiles at a given P were very similar. Representative of predictions produced at other pressures, Figure 13 compares the $X_{H/D}(x)$ predictions generated by simulations in which the pressure was 30.6 atm.

* ATOL is actually a convergence criterion for $Y_{k,g}$. However, due to H's and D's low molecular weights, their $Y_{k,g}$ values are even lower than their $X_{k,g}$ values. We also note that rerunning the simulations with tighter convergence criteria might have addressed this issue. However, we did not believe the effort required to do so was warranted. Instead, we reran a couple of simulations with ATOL = 1×10^{-11} to ascertain whether they would yield $r(P)$ predictions that were different from the corresponding ATOL = 1×10^{-10} case. They did not, reaffirming the conclusion based on preproduction simulations that ATOL = 1×10^{-10} was sufficiently small for the purposes of the study.

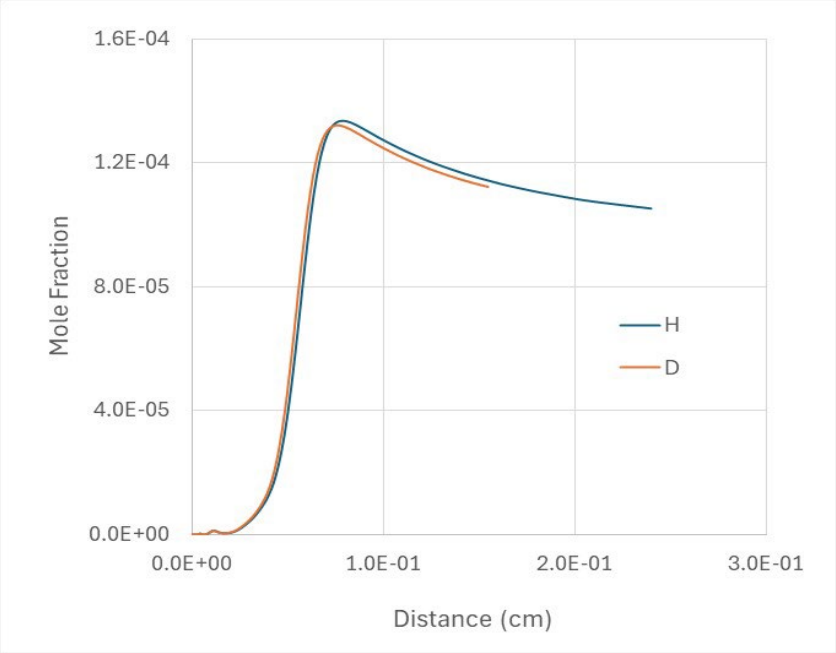


Figure 13. Comparison of $X_H(x)$ and $X_D(x)$ predictions: Case A; P = 30.6 atm.

Because we expected $X_H(x)$ and $X_D(x)$ profiles to be considerably different, such results caused us to question the model's capacity to represent well the diffusion of H (and D). To address that concern, we extracted $V_H(x)$ and $V_D(x)$ profiles from the output. Plots for the 30.6 atm case are shown in Figure 14. They indicate that the model predicted lower diffusion velocities for D in regions where the concentration gradients of H and D were relatively large. However, they also made it apparent that diffusion velocities are not by themselves important. Instead, as suggested by Equations 10 and 11, it is $Y_k(x)V_k(x)$ values that establish the relative importance of diffusion with respect to other subprocesses. And comparing $Y_H(x)V_H(x)$ and $Y_D(x)V_D(x)$ values, we found them to be very similar. Figure 15 compares predictions derived from the 13.6-atm Case A simulations. On such bases, we were satisfied that the model's representation of H-atom diffusion was reasonable, giving us confidence in the conclusions drawn from its predictions.

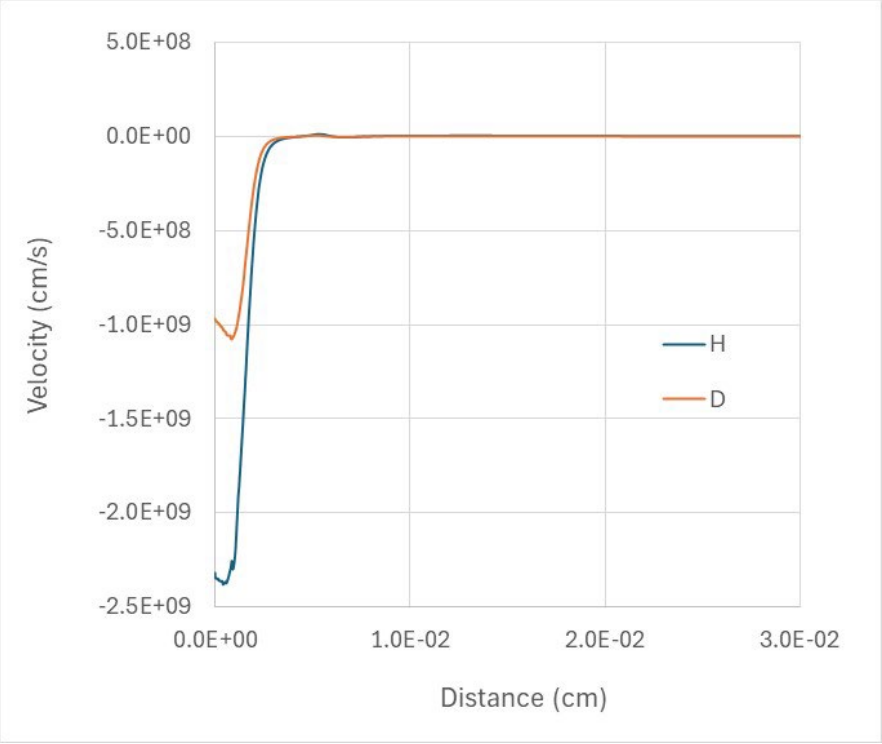


Figure 14. Comparison of $V_H(x)$ and $V_D(x)$ predictions: Case A; P = 30.6 atm.

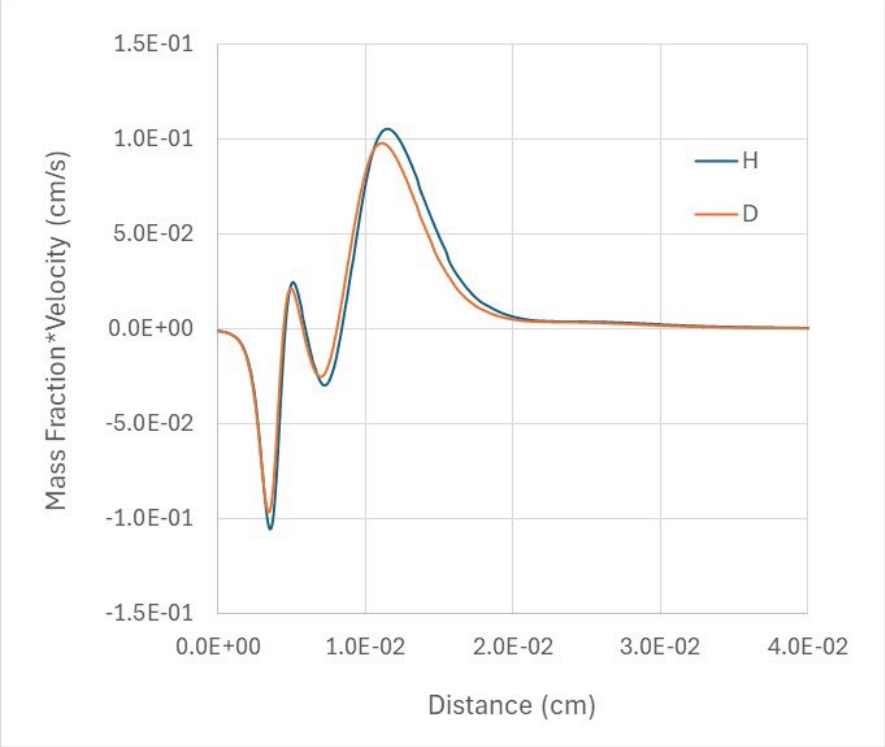


Figure 15. Comparison of $Y_H(x)V_H(x)$ and $Y_D(x)V_D(x)$ predictions: Case A; P = 30.6 atm.

Given that the $r(P)$ predictions produced by the baseline model were a factor of three lower than measured values, we considered it possible that refinements to the *g*-phase chemical kinetics mechanism that yielded $r(P)$ predictions that were in better agreement with measured values could indicate that H-atoms play a more important role near the liquid–gas interface than the present model-mechanism combination admits. That speculation notwithstanding, these results indicated that diffusion-driven differences in the fluxes of H and D were not responsible for the differences in the model-based $r(P)$ predictions for EthN and *d*$_5$-EthN.

Searching for an alternative explanation, we turned our attention to the models' predictions for λ_g. All else being equal, the larger mass and moments of inertia of molecules with D substituted for H lower their molecular velocities and capacities to transfer rotational energy. Therefore, the λ_g values for deuterated molecules are generally lower than their normal analogs. Based on the kinetic theory of gases for pure species, a first-order approximation of the reduction is calculable per

$$\lambda_g \propto 1/\sqrt{W_k}. \tag{36}$$

As such, we expected the λ_g values in the *d*$_5$-EthN system to be lower, and through Equation 12, have the potential to produce lower $r(P)$ predictions.

Because of the coupling between the subprocesses involved in the *g*-phase's dynamics, the $\lambda_g(x)$ values derivable from the $\{T(x), X_k(x)\}$ solutions for the two systems at a given *P* are not an optimal basis for quantifying the difference that the change in $\{W_k\}$ (alone) would make. Therefore, we computed and recorded the $\lambda_g(x)$ values for the solution to an EthN problem, then used the $\{T(x), X_k(x)\}$ predictions from that solution to compute $\lambda_g(x)$ values for the analogous *d*$_5$-EthN system. The results derived from the 30.6 atm EthN simulation are shown in Figure 16. Consistent with expectations, $\lambda_{d_5-EthN\ sys}(x)$ values were less than $\lambda_{EthN\ sys}(x)$ values for all x. Moreover, we observed that near the liquid–gas interface, the $\lambda_g(x)$ predictions for the *d*$_5$-EthN system were almost 12% lower than those for the EthN system. That reduction was larger than the 9% reduction in the $r(P)$ predictions.

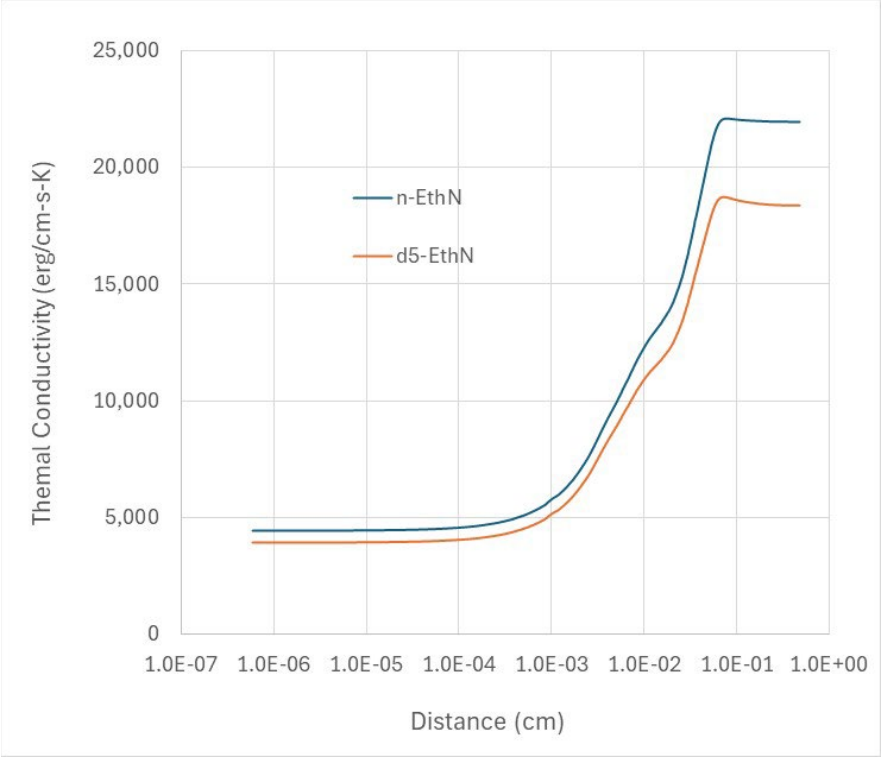


Figure 16. Comparison of $\lambda_{EthN\ sys}(x)$ and $\lambda_{d_5-EthN\ sys}(x)$ predictions: P = 30.6 atm.

We note that the magnitude of the difference between the λ_g predictions for the two systems is much greater than the 3.5% difference one might guess based on Equation 36 and considering only W_{EthN} (91 amu) and W_{d_5-EthN} (96 amu). The larger difference is a consequence of the chemical compositions of the mixtures containing significant concentrations of H_2 and H_2O. Percentagewise, W_{D_2} and W_{D_2O} are significantly larger than W_{H_2} and W_{H_2O}, respectively.

Due to the coupling and feedback between the subprocesses of the g-phase's dynamics, a linear relationship between $\lambda_g(P)$ and $r(P)$ for two systems was not expected. Therefore, we do not believe this result conclusively demonstrates that differences in the two systems' $\lambda_g(P)$ predictions are the sole reason for the difference in the $r(P)$ predictions for them. Nonetheless, we take these results to suggest that 1) this difference accounts (in large part) for the differences in the $r(P)$ predictions calculated for them and 2) this same mechanism could account for a significant fraction of the 25% difference between the two systems' measurement-based $r(P)$ values.

5. Discussion

As mentioned in the Introduction, a basic CYCLOPS model of EthN's deflagration that we have been developing (intermittently) since 2012 has consistently

underpredicted measurement-based $r(P)$ values by a factor of approximately three. Although we have always considered discrepancies of this magnitude "large," from the standpoint of model validation they are within a range we generally accept as adequate for rocket motor development efforts. In such applications, a model's primary purpose is not to reproduce measured burning rates with high accuracy. (That can readily be done with empirical formulae.) Rather, it is to reliably *predict* the impact that changes to a propellant's chemical composition or physical properties will have on its $r(P)$ values and thereby provide guidance for design changes. Based on 1) postulating various deviations between the models' idealization of the experiments and their reality and 2) observing that relatively minor refinements of a g-phase chemical kinetics mechanism could have a large impact on the $r(P)$ predictions it would produce, we have consistently concluded that discrepancies of the observed magnitude and direction could be significantly reduced by including higher fidelity representations for some (select) aspects of the system's dynamics. In this study, we sought additional evidence for that conclusion.

Among the idealizations of the deflagration process that we have shown can underlie a basic CYCLOPS model's underprediction of $r(P)$ values is their (default) representation of the liquid–gas interface as a (flat) plane. As mentioned in the Introduction, CYCLOPS models produce a prediction for $\dot{M}(P)$, and a prediction for $r(P)$ follows from it via Equation 3. However, as demonstrated in studies of MeN's and AP's deflagrations (Nusca 2014b; McQuaid and Chen 2016), $\dot{M}(P)$ is a function of A^{c-g}, and the system's cross-sectional area (A^0) corresponds to the minimum value that A^{c-g} can be. Unable to imagine that EthN(l)'s surface could be "stable" under the conditions of the experiments, we assumed the default representation yielded an underprediction for $\dot{M}(P)$, and therefore $r(P)$.

In addition, because the Pyrex tubes that radially confined the deflagration process in the experiments had a higher thermal conductivity than EthN(l), we could imagine that some preheating of the EthN(l) may have occurred. Similar to the mechanism that produces an increase in an MSP's "effective" $r(P)$ values when it is embedded with thermally conductive wires, such preheating would produce an increase in the $r(P)$ values relative to those of strands at the temperature assumed. Moreover, although our experience has strongly suggested that condensed-phase chemical kinetics do not play a role in determining the $r(P)$ values of uncatalyzed MSPs, we imagined that if they did play a role, they would act to increase $r(P)$ values. Finally, given the $\exp(-B^i/RT)$ dependence of most k_g^i, we could imagine that small (physically plausible) refinements to a subset of the B^i in the mechanism could significantly increase the $r(P)$ predictions.

With respect to the possibility that the model's representation of the liquid–gas interface might (significantly) underestimate A^{c-g}, and therefore $r(P)$ values, Faeth's (1972) paper is notable. He closely observed the interface and the model's representation is consistent with the findings he reported. Thus, we did not believe that the difference between the representation and reality of A^{c-g} could account for more than 5%–10% of the (200%) difference between measured and predicted $r(P)$ values.

To quantify the potential for heat transfer from the *g*-phase flame to the liquid via a Pyrex tube to preheat the liquid and increase $r(P)$ values, we performed simulations with the liquid's temperature 50 K higher than reported by the experimentalists. However, the $r(P)$ predictions increased only 10%, which is a small fraction of the 200% differences observed.

In addition, consistent with much previous conjecture, we found that the inclusion of representations for *l*-phase reaction chemistry and conductive processes did not significantly change the $r(P)$ predictions. Thus, we do not think that their omission from prior models has contributed to the discrepancies. Nonetheless, we still believe that *l*-phase reaction chemistry may play an important role in catalyzed systems.

Although the data are not presented in this report, we found that refinements to the thermodynamic properties of a small subset of species in the EthN mechanism were able to produce much better agreement between CNVT-based predictions for the decomposition of EthN(*g*) and results generated by experiments conducted by Levy (1952, 1954a). However, CYCLOPS-based $r(P)$ predictions produced with a *g*-phase mechanism that included those refinements were similar to those produced by the baseline mechanism.

That result notwithstanding, we still believe that the difference between measured and model-predicted $r(P)$ values is likely due in large part to a missing or poorly represented chemical kinetics submechanism. Seeking to inform the search for such a submechanism, we compared the $\{X_{k,g}\}^{+0}$ predictions produced by the unscaled (Case A) and globally scaled (Case E) $\dot{\omega}_{k,g}$ estimates to identify species whose $X_{k,g}^{+0}$ values were "significant" in the Case E simulations and were significantly different from their Case A counterpart.

Table 6 shows species whose $X_{k,g}^{+0}$ values were greater than 0.001 in the Case E simulations at 13.6 and 61.2 atm. Consistent with our belief that it might be possible to effect a factor-of-three increase in the $r(P)$ predictions via relatively minor changes to the chemical kinetics mechanism, we observed that the $X_{k,g}^{+0}$ values of the eight species with the highest values summed to greater than 0.90, the change

in $X^{+0}_{EthN/ETONO_2,g}$ was only 7%, and no value changed by more than 22%. Therefore, we believe that modifications to the mechanism within plausible uncertainties in parameterizations of the mechanism's k^i_g could produce much better agreement between measured and predicted $r(P)$ values.

Table 6. Comparison of $\{X_{k,g}\}^{+0}$ predictions for Cases A and E.

	13.6 (atm)			61.2 (atm)		
Species	**Case A**	**Case E**	**Difference[a] (%)**	**Case A**	**Case E**	**Difference[a] (%)**
$ETONO_2$	0.4247	0.3959	−7	0.3713	0.3439	−7
H_2O	0.0818	0.0908	11	0.0934	0.1012	8
CH_2O	0.0779	0.0898	15	0.0847	0.0959	13
H_2	0.1151	0.0894	−22	0.1115	0.0873	−22
CO	0.0713	0.0744	4	0.0832	0.0854	3
CH_3NO_2	0.0591	0.0728	23	0.0687	0.0829	21
NO	0.0557	0.0594	7	0.0565	0.0579	3
CH_4	0.0397	0.0426	7	0.0475	0.0505	7
C_2H_5ONO	0.0140	0.0222	59	0.0183	0.0279	53
CH_3CHO	0.0180	0.0203	13	0.0157	0.0175	12
NO_2	0.0093	0.0138	48	0.0109	0.0150	37
N_2O	0.0086	0.0093	8	0.0096	0.0106	11
CO_2	0.0040	0.0050	27	0.0050	0.0065	30
HONO	0.0079	0.0035	−55	0.0076	0.0035	−54
N_2	0.0033	0.0030	−9	0.0049	0.0044	−9
CH3OH	0.0029	0.0023	−22	0.0036	0.0029	−19
CH_3ONO	0.0009	0.0010	4	0.0010	0.0011	5

[a] $100*(X_{k,g}(\text{Case E}) - X_{k,g}(\text{Case A})/X_{k,g}(\text{Case A})$

For the remaining species, all $X^{+0}_{k,g}$ predictions were less than 0.03. The relative changes in the values for NO_2, HONO, and C_2H_5ONO were the largest. The changes in the $X^{+0}_{k,g}$ values of NO_2 and HONO seem likely to be related, perhaps reflecting a difference in the branching ratio between the two species. The result for C_2H_5ONO is notable because (as discussed in Section 4.1.2) we found that refinements to the thermodynamic properties of species in a submechanism that dictates C_2H_5ONO's production and consumption produced a significant improvement between measurement-based and CNVT-predicted $X_{k,g}(t)$ values for EthN(g)'s decomposition. However, those changes alone did not significantly change model-based $r(P)$ predictions.

The significant concentration of CH_3NO_2 (nitromethane) near the liquid–gas interface ($X^{+0}_{k,g}$ = 0.07–0.08) as well as its significantly higher value in the Case E simulation was surprising. Intuitively, multiple reaction steps are required to create precursors (besides NO_2) for its formation. In addition, we note that C_2H_5ONO formation is favored over the formation of its isomer $C_2H_5NO_2$ (nitroethane). Therefore, we expect the formation of CH_3ONO to be competitive with the

formation of CH_3NO_2. However, as observed in Table 6, $X^{+0}_{CH_3ONO,g}$ was almost a factor of 10 lower than $X^{+0}_{CH_3NO_2,g}$. Therefore, because it could also be important in mechanisms for modeling the decomposition and combustion of MSPs and their ingredients, we plan to investigate this matter.

6. Summary and Conclusion

Toward developing and applying multiphase physics-based deflagration models with better potential to computationally design and screen MSP formulations, we formulated and applied a quasi-1D two-phase model of EthN's deflagration that included detailed finite-rate chemical kinetics mechanisms for both phases. Informed by the prior development and application of a model of $O_{3,s}$'s deflagration, we sought to identify issues that might arise in representing the l-phase thermochemical kinetics and transport involved in the deflagration of MSPs. In addition, we sought to identify sources of error that could account for factor-of-three differences between measured EthN $r(P)$ values and $r(P)$ predictions produced by prior CYCLOPS models.

Employing a skeletal version of a recently developed chemical kinetics mechanism that was specifically designed to represent the decomposition and combustion of NQ(g), the baseline model produced $r(P)$ predictions that were similar to those produced by CYCLOPS models that predated it. The inclusion of a representation for l-phase reaction chemistry did not improve the predictions. Seeking other possibilities that might account for the predictions' lack of agreement with measured values, we investigated several hypotheses by heuristically modifying the baseline model's parameters. The modifications included 1) raising the l-phase's starting temperature (and enthalpy) and 2) globally increasing $\dot{\omega}_{k,g}$ estimates. Only the latter change made a significant difference.

In addition, we found that the baseline model produced predictions for the temperature of the liquid–gas interface and the temperature profile in the liquid that were in reasonable agreement with measurement-based values. Taken together with the other findings of the study, we concluded that the primary source of the factor-of-three difference between the baseline model's predictions and measured values is likely a missing or poorly represented chemical kinetics submechanism (or submechanisms).

Attempting to identify such submechanisms, we formulated and applied two other models. One was an HR model for simulating EthN(g)'s decomposition in a closed, constant-volume, constant-temperature bulb. We found that by refining the thermochemical properties of a small subset of species in the NQ(g) mechanism, the model's predictions for the temporal evolutions of the parent molecule and three

major products were brought into good agreement with measurement-based values. However, those refinements did not produce a concomitant improvement in the deflagration model's $r(P)$ predictions.

In addition, a variation of the deflagration model was designed to investigate whether the diffusion of H atoms was an important source of energy feedback from the flame to the liquid–gas interface. Investigated by experimental means, that mechanism's importance appeared to be corroborated by the observation that the $r(P)$ values of *d*$_5$-EthN were 25% lower than their (normal) EthN counterpart. However, we found that simply changing the atomic weight of all the system's H atoms to the value for D atoms and estimating *d*$_5$-EthN's ρ_l and h_v to account for the difference in their molecular weights, the $r(P)$ predictions for *d*$_5$-EthN were approximately 9% lower than those of EthN. Moreover, the results did not corroborate the importance of H-atom diffusion in the process. Rather, our analysis suggested that a reduction in the *g*-phase's thermal conductivity (λ_g) produced by the change in molecular weight alone could account for most of the difference in the predictions for the two systems.

Providing insight into the relative importance of various mechanisms that determine the rate at which MSPs deflagrate, this study constitutes a step toward establishing models with better potential to design and screen MSPs formulations for tactical rocket motor applications.

7. References

Anderson WR, Meagher NE, Vanderhoff JA. Dark zones of solid propellant flames: critically assessed datasets, quantitative model comparison, and detailed chemical analysis. Combust Flame. 2011;158:1228–1244.

Chen CC, Anderson WR, McQuaid MJ. Computationally based predictions for the burning rates and flame structures of nitroglycerin doped with various small molecules. Army Research Laboratory (US); 2019 June. Report No.: ARL-TR-8721.

Chen CC et al. A detailed, finite-rate chemical kinetics mechanism for modeling the thermal decomposition and combustion of gaseous nitroguanidine. Proceedings of the 45th JANNAF PEDCS Meeting; 2024; Charlotte, NC.

Chen CC, McQuaid MJ. A detailed, finite-rate chemical kinetics mechanism for modeling the thermal decomposition and combustion of gaseous nitroglycerin. Army Research Laboratory (US); 2022 Aug. Report No.: ARL-TR-9536.

Chen CC, McQuaid MJ. Tetramethylenediamine/red fuming nitric acid (TMEDA/RFNA) reaction kinetics. Proceedings of the 34th JANNAF Propellant and Explosives Development and Characterization Subcommittee (PEDCS) Meeting; 2007; Reno, NV.

Chen CC, McQuaid MJ. A detailed, gas-phase, finite-rate chemical kinetics mechanism for modeling the combustion of methyl and ethyl nitrate. Proceedings of the 60th JANNAF Propulsion Meeting; 2013; Colorado Springs, CO.

Chen CC, McQuaid MJ, Veals JD. Modeling the condensed-phase decomposition of nitrate esters. II: progress in developing a detailed finite-rate chemical kinetics mechanism for modeling the decomposition of nitrocellulose. Proceedings of the 43rd JANNAF PEDCS Meeting; 2021; Virtual.

Dauerman L, Tajima Y. Solid-phase reactions of a double-base propellant. AIAA J. 1968;6:678–683.

Faeth GM. High-pressure liquid-monopropellant strand combustion. Combust Flame. 1972;18(1):103–113.

Fairbrother DM, Skinner HA, Evans FW. The heats of combustion of organic compounds of nitrogen. Trans Faraday Soc. 1957;53:779–783.

Farber M, Srivastava RD. As mass-spectrometric investigation of the chemistry of plateau burning propellants. Combust Flame. 1978;31:309–323.

Fifer RA, Lannon JA. The effect of pressure and some lead salts on the chemistry of solid propellant combustion. Combust Flame. 1975;24:369–380.

Gray P, Pratt MWT, Larkin MJ. The latent heat of vaporization and the thermochemistry of ethyl nitrate. J Chem Soc. 1956;210–212.

Gray P, Smith PL. Low-temperature calorimetry and the thermodynamic properties of ethyl nitrate. J Chem Soc. 1954;769–773.

Grcar JF. The TWOPNT program for boundary value problems. Sandia National Laboratories (US); 1992 Apr. Report No.: SAND91-8230.

Hildenbrand DL, Happe JA. The thermal conductivities of some liquid nitrate esters. J Phys Chem. 1957;61:1415–1417.

Hildenbrand DL, Whittaker AG. Burning rate studies. II. Variation of temperature distribution with consumption rate for burning liquid systems. J Phys Chem. 1955;59:1024–1028.

Hildenbrand DL, Whittaker AG, Euston CB. Burning rate studies. I. Measurement of the temperature distribution in burning liquid strands. J Phys Chem. 1954;58:1130–1133.

Irwin OR, Salzman PK, Anderson WH. Deflagration characteristics of ammonium perchlorate at high pressures. Ninth Symposium (International) on Combustion, Academic. 1963. 1962 Aug 27–Sep 1; Cornell University, Ithaca, NY. p. 358–364.

Kee RJ et al. CHEMKIN collection. Release 3.6: PREMIX. Reaction Design, Inc.; 2000.

Kee RJ, Rupley FM, Miller JA. CHEMKIN-II: a Fortran chemical kinetics package for the analysis of gas-phase chemical kinetics. Sandia National Laboratories (US); 1989 Sep. Report No.: SAND89-8009. https://doi.org/10.2172/5681118

Kotlar AJ. A general approach for the reduction of chemical reaction mechanisms I: methodology and application to MMH-RFNA. Proceedings of the 5th JANNAF Liquid Propulsion Subcommittee Meeting, CPIA Publication JSC-CD-62; 2010; Colorado Springs, CO.

Levy JB. A kinetic study of the thermal decomposition of ethyl nitrate. Naval Ordnance Laboratory (US); 1952 June. NAVORD Report 2313.

Levy JB. The thermal decomposition of nitrate esters. I. Ethyl nitrate. J Am Chem Soc. 1954a;76:3254–3257.

Levy JB. The thermal decomposition of nitrate esters. II. The effect of additives on the thermal decomposition of ethyl nitrate. J Am Chem Soc. 1954b;76:3790–3793.

Li S, Petzold LR. Design of new DASPK for sensitivity analysis. Santa Barbara (CA): Department of Computer Science, University of California; 1999. Report No.: TRC99-28.

McQuaid MJ. The trial mechanism method for chemical kinetics mechanism reduction: an approach to generating reduced mechanisms with wider ranges of applicability. Proceeding of the 7th JANNAF Liquid Propulsion Subcommittee Meeting; 2013; Colorado Springs, CO.

McQuaid MJ. A quasi-1D three-phase deflagration model with detailed finite-rate chemical kinetics mechanisms: frozen ozone (revisited) and plateau burning rates. DEVCOM Army Research Laboratory (US); 2025 Mar. Report No.: ARL-TR-10075.

McQuaid MJ, Chen CC. Modeling the deflagration of ammonium perchlorate at pressures from 300 to 30000 psia. Part II: Considerations besides the gas-phase, finite-rate chemical kinetics mechanism. Proceedings of the 45th JANNAF Combustion Subcommittee Meeting; 2014.

McQuaid MJ, Chen CC. A computationally based study of fizz zone effects on the linear burning rate of methyl nitrate. Proceedings of the 47th JANNAF Combustion Subcommittee Meeting; 2016; Newport News, VA.

McQuaid MJ, Chen CC, Veals JD, Yeh IC. Detailed finite-rate chemical kinetics based modeling of the decomposition of nitroglycerin in systems comprising liquid and gas phases. Proceedings of the 43rd JANNAF PEDCS Meeting; 2021; Virtual.

McQuaid MJ, Stone CP. CYCLOPS3 burning rate predictor: PREMIX3_WPSB version. DEVCOM Army Research Laboratory (US); 2024 Sep. Report No.: ARL-TR-9971.

McQuaid MJ, Veals J. Yeh IC, Chen CC. The development of detailed finite rate chemical kinetics mechanisms for modeling decomposition in condensed phases. Part 2. The parameterization of free volume theory for liquid nitrate esters. Proceedings of the 50th JANNAF Combustion Subcommittee Meeting; 2020; Virtual.

Miller MS. Development of a 3-phase, detailed-kinetics, steady-state combustion model with heterogeneous reaction: application to frozen ozone. Proceedings of the 32nd JANNAF Combustion Subcommittee Meeting; 1995; Huntsville, AL.

Miller MS. Three-phase combustion modeling: frozen ozone, a prototype system. Army Research Laboratory (US); 1997 Mar. Report No.: ARL-TR-1320.

Miller MS, Anderson WR. Burning-rate predictor for multi-ingredient propellants: nitrate-ester propellants. J Propuls Power. 2004;20:440–453.

Nusca MJ. Modeling the burning rate of sold propellants with embedded metal wires. Proceedings of the 38th JANNAF PEDCS Meeting; 2014a; Charleston, SC.

Nusca MJ. Computational fluid dynamics model of laminate AP/HTPB propellant strands: initial results for burn rate prediction. Proceedings of the 46th JANNAF Combustion Subcommittee Meeting; 2014b; Albuquerque, NM.

Steinberger R, Orlick CA, Schaaf VP. Burning rates of deuterated nitrate esters. J Am Chem Soc. 1955;77:4748–4750.

Suh NP, Adams GF, Lenchitz C. Observations on the role of lead modifiers in super-rate burning of nitrocellulose propellants. Combust Flame. 1974;22:289–293.

Timmermans J, Mattaar JF. Freezing points of organic substances. VI. New experimental determinations. Bull Soc Chim Belg. 1921;30:213.

Tummers B. DataThief. III. 2006. http://datathief.org/

Veals JD, Lansford JL, Chen CC, Stone CP. Condensed-phase property estimates for ethyl nitrate derived from atomistic equilibrium molecular dynamics simulations. DEVCOM Army Research Laboratory (US); 2025 Sep. Report No.: ARL-TR-10192.

Veals JD, Yeh IC, Chen CC, Andzelm J, McQuaid MJ. Establishing and parameterizing rate coefficient functions for steps in the decomposition of nitrate esters in condensed phases: progress in developing a practical approach. Proceedings of the 41st JANNAF PEDCS Meeting; 2018; Vancouver, WA.

Warren LR, Wang Z, Pulham CR, Morrison CA. A review of the catalytic effects of lead-based ballistic modifiers on the combustion chemistry of double-base propellants. Propellants, Explos, Pyrotech. 2021;46:13–25.

Appendix A. The Skeletal Chemical Kinetics Mechanism for the Deflagration Model

As discussed in the main body of this report, a chemical kinetics mechanism that was specifically designed to represent the decomposition and combustion of gaseous nitroguanidine (NQ(g)) was our group's most recently developed mechanism that would be suitable for modeling the decomposition and combustion of gaseous ethyl nitrate (EthN(*g*)).[1] That mechanism comprised coefficients for computing the rates of 1881 reversible elementary reactions and the thermochemical kinetic and transport properties for 345 species. Because that mechanism was expected to contain a large number of reactions and species that were irrelevant with respect to modeling the decomposition and combustion of EthN(*g*) under the conditions of interest, and the computational cost to perform calculations with the full NQ(*g*) mechanism were excessive, we reduced it using the (original) trial mechanism method that was invented by Kotlar[2] and extended by McQuaid.[3]

Briefly, results produced by skeletal mechanisms for two homogenous reactor simulations for closed, adiabatic, constant-pressure (CONP) systems containing only EthN(*g*) at time (*t*) zero were compared with those produced by the full NQ(*g*) mechanism. The initial temperature in both simulations was 500 K. The pressures chosen for the two simulations were the extremes of the pressure and density range within which reaction rates were to be calculated: 1 and 500 atm. In the three open-literature papers that were the basis for model validation, 7.3 atm was the lowest pressure at which EthN's effective linear burning rate was measured. The highest *g*-phase *P* was less than 70 atm. However, to compute reaction rates in the liquid phase, the liquid's density was computed with an equation of state, and that value was converted into an "effective pressure" via the ideal gas law to compute the concentrations of third bodies. Based on that consideration, 500 atm was deemed an appropriate upper limit.

Results that were compared included the magnitudes of three rate-of-heat release peaks (in each simulation), the time at which those peaks occurred, and the final temperature. The maximum deviation allowed in the results for the rate-of-heat-release parameters was 1.25%. The maximum deviation allowed in the final temperature was 1 K.

Reductions based on 10 different initial orderings of the NQ mechanism were performed. All produced skeletal mechanisms with similar numbers of reactions and species. The one selected for use in the study had 82 species and 245 reactions. All the inputs needed to parameterize this mechanism are provided herein.

---

[1] Chen CC et al. A detailed, finite-rate chemical kinetics mechanism for modeling the thermal decomposition and combustion of gaseous nitroguanidine. Proceedings of the 45th JANNAF Propellant and Explosives Development and Characterization Subcommittee Meeting; 2024.

[2] Kotlar AJ. A general approach for the reduction of chemical reaction mechanisms I: methodology and application to MMH-RFNA. Proceedings of the 5th JANNAF Liquid Propulsion Subcommittee Meeting, CPIA Publication JSC-CD-62; 2010; Colorado Springs, CO.

[3] McQuaid MJ. The trial mechanism method for chemical kinetics mechanism reduction: an approach to generating reduced mechanisms with wider ranges of applicability. Proceeding of the 7th JANNAF Liquid Propulsion Subcommittee Meeting; 2013; Colorado Springs, CO.

A.1 chem.out

ELEMENTS CONSIDERED	ATOMIC WEIGHT
1. C	12.0112
2. H	1.00797
3. N	14.0067
4. O	15.9994

SPECIES CONSIDERED	PHASE	CHARGE	MOLECULAR WEIGHT	TEMPERATURE LOW	TEMPERATURE HIGH	ELEMENT COUNT C	H	N	O	HE	AR
1. ETONO2	G	0	91.06705	300	5000	2	5	1	3	0	0
2. NO2	G	0	46.00550	300	5000	0	0	1	2	0	0
3. HONO	G	0	47.01347	300	5000	0	1	1	2	0	0
4. NO	G	0	30.00610	200	6000	0	0	1	1	0	0
5. O	G	0	15.99940	300	5000	0	0	0	1	0	0
6. N2O	G	0	44.01280	300	5000	0	0	2	1	0	0
7. H2O	G	0	18.01534	300	5000	0	2	0	1	0	0
8. N2	G	0	28.01340	300	5000	0	0	2	0	0	0
9. CO2	G	0	44.00995	300	5000	1	0	0	2	0	0
10. O2	G	0	31.99880	300	5000	0	0	0	2	0	0
11. H	G	0	1.00797	300	5000	0	1	0	0	0	0
12. HNO	G	0	31.01407	200	6000	0	1	1	1	0	0
13. OH	G	0	17.00737	300	5000	0	1	0	1	0	0
14. HCN	G	0	27.02582	200	6000	1	1	1	0	0	0
15. HNCO	G	0	43.02522	200	6000	1	1	1	1	0	0
16. NH	G	0	15.01467	200	6000	0	1	1	0	0	0
17. CO	G	0	28.01055	300	5000	1	0	0	1	0	0
18. H2CN	G	0	28.03379	300	4000	1	2	1	0	0	0
19. N	G	0	14.00670	300	5000	0	0	1	0	0	0
20. NO3	G	0	62.00490	300	5000	0	0	1	3	0	0
21. NH2	G	0	16.02264	200	6000	0	2	1	0	0	0
22. NH3	G	0	17.03061	300	5000	0	3	1	0	0	0
23. HCO	G	0	29.01852	200	6000	1	1	0	1	0	0
24. H2	G	0	2.01594	300	5000	0	2	0	0	0	0
25. HCCO	G	0	41.02967	300	4000	2	1	0	1	0	0
26. HCNO	G	0	43.02522	250	4000	1	1	1	1	0	0
27. NCO	G	0	42.01725	200	6000	1	0	1	1	0	0
28. NNH	G	0	29.02137	250	4000	0	1	2	0	0	0
29. HNC	G	0	27.02582	300	5000	1	1	1	0	0	0
30. HOCO	G	0	45.01792	300	4000	1	1	0	2	0	0
31. HNNO	G	0	45.02077	300	5000	0	1	2	1	0	0
32. HNO3	G	0	63.01287	300	5000	0	1	1	3	0	0
33. CH2	G	0	14.02709	250	4000	1	2	0	0	0	0
34. CH2(S)	G	0	14.02709	300	4000	1	2	0	0	0	0
35. CH3	G	0	15.03506	300	5000	1	3	0	0	0	0
36. CH2O	G	0	30.02649	200	3500	1	2	0	1	0	0
37. CH4	G	0	16.04303	300	5000	1	4	0	0	0	0
38. CH2OH	G	0	31.03446	250	4000	1	3	0	1	0	0
39. CH3O	G	0	31.03446	300	3000	1	3	0	1	0	0
40. CH3OH	G	0	32.04243	300	5000	1	4	0	1	0	0
41. C2H2	G	0	26.03824	300	5000	2	2	0	0	0	0
42. C2H5	G	0	29.06215	300	5000	2	5	0	0	0	0
43. C2H6	G	0	30.07012	300	4000	2	6	0	0	0	0
44. CH2CO	G	0	42.03764	300	5000	2	2	0	1	0	0
45. C2H3	G	0	27.04621	300	5000	2	3	0	0	0	0

```
 46. C2H4              G  0   28.05418   300   5000   2  4  0  0  0  0
 47. HCCOH             G  0   42.03764   300   4000   2  2  0  1  0  0
 48. HNO2              G  0   47.01347   300   5000   0  1  1  2  0  0
 49. HNOH              G  0   32.02204   300   5000   0  2  1  1  0  0
 50. NH2O              G  0   32.02204   300   5000   0  2  1  1  0  0
 51. C2H4O             G  0   44.05358   300   5000   2  4  0  1  0  0
 52. CH2CHO            G  0   43.04561   300   5000   2  3  0  1  0  0
 53. CH3CHO            G  0   44.05358   200   6000   2  4  0  1  0  0
 54. HOCN              G  0   43.02522   300   4000   1  1  1  1  0  0
 55. CH3NH             G  0   30.04973   200   6000   1  4  1  0  0  0
 56. CH2NH             G  0   29.04176   300   5000   1  3  1  0  0  0
 57. N2O4              G  0   92.01100   300   5000   0  0  2  4  0  0
 58. CH3NO2            G  0   61.04056   300   4000   1  3  1  2  0  0
 59. CH3NO             G  0   45.04116   300   4000   1  3  1  1  0  0
 60. H2CNO2            G  0   60.03259   300   4000   1  2  1  2  0  0
 61. CH3ONO            G  0   61.04056   300   4000   1  3  1  2  0  0
 62. C3H8              G  0   44.09721   300   5000   3  8  0  0  0  0
 63. CH3ONO2           G  0   77.03996   300   5000   1  3  1  3  0  0
 64. C2H5O             G  0   45.06155   300   5000   2  5  0  1  0  0
 65. CH3CO             G  0   43.04561   300   5000   2  3  0  1  0  0
 66. CNO2CDO           G  0   89.05111   300   5000   2  3  1  3  0  0
 67. CNO2CDJO          G  0   88.04314   300   5000   2  2  1  3  0  0
 68. CJCONO2           G  0   90.05908   300   5000   2  4  1  3  0  0
 69. COJCONO2          G  0  106.05848   300   5000   2  4  1  4  0  0
 70. CDOCOJ            G  0   59.04501   300   5000   2  3  0  2  0  0
 71. C2H5OH            G  0   46.06952   300   5000   2  6  0  1  0  0
 72. HOCHO             G  0   46.02589   300   4000   1  2  0  2  0  0
 73. OCHO              G  0   45.01792   300   5000   1  1  0  2  0  0
 74. CH3CO2            G  0   59.04501   300   5000   2  3  0  2  0  0
 75. PC2H4OH           G  0   45.06155   300   5000   2  5  0  1  0  0
 76. C2H5ONO           G  0   75.06765   300   5000   2  5  1  2  0  0
 77. NH2NO             G  0   46.02874   300   5000   0  2  2  1  0  0
 78. NH2OH             G  0   33.03001   300   5000   0  3  1  1  0  0
 79. ONONO2            G  0   92.01100   300   5000   0  0  2  4  0  0
 80. HONNH             G  0   46.02874   300   5000   0  2  2  1  0  0
 81. ONOCHO            G  0   75.02402   300   5000   1  1  1  3  0  0
 82. NOHT              G  0   31.01407   300   5000   0  1  1  1  0  0
--------------------------------------------------------------------------------

                                                  (k = A T**b exp(-E/RT))
   REACTIONS CONSIDERED                             A        b        E

 1. NO2+HCO(+M)=HONO+CO(+M)                      1.00E+00    0.0        0.0
    Declared duplicate reaction...
    I04:   6.7200E+09  7.2000E-01 -4.8500E+02  1.0000E+00
    I05:   6.7100E+09  7.2000E-01 -4.8500E+02  1.0000E+01
    I06:   6.7100E+09  7.2000E-01 -4.8500E+02  2.5000E+01
    I07:   6.7000E+09  7.2000E-01 -4.8500E+02  5.0000E+01
    I08:   6.6900E+09  7.2000E-01 -4.8500E+02  7.5000E+01
    I09:   6.6700E+09  7.2000E-01 -4.8600E+02  1.0000E+02
    I10:   6.6300E+09  7.2000E-01 -4.8700E+02  1.5000E+02
    I11:   6.5500E+09  7.3000E-01 -4.8800E+02  2.0000E+02
    I12:   6.4500E+09  7.3000E-01 -4.9000E+02  2.5000E+02
    I13:   6.3200E+09  7.3000E-01 -4.9200E+02  3.0000E+02
    I14:   6.1600E+09  7.3000E-01 -4.9500E+02  3.5000E+02
    I15:   5.9900E+09  7.4000E-01 -4.9800E+02  4.0000E+02
    I16:   5.8000E+09  7.4000E-01 -5.0100E+02  4.5000E+02
    I17:   5.6000E+09  7.5000E-01 -5.0500E+02  5.0000E+02
 2. NO2+HCO(+M)=OCHO+NO(+M)                      1.00E+00    0.0        0.0
    I04:   7.3300E+00  3.1800E+00 -3.1200E+02  1.0000E+00
    I05:   7.3400E+00  3.1800E+00 -3.1200E+02  1.0000E+01
    I06:   7.3600E+00  3.1800E+00 -3.1200E+02  2.5000E+01
    I07:   7.3800E+00  3.1800E+00 -3.1200E+02  5.0000E+01
    I08:   7.4100E+00  3.1800E+00 -3.1200E+02  7.5000E+01
```

```
    I09:   7.4500E+00  3.1800E+00 -3.1200E+02  1.0000E+02
    I10:   7.5400E+00  3.1800E+00 -3.1000E+02  1.5000E+02
    I11:   7.6700E+00  3.1800E+00 -3.0600E+02  2.0000E+02
    I12:   7.8300E+00  3.1700E+00 -2.9900E+02  2.5000E+02
    I13:   8.0300E+00  3.1700E+00 -2.9000E+02  3.0000E+02
    I14:   8.2700E+00  3.1700E+00 -2.7900E+02  3.5000E+02
    I15:   8.5300E+00  3.1600E+00 -2.6600E+02  4.0000E+02
    I16:   8.8200E+00  3.1600E+00 -2.5200E+02  4.5000E+02
    I17:   9.1100E+00  3.1600E+00 -2.3600E+02  5.0000E+02
 3. NO2+HCO(+M)=HONO+CO(+M)                  1.00E+00    0.0        0.0
    Declared duplicate reaction...
    I04:   5.8900E+00  2.9500E+00 -5.5800E+02  1.0000E+00
    I05:   5.8900E+00  2.9500E+00 -5.5800E+02  1.0000E+01
    I06:   5.8800E+00  2.9500E+00 -5.5600E+02  2.5000E+01
    I07:   5.8800E+00  2.9500E+00 -5.5400E+02  5.0000E+01
    I08:   5.8800E+00  2.9500E+00 -5.5100E+02  7.5000E+01
    I09:   5.8800E+00  2.9500E+00 -5.4800E+02  1.0000E+02
    I10:   5.9000E+00  2.9500E+00 -5.4100E+02  1.5000E+02
    I11:   5.9500E+00  2.9500E+00 -5.3200E+02  2.0000E+02
    I12:   6.0300E+00  2.9500E+00 -5.2000E+02  2.5000E+02
    I13:   6.1200E+00  2.9500E+00 -5.0700E+02  3.0000E+02
    I14:   6.2300E+00  2.9400E+00 -4.9200E+02  3.5000E+02
    I15:   6.3500E+00  2.9400E+00 -4.7500E+02  4.0000E+02
    I16:   6.4700E+00  2.9400E+00 -4.5800E+02  4.5000E+02
    I17:   6.6000E+00  2.9400E+00 -4.3900E+02  5.0000E+02
 4. ONOCHO(+M)=HNO+CO2(+M)                   1.00E+00    0.0        0.0
    I04:   2.0000E+31 -6.1000E+00  2.8393E+04  1.0000E+00
    I05:   8.7300E+28 -5.1500E+00  2.8478E+04  1.0000E+01
    I06:   2.0500E+27 -4.5800E+00  2.8186E+04  2.5000E+01
    I07:   8.5200E+25 -4.1200E+00  2.7877E+04  5.0000E+01
    I08:   1.3100E+25 -3.8500E+00  2.7682E+04  7.5000E+01
    I09:   3.5100E+24 -3.6600E+00  2.7537E+04  1.0000E+02
    I10:   5.6800E+23 -3.4000E+00  2.7332E+04  1.5000E+02
    I11:   1.6700E+23 -3.2200E+00  2.7191E+04  2.0000E+02
    I12:   6.3100E+22 -3.0900E+00  2.7075E+04  2.5000E+02
    I13:   2.9100E+22 -2.9800E+00  2.6983E+04  3.0000E+02
    I14:   1.5200E+22 -2.8900E+00  2.6904E+04  3.5000E+02
    I15:   8.2000E+21 -2.8000E+00  2.6827E+04  4.0000E+02
    I16:   5.1200E+21 -2.7300E+00  2.6769E+04  4.5000E+02
    I17:   3.3100E+21 -2.6700E+00  2.6715E+04  5.0000E+02
 5. HOCHO+HONO=ONOCHO+H2O                    8.09E+03    2.2    10633.0
 6. CH2O+NO2=HCO+HNO2                        3.48E+13    0.0    23720.0
 7. CH2OH+NO2=CH2O+HONO                      1.17E+15   -0.5        0.0
 8. NO2+HCCO=CO+HCO+NO                       8.76E+12   -0.3        0.0
 9. HCCOH+H=HCCO+H2                          2.40E+08    1.5        0.0
10. HCCOH+CH3=HCCO+CH4                       8.10E+05    1.9        0.0
11. HOCHO+M=CO+H2O+M                         9.04E+14    0.0    50300.0
12. HOCHO+M=CO2+H2+M                         2.02E+15    0.0    51350.0
13. HOCHO+H=HOCO+H2                          2.40E+08    1.5     5678.3
14. HOCHO+OH=HOCO+H2O                        1.20E+06    2.0     -122.9
15. CH3CHO+OH<=>CH3+HOCHO                    3.00E+15   -1.1        0.0
16. HOCO(+M)<=>CO+OH(+M)                     1.00E+00    0.0        0.0
    I04:   1.6800E+18 -3.0500E+00  2.4323E+04  9.8700E-02
    I05:   2.5000E+24 -4.6300E+00  2.7067E+04  2.9610E-01
    I06:   4.5400E+26 -5.1200E+00  2.7572E+04  9.8690E-01
    I07:   7.1200E+28 -5.6000E+00  2.8535E+04  2.9607E+00
    I08:   5.4800E+29 -5.7000E+00  2.8899E+04  9.8690E+00
    I09:   9.8900E+31 -6.1900E+00  3.0518E+04  2.9607E+01
    I10:   5.7400E+33 -6.5300E+00  3.2068E+04  9.8690E+01
    I10:   5.7400E+33 -6.5300E+00  3.2068E+04  9.8690E+01
    I11:   2.6100E+33 -6.2900E+00  3.2231E+04  2.9607E+02
    I12:   6.3000E+32 -5.9600E+00  3.2470E+04  9.8690E+02
17. HOCO=OCHO                                2.84E+11    0.6    32065.0
18. HOCO+NO2=OH+CO2+NO                       1.00E+11    0.0        0.0
```

```
19. OCHO=H+CO2                                    1.34E+18   -1.3     2181.2
20. O+H2=H+OH                                     5.08E+04    2.7     6292.0
21. OH+H2=H+H2O                                   4.38E+13    0.0     6990.0
22. O+H2O=OH+OH                                   2.97E+06    2.0    13400.0
23. CO+OH=CO2+H                                   7.02E+04    2.0     -355.7
    Declared duplicate reaction...
24. CO+OH=CO2+H                                   5.76E+12   -0.7      331.8
    Declared duplicate reaction...
25. HCO+M=H+CO+M                                  4.75E+11    0.7    14870.0
    H2              Enhanced by    2.000E+00
    H2O             Enhanced by    1.200E+01
    CO              Enhanced by    1.500E+00
    CO2             Enhanced by    2.000E+00
26. NH2+OH=NH2OH                                  2.98E+14   -0.3      -55.6
27. NH2OH+OH=HNOH+H2O                             1.54E+04    2.6    -3536.9
28. NH2OH+OH=NH2O+H2O                             1.53E+05    2.3    -1295.5
29. NH+OH=HNO+H                                   3.24E+14   -0.4      -45.7
30. NH+OH=NO+H2                                   2.00E+13    0.0        0.0
31. NH2+NO2(+M)=NH2O+NO(+M)                       1.00E+00    0.0        0.0
    I04:   2.4000E+07  1.5300E+00 -2.1220E+03  1.0000E+00
    I05:   2.4000E+07  1.5300E+00 -2.1220E+03  1.0000E+01
    I06:   2.4000E+07  1.5300E+00 -2.1220E+03  2.5000E+01
    I07:   2.4000E+07  1.5300E+00 -2.1220E+03  5.0000E+01
    I08:   2.4000E+07  1.5300E+00 -2.1220E+03  7.5000E+01
    I09:   2.4000E+07  1.5300E+00 -2.1220E+03  1.0000E+02
    I10:   2.4000E+07  1.5300E+00 -2.1220E+03  1.5000E+02
    I11:   2.4000E+07  1.5300E+00 -2.1220E+03  2.0000E+02
    I12:   2.4000E+07  1.5300E+00 -2.1220E+03  2.5000E+02
    I13:   2.4000E+07  1.5300E+00 -2.1220E+03  3.0000E+02
    I14:   2.4000E+07  1.5300E+00 -2.1220E+03  3.5000E+02
    I15:   2.4000E+07  1.5300E+00 -2.1220E+03  4.0000E+02
    I16:   2.4000E+07  1.5300E+00 -2.1220E+03  4.5000E+02
    I17:   2.4000E+07  1.5300E+00 -2.1220E+03  5.0000E+02
32. NH2OH+NO2=NH2O+HNO2                           4.63E+01    3.3     4369.0
33. NH2OH+NO2=NH2O+HONO                           4.39E-03    4.4      556.0
34. NH2OH+H=HNOH+H2                               4.80E+08    1.5     6246.0
35. NH2OH+H=NH2O+H2                               2.40E+08    1.5     5064.0
36. NH2O+M=HNO+H+M                                2.80E+24   -2.8    64915.0
    H2O             Enhanced by    1.000E+01
37. NH2O+M=HNOH+M                                 1.10E+29   -4.0    44000.0
    H2O             Enhanced by    1.000E+01
38. NH2O+NO=HNO+HNO                               3.02E+03    2.1    16082.0
39. NH2O+NO2=HNO+HONO                             5.60E+04    2.5        0.0
40. HNO3+HONO=H2O+ONONO2                          2.00E+06    2.1     6463.7
41. NO2+NO2=ONONO2                                1.44E+01    2.9     6332.9
42. HNO2(+M)=HONO(+M)                             2.50E+14    0.0    32300.0
    Low pressure limit:  0.31000E+19  0.00000E+00  0.31500E+05
    TROE centering:      0.11490E+01  0.10000E-29  0.31250E+04  0.10000E+31
43. HNOH+M=H+HNO+M                                2.00E+24   -2.8    58901.0
44. HNNO+NO=N2O+HNO                               1.00E+12    0.0        0.0
45. NNH+OH=HONNH                                  5.00E+13    0.0        0.0
46. HONNH=H2O+N2                                  2.55E+11    0.7     9923.7
47. NOHT=HNO                                      1.24E-25   10.9    17576.0
48. NOHT=H+NO                                     5.16E+05    2.4    31045.0
49. N2O(+M)=N2+O(+M)                                  1.26E+12    0.0    62620.0
    Low pressure limit:  0.59700E+15  0.00000E+00  0.56640E+05
    N2O             Enhanced by    5.000E+00
    H2O             Enhanced by    9.000E+00
    N2              Enhanced by    1.000E+00
    CO2             Enhanced by    3.200E+00
    O2              Enhanced by    8.200E-01
50. H+NO(+M)=HNO(+M)                              1.52E+15   -0.4        0.0
    Low pressure limit:  0.40000E+21 -0.17500E+01  0.00000E+00
    N2O             Enhanced by    5.000E+00
```

```
    H2O             Enhanced by    5.000E+00
    N2              Enhanced by    1.000E+00
    CO2             Enhanced by    1.300E+00
51. NO+OH(+M)=HONO(+M)                        1.99E+12   -0.1     -721.0
    Low pressure limit:  0.50800E+24 -0.25100E+01 -0.67600E+02
    TROE centering:      0.62000E+00  0.13000E+01  0.58261E+12  0.40701E+05
    N2O             Enhanced by    5.000E+00
    H2O             Enhanced by    8.300E+00
    N2              Enhanced by    1.000E+00
    CO2             Enhanced by    1.500E+00
52. HNCO(+M)=NH+CO(+M)                        6.00E+13    0.0    99800.0
    Low pressure limit:  0.21700E+29 -0.31000E+01  0.10190E+06
    TROE centering:      0.92701E+00  0.13000E+01  0.34169E+04  0.50814E+05
    N2O             Enhanced by    5.000E+00
    H2O             Enhanced by    5.000E+00
    N2              Enhanced by    1.000E+00
    CO2             Enhanced by    1.600E+00
53. NO2+NO2=NO+NO3                            9.64E+09    0.7    20920.0
54. NO2+NO2=NO+NO+O2                          4.51E+12    0.0    27600.0
55. HNO+NO=N2O+OH                             1.70E+13    0.0    29590.0
56. HNO+NO2=HONO+NO                           4.42E+04    2.6     8792.0
57. HONO+OH=H2O+NO2                           1.27E+10    1.0      135.0
58. HCCO+NO=HCNO+CO                           2.00E+13    0.0        0.0
59. OH+HCN=HNCO+H                             1.98E-03    4.0     1000.0
60. HCN+O=NCO+H                               1.38E+04    2.6     4980.0
61. NO2+H=NO+OH                               1.30E+14    0.0      361.0
62. NCO+M=N+CO+M                              1.14E+23   -1.9    59930.0
    N2O             Enhanced by    5.000E+00
    H2O             Enhanced by    5.000E+00
    N2              Enhanced by    1.000E+00
    CO2             Enhanced by    1.500E+00
63. NCO+NO=N2O+CO                             3.98E+19   -2.2     1743.0
64. NCO+NO=CO2+N2                             1.46E+21   -2.7     1824.0
65. NCO+H2=HNCO+H                             2.07E+06    2.0     6020.0
66. NH+NO=N2O+H                               3.50E+14   -0.5       16.1
67. N2O+H=N2+OH                               1.30E+11    0.9    15210.0
68. NNH+O=NO+NH                               3.30E+14   -0.2    -1013.0
69. NH2+O=HNO+H                               4.60E+13    0.0        0.0
70. NH2+H=NH+H2                               4.00E+13    0.0     3650.0
71. NH2+NO=NNH+OH                             2.29E+10    0.4     -815.0
72. NH2+NO=N2+H2O                             2.77E+20   -2.6     1258.0
73. NH3+OH=NH2+H2O                            2.04E+06    2.0      566.0
74. NH3+H=NH2+H2                              5.42E+05    2.4     9917.0
75. HNO+OH=NO+H2O                             1.30E+07    1.9     -958.0
76. H+HNO=H2+NO                               4.46E+11    0.7      655.0
77. HNO+NH2=NH3+NO                            2.00E+13    0.0     1000.0
78. N+NO=N2+O                                 3.27E+12    0.3        0.0
79. NO+H=N+OH                                 1.70E+14    0.0    48800.0
80. HNO+HNO=N2O+H2O                           3.63E-03    4.0     1190.0
81. HNC+OH=HNCO+H                             2.80E+13    0.0     3696.0
82. N2O+NO=N2+NO2                             4.29E+13    0.0    47130.0
83. HNCO+H=NH2+CO                             2.25E+07    1.7     3800.0
84. CO+NO2=NO+CO2                             9.04E+13    0.0    33780.0
85. H2+NO2=HONO+H                             1.30E+04    2.8    29770.0
86. HONO+H=HNO+OH                             5.63E+10    0.9     4969.0
87. 2HONO=NO+NO2+H2O                          3.49E-01    3.6    12140.0
88. NNH(+M)=N2+H(+M)                          4.10E+09    1.1     5186.0
    Low pressure limit:  0.10000E+14  0.50000E+00  0.30600E+04
    N2O             Enhanced by    5.000E+00
    H2O             Enhanced by    9.000E+00
    N2              Enhanced by    1.000E+00
    O2              Enhanced by    8.200E-01
    HNO3            Enhanced by    5.000E+00
    NH3             Enhanced by    5.000E+00
```

```
     NO3               Enhanced by    5.000E+00
 89. HCN+M=HNC+M                                  4.36E+26   -3.3    50194.0
 90. HNO+NO+NO=HNNO+NO2                           1.70E+11    0.0     2100.0
 91. HNNO+NO=NNH+NO2                              3.20E+12    0.0      270.0
 92. HNNO+M=H+N2O+M                               2.20E+15    0.0    21600.0
 93. HNNO+M=N2+OH+M                               1.00E+15    0.0    25600.0
 94. HCO+NO=HNO+CO                                7.23E+12    0.0        0.0
 95. O+CH3<=>H+CH2O                               5.06E+13    0.0        0.0
 96. O+CH4<=>OH+CH3                               1.02E+09    1.5     8600.0
 97. O+C2H2<=>H+HCCO                              1.35E+07    2.0     1900.0
 98. O+C2H2<=>CO+CH2                              6.94E+06    2.0     1900.0
 99. O+C2H4<=>CH3+HCO                             1.25E+07    1.8      220.0
100. O+C2H6<=>OH+C2H5                             8.98E+07    1.9     5690.0
101. H+CH3(+M)<=>CH4(+M)                          1.39E+16   -0.5      536.0
     Low pressure limit:  0.26200E+34 -0.47600E+01  0.24400E+04
     TROE centering:      0.78300E+00  0.74000E+02  0.29410E+04  0.69640E+04
     H2               Enhanced by    2.000E+00
     H2O              Enhanced by    6.000E+00
     CH4              Enhanced by    3.000E+00
     CO               Enhanced by    1.500E+00
     CO2              Enhanced by    2.000E+00
     C2H6             Enhanced by    3.000E+00
102. H+CH4<=>CH3+H2                               6.60E+08    1.6    10840.0
103. H+CH2O(+M)<=>CH2OH(+M)                       5.40E+11    0.5     3600.0
     Low pressure limit:  0.12700E+33 -0.48200E+01  0.65300E+04
     TROE centering:      0.71870E+00  0.10300E+03  0.12910E+04  0.41600E+04
     H2               Enhanced by    2.000E+00
     H2O              Enhanced by    6.000E+00
     CH4              Enhanced by    2.000E+00
     CO               Enhanced by    1.500E+00
     CO2              Enhanced by    2.000E+00
     C2H6             Enhanced by    3.000E+00
104. H+CH2O<=>HCO+H2                              5.74E+07    1.9     2742.0
105. H+CH2OH<=>OH+CH3                             1.65E+11    0.7     -284.0
106. H+CH3OH<=>CH2OH+H2                           1.70E+07    2.1     4870.0
107. H+CH3OH<=>CH3O+H2                            4.20E+06    2.1     4870.0
108. H+C2H2(+M)<=>C2H3(+M)                        5.60E+12    0.0     2400.0
     Low pressure limit:  0.38000E+41 -0.72700E+01  0.72200E+04
     TROE centering:      0.75070E+00  0.98500E+02  0.13020E+04  0.41670E+04
     H2               Enhanced by    2.000E+00
     H2O              Enhanced by    6.000E+00
     CH4              Enhanced by    2.000E+00
     CO               Enhanced by    1.500E+00
     CO2              Enhanced by    2.000E+00
     C2H6             Enhanced by    3.000E+00
109. H+C2H4(+M)<=>C2H5(+M)                        5.40E+11    0.5     1820.0
     Low pressure limit:  0.60000E+42 -0.76200E+01  0.69700E+04
     TROE centering:      0.97530E+00  0.21000E+03  0.98400E+03  0.43740E+04
     H2               Enhanced by    2.000E+00
     H2O              Enhanced by    6.000E+00
     CH4              Enhanced by    2.000E+00
     CO               Enhanced by    1.500E+00
     CO2              Enhanced by    2.000E+00
     C2H6             Enhanced by    3.000E+00
110. H+C2H4<=>C2H3+H2                             1.32E+06    2.5    12240.0
111. H+C2H6<=>C2H5+H2                             1.15E+08    1.9     7530.0
112. H+HCCOH<=>H+CH2CO                            1.00E+13    0.0        0.0
113. OH+CH3(+M)<=>CH3OH(+M)                       2.79E+18   -1.4     1330.0
     Low pressure limit:  0.40000E+37 -0.59200E+01  0.31400E+04
     TROE centering:      0.41200E+00  0.19500E+03  0.59000E+04  0.63940E+04
     H2               Enhanced by    2.000E+00
     H2O              Enhanced by    6.000E+00
     CH4              Enhanced by    2.000E+00
     CO               Enhanced by    1.500E+00
```

```
     CO2             Enhanced by    2.000E+00
     C2H6            Enhanced by    3.000E+00
114. OH+CH3<=>CH2(S)+H2O                        6.44E+17   -1.3     1417.0
115. OH+CH4<=>CH3+H2O                           1.00E+08    1.6     3120.0
116. OH+CH2O<=>HCO+H2O                          3.43E+09    1.2     -447.0
117. OH+CH3OH<=>CH2OH+H2O                       1.44E+06    2.0     -840.0
118. OH+CH3OH<=>CH3O+H2O                        6.30E+06    2.0     1500.0
119. OH+C2H2<=>H+CH2CO                          2.18E-04    4.5    -1000.0
120. OH+C2H2<=>H+HCCOH                          5.04E+05    2.3    13500.0
121. OH+C2H6<=>C2H5+H2O                         3.54E+06    2.1      870.0
122. OH+CH2CO<=>HCCO+H2O                        7.50E+12    0.0     2000.0
123. CH2+H2<=>H+CH3                             5.00E+05    2.0     7230.0
124. CH2+CH3<=>H+C2H4                           4.00E+13    0.0        0.0
125. CH2+CH4<=>2CH3                             2.46E+06    2.0     8270.0
126. CH2(S)+H2<=>CH3+H                          7.00E+13    0.0        0.0
127. CH2(S)+H2O(+M)<=>CH3OH(+M)                 4.82E+17   -1.2     1145.0
     Low pressure limit:  0.18800E+39 -0.63600E+01  0.50400E+04
     TROE centering:      0.60270E+00  0.20800E+03  0.39220E+04  0.10180E+05
     H2              Enhanced by    2.000E+00
     H2O             Enhanced by    6.000E+00
     CH4             Enhanced by    2.000E+00
     CO              Enhanced by    1.500E+00
     CO2             Enhanced by    2.000E+00
     C2H6            Enhanced by    3.000E+00
128. CH2(S)+H2O<=>CH2+H2O                       3.00E+13    0.0        0.0
129. CH2(S)+CO<=>CH2+CO                         9.00E+12    0.0        0.0
130. CH2(S)+CO2<=>CO+CH2O                       1.40E+13    0.0        0.0
131. 2CH3(+M)<=>C2H6(+M)                        6.77E+16   -1.2      654.0
     Low pressure limit:  0.34000E+42 -0.70300E+01  0.27620E+04
     TROE centering:      0.61900E+00  0.73200E+02  0.11800E+04  0.99990E+04
     H2              Enhanced by    2.000E+00
     H2O             Enhanced by    6.000E+00
     CH4             Enhanced by    2.000E+00
     CO              Enhanced by    1.500E+00
     CO2             Enhanced by    2.000E+00
     C2H6            Enhanced by    3.000E+00
132. 2CH3<=>H+C2H5                              6.84E+12    0.1    10600.0
133. CH3+HCO<=>CH4+CO                           2.65E+13    0.0        0.0
134. CH3+CH2O<=>HCO+CH4                         3.32E+03    2.8     5860.0
135. CH3+CH3OH<=>CH2OH+CH4                      3.00E+07    1.5     9940.0
136. CH3+C2H6<=>C2H5+CH4                        6.14E+06    1.7    10450.0
137. C2H4(+M)<=>H2+C2H2(+M)                     8.00E+12    0.4    86770.0
     Low pressure limit:  0.15800E+52 -0.93000E+01  0.97800E+05
     TROE centering:      0.73450E+00  0.18000E+03  0.10350E+04  0.54170E+04
     H2              Enhanced by    2.000E+00
     H2O             Enhanced by    6.000E+00
     CH4             Enhanced by    2.000E+00
     CO              Enhanced by    1.500E+00
     CO2             Enhanced by    2.000E+00
     C2H6            Enhanced by    3.000E+00
138. CH2+NO<=>H+HNCO                            3.10E+17   -1.4     1270.0
139. CH2+NO<=>OH+HCN                            2.90E+14   -0.7      760.0
140. CH2+NO<=>H+HCNO                            3.80E+13   -0.4      580.0
141. CH2(S)+NO<=>H+HNCO                         3.10E+17   -1.4     1270.0
142. CH3+NO<=>HCN+H2O                           9.60E+13    0.0    28800.0
143. CH3+NO<=>H2CN+OH                           1.00E+12    0.0    21750.0
144. HCNO+H<=>H+HNCO                            2.10E+15   -0.7     2850.0
145. HCNO+H<=>OH+HCN                            2.70E+11    0.2     2120.0
146. HCNO+H<=>NH2+CO                            1.70E+14   -0.8     2890.0
147. OH+NO2(+M)=HNO3(+M)                        2.41E+13    0.0        0.0
     Low pressure limit:  0.64200E+33 -0.54900E+01  0.23500E+04
     TROE centering:      0.78738E+00  0.13000E+01  0.18330E+04  0.85500E+05
     N2O             Enhanced by    5.000E+00
     H2O             Enhanced by    9.000E+00
```

```
     N2              Enhanced by    1.000E+00
     HNO3            Enhanced by    5.000E+00
     NH3             Enhanced by    5.000E+00
     NO3             Enhanced by    5.000E+00
148. HNO3+NO=HONO+NO2                          8.00E+06    2.0    11000.0
149. HNOH+NO2=HONO+HNO                         6.00E+11    0.0     2000.0
150. HNOH+H=NH2+OH                             4.00E+13    0.0        0.0
151. HNOH+H=HNO+H2                             4.80E+08    1.5      378.0
152. NH2O+H=NH2+OH                             4.00E+13    0.0        0.0
153. NH2O+H=HNO+H2                             4.80E+08    1.5     1560.0
154. HNO2+OH=H2O+NO2                           1.20E+06    2.0     -795.0
155. NO3+CH2O=HNO3+HCO                         1.70E+12    0.0     5000.0
156. C2H4O+NO2=HONO+CH2CHO                     1.30E+12    0.0     3700.0
157. CH2CHO+NO=HNO+CH2CO                       1.00E+12    0.0     8600.0
158. CH2CHO+NO2=HONO+CH2CO                     8.90E+12    0.0     -160.0
159. H+CH3CHO<=>CH2CHO+H2                      2.05E+09    1.2     2405.0
160. H+CH3CHO=>CH3+H2+CO                       2.05E+09    1.2     2405.0
161. OH+CH3CHO=>CH3+H2O+CO                     2.34E+10    0.7    -1113.0
162. CH3+CH3CHO=>CH3+CH4+CO                    2.72E+06    1.8     5920.0
163. O+C2H4<=>H+CH2CHO                         6.70E+06    1.8      220.0
164. H+CH2CO(+M)<=>CH2CHO(+M)                  4.86E+11    0.4    -1755.0
     Low pressure limit:  0.10120E+43 -0.76300E+01  0.38540E+04
     TROE centering:      0.46500E+00  0.20100E+03  0.17730E+04  0.53330E+04
     H2              Enhanced by    2.000E+00
     H2O             Enhanced by    6.000E+00
     CO              Enhanced by    1.500E+00
     CO2             Enhanced by    2.000E+00
165. HCO+HNO=CH2O+NO                           6.00E+11    0.0     2000.0
166. CH2O+NO2=HCO+HONO                         8.35E-11    6.7     8310.0
167. HCO+NO2=CO+HONO                           1.24E+23   -3.3     2355.0
168. HCO+NO2=H+CO2+NO                          8.39E+15   -0.8     1930.0
169. CH4+NO2=CH3+HONO                          1.20E+13    0.0    30000.0
170. CH3+NO2=CH3O+NO                           1.40E+13    0.0        0.0
171. OH+HCN=HOCN+H                             1.10E+06    2.0    13373.0
172. HOCN+H<=>H+HNCO                           2.00E+07    2.0     2000.0
173. HOCN+H=H2+NCO                             2.40E+08    1.5     6617.0
174. CH3NH=CH3+NH                              8.38E+11    1.6    77500.0
175. CH3NH=CH2NH+H                             2.61E+09    1.4    32900.0
176. CH2NH+M=HCN+H2+M                          1.00E+14    0.0    10000.0
177. H2CN+NO=HCN+HNO                           1.00E+07    2.0     4400.0
178. N2O4(+M)=NO2+NO2(+M)                      4.05E+18   -1.1    12840.0
     Low pressure limit:  0.19600E+29 -0.38000E+01  0.12800E+05
179. CH3NO2(+M)=CH3+NO2(+M)                    1.00E+00    0.0        0.0
     IO1:   2.5562E+26 -5.0579E+00  5.5587E+04  1.0000E-04
     IO2:   3.2719E+28 -5.3395E+00  5.7248E+04  1.0000E-03
     IO3:   1.1509E+30 -5.4650E+00  5.8762E+04  1.0000E-02
     IO4:   6.7137E+30 -5.3758E+00  6.0024E+04  1.0000E-01
     IO5:   2.6910E+30 -4.9697E+00  6.0841E+04  1.0000E+00
     IO6:   4.0835E+28 -4.1847E+00  6.1043E+04  1.0000E+01
     IO7:   4.1061E+25 -3.1088E+00  6.0626E+04  1.0000E+02
     IO8:   3.2389E+23 -2.3522E+00  6.0350E+04  1.0000E+03
     IO9:   2.0049E+22 -1.8820E+00  6.0365E+04  1.0000E+04
     IO8:   3.2389E+23 -2.3522E+00  6.0350E+04  1.0000E+03
     IO9:   2.0049E+22 -1.8820E+00  6.0365E+04  1.0000E+04
180. CH3NO2+H=CH3+HONO                         3.30E+12    0.0     3730.0
181. CH3NO2+H=CH3NO+OH                         1.40E+12    0.0     3730.0
182. CH3NO2+H=H2CNO2+H2                        5.40E+02    3.5     5200.0
183. CH3NO2+OH=H2CNO2+H2O                      5.00E+05    2.0     1000.0
184. CH3NO2+OH=CH3OH+NO2                       2.00E+10    0.0    -1000.0
185. CH3NO2+CH3=H2CNO2+CH4                     5.50E-01    4.0     8300.0
186. H2CNO2=CH2O+NO                            1.00E+13    0.0    36000.0
187. CH3+NO(+M)=CH3NO(+M)                      9.00E+12    0.0      119.0
     Low pressure limit:  0.32000E+24 -0.18700E+01  0.00000E+00
188. CH3O+NO=CH2O+HNO                          1.30E+14   -0.7        0.0
```

```
189. CH3O+NO(+M)=CH3ONO(+M)                     6.60E+14   -0.6        0.0
     Low pressure limit:  0.27000E+28 -0.35000E+01  0.00000E+00
190. CH3O+NO2=CH2O+HONO                         6.00E+12    0.0     2285.0
191. CH2CO+OH=CH2O+HCO                          3.33E+12    0.0        0.0
192. CH2CO+OH=CH2OH+CO                          3.33E+12    0.0        0.0
193. CH2CO+OH=CH3+CO2                           3.33E+12    0.0        0.0
194. H+CH2O(+M)<=>CH3O(+M)                      5.40E+11    0.5     2600.0
     Low pressure limit:  0.22000E+31 -0.48000E+01  0.55600E+04
     TROE centering:      0.75800E+00  0.94000E+02  0.15550E+04  0.42000E+04
     H2               Enhanced by    2.000E+00
     H2O              Enhanced by    6.000E+00
     CH4              Enhanced by    2.000E+00
     CO               Enhanced by    1.500E+00
     CO2              Enhanced by    2.000E+00
     C2H6             Enhanced by    3.000E+00
195. H+CH2CO<=>HCCO+H2                          5.00E+13    0.0     8000.0
196. H+CH2CO<=>CH3+CO                           1.13E+13    0.0     3428.0
197. CH2+CO(+M)<=>CH2CO(+M)                     8.10E+11    0.5     4510.0
     Low pressure limit:  0.26900E+34 -0.51100E+01  0.70950E+04
     TROE centering:      0.59070E+00  0.27500E+03  0.12260E+04  0.51850E+04
     H2               Enhanced by    2.000E+00
     H2O              Enhanced by    6.000E+00
     CH4              Enhanced by    2.000E+00
     CO               Enhanced by    1.500E+00
     CO2              Enhanced by    2.000E+00
     C2H6             Enhanced by    3.000E+00
198. O+CH3<=>H+H2+CO                            3.37E+13    0.0        0.0
199. CH3+C2H5(+M)<=>C3H8(+M)                    9.43E+12    0.0        0.0
     Low pressure limit:  0.27100E+75 -0.16820E+02  0.13065E+05
     TROE centering:      0.15270E+00  0.29100E+03  0.27420E+04  0.77480E+04
     H2               Enhanced by    2.000E+00
     H2O              Enhanced by    6.000E+00
     CH4              Enhanced by    2.000E+00
     CO               Enhanced by    1.500E+00
     CO2              Enhanced by    2.000E+00
     C2H6             Enhanced by    3.000E+00
200. CH3ONO2(+M)=CH3O+NO2(+M)                   1.00E+00    0.0        0.0
     I04:   1.9300E+42 -8.9500E+00  4.6868E+04  1.0000E+00
     I05:   3.9700E+39 -7.8600E+00  4.6774E+04  1.0000E+01
     I06:   4.7300E+37 -7.1800E+00  4.6437E+04  2.5000E+01
     I07:   1.5500E+36 -6.6700E+00  4.6153E+04  5.0000E+01
     I08:   2.0300E+35 -6.3600E+00  4.5972E+04  7.5000E+01
     I09:   4.5300E+34 -6.1400E+00  4.5831E+04  1.0000E+02
     I10:   5.3300E+33 -5.8300E+00  4.5620E+04  1.5000E+02
     I11:   1.0700E+33 -5.6000E+00  4.5453E+04  2.0000E+02
     I12:   3.0600E+32 -5.4200E+00  4.5320E+04  2.5000E+02
     I13:   1.0900E+32 -5.2700E+00  4.5207E+04  3.0000E+02
     I14:   4.5600E+31 -5.1400E+00  4.5111E+04  3.5000E+02
     I15:   2.1300E+31 -5.0300E+00  4.5027E+04  4.0000E+02
     I16:   1.0400E+31 -4.9300E+00  4.4944E+04  4.5000E+02
     I17:   5.8300E+30 -4.8500E+00  4.4879E+04  5.0000E+02
201. CH3O+CH3O=CH2O+CH3OH                       6.03E+13    0.0        0.0
202. CH3O+CH2O=CH3OH+HCO                        1.02E+11    0.0     2980.0
203. ETONO2+OH=CJCONO2+H2O                      5.50E+12    0.0     2400.0
204. ETONO2+H=CJCONO2+H2                        3.18E+13    0.0     8700.0
205. ETONO2+NO2=CJCONO2+HNO2                    8.00E+13    0.0    33800.0
206. ETONO2+NO2=CJCONO2+HONO                    1.10E+13    0.0    31100.0
207. CJCONO2=C2H4+NO3                           3.19E+11    0.7    22353.0
208. CJCONO2=C2H4O+NO2                          3.36E+08    1.3    18998.0
209. CJCONO2+NO2(+M)=COJCONO2+NO(+M)            1.00E+00    0.0        0.0
     I04:   6.9500E+15 -7.3000E-01  1.4900E+03  1.0000E+00
     I05:   1.9600E+19 -1.6900E+00  4.1100E+03  1.0000E+01
     I06:   4.4900E+19 -1.7700E+00  4.9210E+03  2.5000E+01
     I07:   1.3000E+19 -1.5800E+00  5.2430E+03  5.0000E+01
```

```
     I08:   2.5500E+18 -1.3600E+00  5.2780E+03  7.5000E+01
     I09:   5.2500E+17 -1.1500E+00  5.2280E+03  1.0000E+02
     I10:   3.2000E+16 -7.9000E-01  5.0540E+03  1.5000E+02
     I11:   3.0400E+15 -4.8000E-01  4.8610E+03  2.0000E+02
     I12:   4.0700E+14 -2.2000E-01  4.6760E+03  2.5000E+02
     I13:   7.1100E+13  0.0000E+00  4.5040E+03  3.0000E+02
     I14:   1.5300E+13  2.0000E-01  4.3450E+03  3.5000E+02
     I15:   3.8800E+12  3.8000E-01  4.2000E+03  4.0000E+02
     I16:   1.1300E+12  5.3000E-01  4.0650E+03  4.5000E+02
     I17:   3.6600E+11  6.8000E-01  3.9410E+03  5.0000E+02
210. COJCONO2=CH2O+CH2O+NO2                    2.81E+09    1.3    13866.0
211. CNO2CDO=CH2CHO+NO2                        1.27E+17   -0.7    50945.0
212. CNO2CDO+NO2=CNO2CDJO+HONO                 2.50E+07    1.3    15579.0
213. CNO2CDJO=H2CNO2+CO                        7.39E+11    0.7    10567.0
214. ETONO2+H=CH3CHO+NO2+H2                    4.80E+08    1.5     5151.8
215. ETONO2+OH=CH3CHO+NO2+H2O                  2.40E+06    2.0     -557.9
216. ETONO2+CH3=CH3CHO+NO2+CH4                 1.62E+06    1.9     8352.8
217. ETONO2+NO2=CH3CHO+NO2+HONO                3.72E-07    6.1    21099.0
218. ETONO2(+M)=C2H5O+NO2(+M)                  1.00E+00    0.0        0.0
     I04:   6.0900E+43 -9.2800E+00  4.6541E+04  1.0000E+00
     I05:   4.0500E+39 -7.7800E+00  4.5975E+04  1.0000E+01
     I06:   1.8200E+37 -6.9900E+00  4.5451E+04  2.5000E+01
     I07:   2.1500E+35 -6.3600E+00  4.4974E+04  5.0000E+01
     I08:   1.3200E+34 -5.9600E+00  4.4658E+04  7.5000E+01
     I09:   1.8500E+33 -5.6800E+00  4.4429E+04  1.0000E+02
     I10:   1.0200E+32 -5.2700E+00  4.4083E+04  1.5000E+02
     I11:   1.2800E+31 -4.9800E+00  4.3830E+04  2.0000E+02
     I12:   2.5300E+30 -4.7500E+00  4.3629E+04  2.5000E+02
     I13:   6.9300E+29 -4.5700E+00  4.3467E+04  3.0000E+02
     I14:   2.3200E+29 -4.4200E+00  4.3330E+04  3.5000E+02
     I15:   8.5200E+28 -4.2800E+00  4.3203E+04  4.0000E+02
     I16:   3.5300E+28 -4.1600E+00  4.3090E+04  4.5000E+02
     I17:   1.7200E+28 -4.0600E+00  4.2998E+04  5.0000E+02
219. ETONO2(+M)=CH3CHO+HONO(+M)                1.00E+00    0.0        0.0
     I04:   7.2700E+37 -8.4900E+00  4.9655E+04  1.0000E+00
     I05:   1.4700E+34 -7.0700E+00  4.9476E+04  1.0000E+01
     I06:   6.1000E+31 -6.2500E+00  4.9013E+04  2.5000E+01
     I07:   5.6700E+29 -5.5700E+00  4.8551E+04  5.0000E+01
     I08:   2.8400E+28 -5.1400E+00  4.8230E+04  7.5000E+01
     I09:   3.3900E+27 -4.8400E+00  4.7994E+04  1.0000E+02
     I10:   1.4400E+26 -4.3900E+00  4.7632E+04  1.5000E+02
     I11:   1.4800E+25 -4.0700E+00  4.7363E+04  2.0000E+02
     I12:   2.4800E+24 -3.8200E+00  4.7148E+04  2.5000E+02
     I13:   5.9100E+23 -3.6200E+00  4.6975E+04  3.0000E+02
     I14:   1.7600E+23 -3.4500E+00  4.6826E+04  3.5000E+02
     I15:   5.8000E+22 -3.2900E+00  4.6688E+04  4.0000E+02
     I16:   2.1800E+22 -3.1500E+00  4.6566E+04  4.5000E+02
     I17:   9.7800E+21 -3.0400E+00  4.6466E+04  5.0000E+02
220. ETONO2(+M)=C2H4+HNO3(+M)                  1.00E+00    0.0        0.0
     I04:   3.8400E+37 -8.4200E+00  5.1785E+04  1.0000E+00
     I05:   3.5300E+34 -7.1600E+00  5.2001E+04  1.0000E+01
     I06:   1.7000E+32 -6.3400E+00  5.1624E+04  2.5000E+01
     I07:   1.4900E+30 -5.6400E+00  5.1196E+04  5.0000E+01
     I08:   6.7900E+28 -5.1900E+00  5.0882E+04  7.5000E+01
     I09:   7.4100E+27 -4.8700E+00  5.0648E+04  1.0000E+02
     I10:   2.6700E+26 -4.4000E+00  5.0282E+04  1.5000E+02
     I11:   2.4100E+25 -4.0600E+00  5.0006E+04  2.0000E+02
     I12:   3.6100E+24 -3.7900E+00  4.9784E+04  2.5000E+02
     I13:   7.8600E+23 -3.5700E+00  4.9604E+04  3.0000E+02
     I14:   2.1500E+23 -3.3900E+00  4.9450E+04  3.5000E+02
     I15:   6.5800E+22 -3.2200E+00  4.9305E+04  4.0000E+02
     I16:   2.3100E+22 -3.0800E+00  4.9176E+04  4.5000E+02
     I17:   9.7700E+21 -2.9600E+00  4.9072E+04  5.0000E+02
221. C2H5O+NO2=CH3CHO+HNO2                     2.93E+00    3.4     -917.0
```

```
222. C2H5O+NO2=CH3CHO+HONO                    2.17E-01    3.6    -1048.4
223. C2H5O+NO=CH3CHO+HNO                      1.06E+00    3.4     -923.7
224. CH3CHO+NO2=CH3CO+HONO                    2.50E+07    1.3    15398.0
225. CH3CHO+NO2=CH3CO+HNO2                    7.10E-03    4.6    19979.0
226. CH3CHO+NO2=CH2CHO+HONO                   2.50E+07    1.3    22674.0
227. CH3CO+NO2=CH3CO2+NO                      4.51E+13    0.0        0.0
228. CH2CHO+NO2=CDOCOJ+NO                     2.35E+13    0.0        0.0
229. CDOCOJ=HCO+CH2O                          2.53E+13    0.4     8090.3
230. CH3CHO=CH3+HCO                           2.61E+15    0.1    80550.0
231. CH2O+OH(+M)=HOCHO+H(+M)                  1.00E+00    0.0        0.0
     I04:   6.3300E+06  1.6300E+00  4.2800E+03  1.0000E+00
     I05:   7.2600E+06  1.6100E+00  4.3130E+03  1.0000E+01
     I06:   1.4000E+07  1.5300E+00  4.4770E+03  2.5000E+01
     I07:   4.5800E+07  1.3800E+00  4.7810E+03  5.0000E+01
     I08:   1.2500E+08  1.2600E+00  5.0480E+03  7.5000E+01
     I09:   2.8600E+08  1.1500E+00  5.2750E+03  1.0000E+02
     I10:   1.0400E+09  1.0000E+00  5.6440E+03  1.5000E+02
     I11:   2.7200E+09  8.8000E-01  5.9320E+03  2.0000E+02
     I12:   5.7500E+09  7.9000E-01  6.1670E+03  2.5000E+02
     I13:   1.0500E+10  7.1000E-01  6.3630E+03  3.0000E+02
     I14:   1.7200E+10  6.5000E-01  6.5310E+03  3.5000E+02
     I15:   2.6000E+10  6.1000E-01  6.6780E+03  4.0000E+02
     I16:   3.6800E+10  5.6000E-01  6.8070E+03  4.5000E+02
     I17:   4.9600E+10  5.3000E-01  6.9210E+03  5.0000E+02
232. CH3CO(+M)=CH3+CO(+M)                     3.00E+12    0.0    16720.0
     Low pressure limit:  0.12000E+16  0.00000E+00  0.12518E+05
233. CH3CO2+M=CH3+CO2+M                       4.40E+15    0.0    10500.0
     Reverse Arrhenius coefficients:          9.65E+12    0.2    21040.0
234. C2H5OH(+M)=CH2OH+CH3(+M)                 5.71E+23   -1.7    94410.0
     Low pressure limit:  0.31100E+86 -0.18840E+02  0.11310E+06
     TROE centering:      0.50000E+00  0.55000E+03  0.82500E+03  0.61000E+04
     H2               Enhanced by    2.000E+00
     H2O              Enhanced by    5.000E+00
     CO               Enhanced by    2.000E+00
     CO2              Enhanced by    3.000E+00
235. C2H5OH(+M)=C2H4+H2O(+M)                  2.79E+13    0.1    66140.0
     Low pressure limit:  0.25700E+84 -0.18850E+02  0.86453E+05
     TROE centering:      0.70000E+00  0.35000E+03  0.80000E+03  0.38000E+04
     H2O              Enhanced by    5.000E+00
236. C2H5OH+OH=C2H5O+H2O                      7.46E+11    0.3     1634.0
237. C2H5OH+H=C2H5O+H2                        1.50E+07    1.6     3038.0
238. C2H5OH+CH3=PC2H4OH+CH4                   1.33E+02    3.2     9362.0
239. C2H5O(+M)=CH3+CH2O(+M)                   1.00E+00    0.0        0.0
     I04:   1.0000E+28 -5.4600E+00  1.8903E+04  1.0000E+00
     I05:   3.2600E+27 -4.9300E+00  1.9638E+04  1.0000E+01
     I06:   6.3300E+24 -3.9500E+00  1.9155E+04  2.5000E+01
     I07:   5.4500E+24 -3.8300E+00  1.9472E+04  5.0000E+01
     I08:   3.7300E+24 -3.7300E+00  1.9606E+04  7.5000E+01
     I09:   3.0600E+24 -3.6700E+00  1.9706E+04  1.0000E+02
     I10:   1.8500E+24 -3.5600E+00  1.9808E+04  1.5000E+02
     I11:   1.2600E+24 -3.4700E+00  1.9875E+04  2.0000E+02
     I12:   9.1200E+23 -3.4000E+00  1.9923E+04  2.5000E+02
     I13:   6.6200E+23 -3.3400E+00  1.9952E+04  3.0000E+02
     I14:   5.2800E+23 -3.3000E+00  1.9980E+04  3.5000E+02
     I15:   4.8600E+23 -3.2700E+00  2.0023E+04  4.0000E+02
     I16:   4.3400E+23 -3.2400E+00  2.0052E+04  4.5000E+02
     I17:   4.1700E+23 -3.2300E+00  2.0086E+04  5.0000E+02
240. C2H5O(+M)=CH3CHO+H(+M)                   1.00E+00    0.0        0.0
     I04:   2.4300E+21 -3.3700E+00  1.7357E+04  1.0000E+00
     I05:   1.3200E+19 -2.4500E+00  1.7351E+04  1.0000E+01
     I06:   1.4100E+16 -1.4300E+00  1.6684E+04  2.5000E+01
     I07:   6.8400E+15 -1.2700E+00  1.6836E+04  5.0000E+01
     I08:   3.5900E+15 -1.1500E+00  1.6882E+04  7.5000E+01
     I09:   2.4500E+15 -1.0700E+00  1.6921E+04  1.0000E+02
```

```
     I10:   1.2000E+15 -9.5000E-01  1.6945E+04  1.5000E+02
     I11:   7.0400E+14 -8.5000E-01  1.6957E+04  2.0000E+02
     I12:   4.5000E+14 -7.8000E-01  1.6961E+04  2.5000E+02
     I13:   2.9900E+14 -7.1000E-01  1.6958E+04  3.0000E+02
     I14:   2.1800E+14 -6.5000E-01  1.6958E+04  3.5000E+02
     I15:   1.8000E+14 -6.2000E-01  1.6971E+04  4.0000E+02
     I16:   1.4700E+14 -5.8000E-01  1.6975E+04  4.5000E+02
     I17:   1.2900E+14 -5.6000E-01  1.6985E+04  5.0000E+02
241. C2H5O+H=CH3CHO+H2                          1.00E+14    0.0        0.0
242. C2H5OH=CH2OH+CH3                           3.10E+15    0.0    80600.0
243. C2H5OH+CH2O=C2H5O+CH3O                     1.50E+12    0.0    79500.0
244. C2H5+NO2(+M)=C2H5O+NO(+M)                  1.00E+00    0.0        0.0
     I04:   2.0800E+13  0.0000E+00  3.0000E+00  1.0000E+00
     I05:   2.0800E+13  0.0000E+00  3.0000E+00  1.0000E+01
     I06:   2.0800E+13  0.0000E+00  3.0000E+00  2.5000E+01
     I07:   2.0900E+13  0.0000E+00  3.0000E+00  5.0000E+01
     I08:   2.1000E+13  0.0000E+00  5.0000E+00  7.5000E+01
     I09:   2.1400E+13 -1.0000E-02  1.0000E+01  1.0000E+02
     I10:   2.3100E+13 -2.0000E-02  2.9000E+01  1.5000E+02
     I11:   2.5900E+13 -3.0000E-02  5.9000E+01  2.0000E+02
     I12:   2.9800E+13 -5.0000E-02  9.6000E+01  2.5000E+02
     I13:   3.4800E+13 -7.0000E-02  1.3800E+02  3.0000E+02
     I14:   4.0900E+13 -9.0000E-02  1.8200E+02  3.5000E+02
     I15:   4.8200E+13 -1.1000E-01  2.2800E+02  4.0000E+02
     I16:   5.6700E+13 -1.3000E-01  2.7400E+02  4.5000E+02
     I17:   6.6600E+13 -1.5000E-01  3.1900E+02  5.0000E+02
245. C2H5ONO(+M)=C2H5O+NO(+M)                   1.00E+00    0.0        0.0
     I04:   2.7800E+51 -1.1540E+01  4.9388E+04  1.0000E+00
     I05:   3.1100E+50 -1.0950E+01  5.0064E+04  1.0000E+01
     I06:   8.6700E+45 -9.4200E+00  4.8948E+04  2.5000E+01
     I07:   3.1800E+44 -8.9000E+00  4.8771E+04  5.0000E+01
     I08:   1.5600E+44 -8.7600E+00  4.8837E+04  7.5000E+01
     I09:   9.0300E+43 -8.6500E+00  4.8874E+04  1.0000E+02
     I10:   3.2700E+43 -8.4800E+00  4.8887E+04  1.5000E+02
     I11:   1.3500E+43 -8.3300E+00  4.8866E+04  2.0000E+02
     I12:   5.7100E+42 -8.2000E+00  4.8824E+04  2.5000E+02
     I13:   2.8200E+42 -8.0900E+00  4.8785E+04  3.0000E+02
     I14:   1.3400E+42 -7.9700E+00  4.8732E+04  3.5000E+02
     I15:   7.5300E+41 -7.8800E+00  4.8693E+04  4.0000E+02
     I16:   4.1900E+41 -7.7900E+00  4.8647E+04  4.5000E+02
     I17:   2.6300E+41 -7.7200E+00  4.8614E+04  5.0000E+02
246. C2H5O+C2H5O=C2H5OH+CH3CHO                  1.44E+13    0.0        0.0
247. HONNH=NH2NO                                3.93E+11    0.5    31407.0
248. NH2+NO=NH2NO                               1.08E+12    0.0    -1290.0

 NOTE:  A units mole-cm-sec-K, E units cal/mole
```

A.2 therm.dat

```
ETONO2    FREQ_CCONO2_I_C   2H   5N   1O   3G   300.000  5000.000 1386.000    31
 1.46515723E+01 1.28951427E-02-4.51624920E-06 7.12471272E-10-4.18026785E-14    2
-2.58655638E+04-4.85145617E+01 1.50837107E+00 4.21061803E-02-2.87403500E-05    3
 9.61518131E-09-1.26461213E-12-2.11697401E+04 2.25733412E+01                   4
NO2               121286N   1O   2          G  0300.00   5000.00  1000.00     1
 0.04682859E+02 0.02462429E-01-0.01042259E-04 0.01976902E-08-0.01391717E-12    2
 0.02261292E+05 0.09885985E+01 0.02670600E+02 0.07838501E-01-0.08063865E-04    3
 0.06161715E-07-0.02320150E-10 0.02896291E+05 0.01161207E+03                   4
HONO               31787H   1N   1O   2     G  0300.00   5000.00  1000.00     1
 0.05486893E+02 0.04218065E-01-0.01649143E-04 0.02971877E-08-0.02021148E-12    2
-0.01126865E+06-0.02997002E+02 0.02290413E+02 0.01409922E+00-0.01367872E-03    3
 0.07498780E-07-0.01876905E-10-0.01043195E+06 0.01328077E+03                   4
NO                MCB93 N   1O   1    0    0G   200.000  6000.000 1000.000    01
 3.26071234E+00 1.19101135E-03-4.29122646E-07 6.94481463E-11-4.03295681E-15    2
 9.92143132E+03 6.36900518E+00 4.21859896E+00-4.63988124E-03 1.10443049E-05    3
-9.34055507E-09 2.80554874E-12 9.84509964E+03 2.28061001E+00 1.09770882E+04    4
O                 120186O   1               G  0300.00   5000.00  1000.00     1
 0.02542060E+02-0.02755062E-03-0.03102803E-07 0.04551067E-10-0.04368052E-14    2
 0.02923080E+06 0.04920308E+02 0.02946429E+02-0.01638166E-01 0.02421032E-04    3
-0.01602843E-07 0.03890696E-11 0.02914764E+06 0.02963995E+02                   4
N2O               121286N   2O   1          G  0300.00   5000.00  1000.00     1
 0.04718977E+02 0.02873714E-01-0.01197496E-04 0.02250552E-08-0.01575337E-12    2
 0.08165811E+05-0.01657250E+02 0.02543058E+02 0.09492193E-01-0.09792775E-04    3
 0.06263845E-07-0.01901826E-10 0.08765100E+05 0.09511222E+02                   4
H2O                20387H   2O   1          G  0300.00   5000.00  1000.00     1
 0.02672146E+02 0.03056293E-01-0.08730260E-05 0.01200996E-08-0.06391618E-13    2
-0.02989921E+06 0.06862817E+02 0.03386842E+02 0.03474982E-01-0.06354696E-04    3
 0.06968581E-07-0.02506588E-10-0.03020811E+06 0.02590233E+02                   4
N2                121286N   2               G  0300.00   5000.00  1000.00     1
 0.02926640E+02 0.01487977E-01-0.05684761E-05 0.01009704E-08-0.06753351E-13    2
-0.09227977E+04 0.05980528E+02 0.03298677E+02 0.01408240E-01-0.03963222E-04    3
 0.05641515E-07-0.02444855E-10-0.01020900E+05 0.03950372E+02                   4
CO2               121286C   1O   2          G  0300.00   5000.00  1000.00     1
 0.04453623E+02 0.03140169E-01-0.01278411E-04 0.02393997E-08-0.01669033E-12    2
-0.04896696E+06-0.09553959E+01 0.02275725E+02 0.09922072E-01-0.01040911E-03    3
 0.06866687E-07-0.02117280E-10-0.04837314E+06 0.01018849E+03                   4
O2                121386O   2               G  0300.00   5000.00  1000.00     1
 0.03697578E+02 0.06135197E-02-0.01258842E-05 0.01775281E-09-0.01136435E-13    2
-0.01233930E+05 0.03189166E+02 0.03212936E+02 0.01127486E-01-0.05756150E-05    3
 0.01313877E-07-0.08768554E-11-0.01005249E+05 0.06034738E+02                   4
H                 120186H   1               G  0300.00   5000.00  1000.00     1
 0.02500000E+02 0.00000000E+00 0.00000000E+00 0.00000000E+00 0.00000000E+00    2
 0.02547163E+06-0.04601176E+01 0.02500000E+02 0.00000000E+00 0.00000000E+00    3
 0.00000000E+00 0.00000000E+00 0.02547163E+06-0.04601176E+01                   4
HNO       RFITHNO_200_60H   1N   1O   1    0G   300.000  5000.000 1000.00    0 1
 3.32506061D+00 3.28074885D-03-1.17988827D-06 1.90627500D-10-1.14185005D-14    2
 1.16469551D+04 6.44374561D+00 4.30275249D+00-3.27872764D-03 1.00572297D-05    3
-6.51594911D-09 1.03982469D-12 1.16696904D+04 2.60372138D+00                   4
OH          Sand/Rusc01 O   1H   1          G  0300.00   5000.00  1000.00     1
 0.02882730E+02 0.01013974E-01-0.02276877E-05 0.02174684E-09-0.05126305E-14    2
 0.03672089E+05 0.05595712E+02 0.03637266E+02 0.01850910E-02-0.01676165E-04    3
 0.02387203E-07-0.08431442E-11 0.03391983E+05 0.01358860E+02                   4
HCN           McB93/GM94 H   1C   1N   1    0G   200.000  6000.000 1000.000    01
 3.80231733E+00 3.14630009E-03-1.06315698E-06 1.66185395E-10-9.79891789E-15    2
 1.47215128E+04 1.57503584E+00 2.25901123E+00 1.00510591E-02-1.33514911E-05    3
 1.00920882E-08-3.00882048E-12 1.50268794E+04 8.91634590E+00 1.60477053E+04    4
HNCO          McB93/GM94 H   1N   1C   1O   1G   200.000  6000.000 1000.000    01
 5.29404664E+00 4.03039650E-03-1.41290348E-06 2.24428234E-10-1.32859380E-14    2
-1.61346328E+04-3.08763130E+00 2.24322454E+00 1.44986380E-02-1.52609054E-05    3
 8.36364453E-09-1.72191967E-12-1.53950081E+04 1.21565469E+01-1.42008857E+04    4
NH           McB93/WRA00 N   1H   1    0    0G   200.000  6000.000 1000.000    01
 2.78372645E+00 1.32985886E-03-4.24785565E-07 7.83494425E-11-5.50451298E-15    2
 4.22190438E+04 5.74084857E+00 3.49295037E+00 3.11795722E-04-1.48906628E-06    3
 2.48167403E-09-1.03570916E-12 4.19788215E+04 1.84834974E+00 4.30253623E+04    4
CO                121286C   1O   1          G  0300.00   5000.00  1000.00     1
 0.03025078E+02 0.01442689E-01-0.05630828E-05 0.01018581E-08-0.06910952E-13    2
-0.01426835E+06 0.06108218E+02 0.03262452E+02 0.01511941E-01-0.03881755E-04    3
 0.05581944E-07-0.02474951E-10-0.01431054E+06 0.04848897E+02                   4
H2CN               41687H   2C   1N   1     G  0300.00   4000.00  1000.00     1
```

```
 0.05209703E+02 0.02969291E-01-0.02855589E-05-0.01635550E-08 0.03043259E-12    2
 0.02767711E+06-0.04444478E+02 0.02851661E+02 0.05695233E-01 0.01071140E-04    3
-0.01622612E-07-0.02351108E-11 0.02863782E+06 0.08992751E+02                   4
N                 120186N   1               G  0300.00   5000.00  1000.00     1
 0.02450268E+02 0.01066146E-02-0.07465337E-06 0.01879652E-09-0.01025984E-13    2
 0.05611604E+06 0.04448758E+02 0.02503071E+02-0.02180018E-03 0.05420529E-06    3
-0.05647560E-09 0.02099904E-12 0.05609890E+06 0.04167566E+02                   4
NO3               121286N   1O   3          G  0300.00   5000.00  1000.00     1
 0.07120307E+02 0.03246228E-01-0.01431613E-04 0.02797053E-08-0.02013008E-12    2
 0.05864479E+05-0.01213730E+03 0.01221076E+02 0.01878797E+00-0.01344321E-03    3
 0.01274601E-07 0.01354060E-10 0.07473144E+05 0.01840203E+03                   4
NH2               McB93 N   1H   2    0    0G   200.000  6000.000 1000.000    01
 2.84768992E+00 3.14280035E-03-8.98641458E-07 1.30318284E-10-7.48812926E-15    2
 2.18239049E+04 6.47165433E+00 4.20556857E+00-2.13561363E-03 7.26851301E-06    3
-5.93069876E-09 1.80690978E-12 2.15352231E+04-1.46662770E-01 2.27475415E+04    4
NH3               121386N   1H   3          G  0300.00   5000.00  1000.00     1
 0.02461904E+02 0.06059166E-01-0.02004977E-04 0.03136003E-08-0.01938317E-12    2
-0.06493270E+05 0.07472097E+02 0.02204352E+02 0.01011476E+00-0.01465265E-03    3
 0.01447235E-06-0.05328509E-10-0.06525488E+05 0.08127138E+02                   4
HCO          McB93 L12/89H   1C   1O   1    0G   200.000  6000.000 1000.000    01
 3.64896209E+00 3.08090819E-03-1.12429876E-06 1.86308085E-10-1.13951828E-14    2
 3.71209048E+03 5.06147406E+00 4.22118584E+00-3.24392532E-03 1.37799446E-05    3
-1.33144093E-08 4.33768865E-12 3.83956496E+03 3.39437243E+00 5.05141013E+03    4
H2                121286H   2               G  0300.00   5000.00  1000.00     1
 0.02991423E+02 0.07000644E-02-0.05633829E-06-0.09231578E-10 0.01582752E-13    2
-0.08350340E+04-0.01355110E+02 0.03298124E+02 0.08249442E-02-0.08143015E-05    3
-0.09475434E-09 0.04134872E-11-0.01012521E+05-0.03294094E+02                   4
HCCO               32387H   1C   2O   1     G  0300.00   4000.00  1000.00     1
 0.06758073E+02 0.02000400E-01-0.02027607E-05-0.01041132E-08 0.01965165E-12    2
 0.01901513E+06-0.09071262E+02 0.05047965E+02 0.04453478E-01 0.02268283E-05    3
-0.01482095E-07 0.02250742E-11 0.01965892E+06 0.04818439E+01                   4
HCNO              120186H   1C   1N   1O   1G  0250.00   4000.00  1000.00     1
 0.06692412E+02 0.02368360E-01-0.02371510E-05-0.01275503E-08 0.02407137E-12    2
 0.01694737E+06-0.01245434E+03 0.03184859E+02 0.09752316E-01-0.01280203E-04    3
-0.06163104E-07 0.03226275E-10 0.01797907E+06 0.06123844E+02                   4
NCO          McB93/WRA98 N   1C   1O   1    0G   200.000  6000.000 1000.000    01
 5.15255717E+00 2.30945594E-03-8.83699519E-07 1.48525346E-10-9.08857905E-15    2
 1.39030086E+04-2.56406350E+00 2.75452392E+00 9.23008037E-03-9.28006629E-06    3
 5.62521381E-09-1.61200144E-12 1.45909290E+04 9.85368773E+00 1.57508051E+04    4
NNH               120186N   2H   1          G  0250.00   4000.00  1000.00     1
 0.04415342E+02 0.01614388E-01-0.01632894E-05-0.08559846E-09 0.01614791E-12    2
 0.02788029E+06 0.09042888E+01 0.03501344E+02 0.02053587E-01 0.07170410E-05    3
 0.04921348E-08-0.09671170E-11 0.02833347E+06 0.06391837E+02                   4
HNC           MEL/LIN92  H   1C   1N   1    0G   300.000  5000.000 1394.000    01
 4.14927436E+00 2.75915497E-03-9.32137975E-07 1.43421369E-10-8.26579656E-15    2
 2.12186267E+04-2.04087166E-02 2.85596031E+00 6.10771202E-03-4.55238112E-06    3
 2.02415456E-09-3.88077938E-13 2.16612862E+04 6.85303990E+00                   4
HOCO              103190C   1H   1O   2     G  0300.00   4000.00  1500.00     1
 0.07517634E+02 0.01259029E-01-0.01910901E-05-0.03136391E-09 0.07547673E-13    2
-0.02634121E+06-0.01448392E+03 0.02285122E+02 0.01351435E+00-0.01160407E-03    3
 0.05047011E-07-0.09032231E-11-0.02448416E+06 0.01367874E+03                   4
HNNO           MELIUS    N   2H   1O   1    0G   300.000  5000.000 1389.000    01
 6.24922910E+00 3.26983002E-03-1.14794284E-06 1.81383141E-10-1.06538637E-14    2
 2.53822106E+04-7.09495778E+00 2.40143922E+00 1.26718648E-02-1.00828306E-05    3
 4.10522736E-09-6.79228705E-13 2.66782646E+04 1.34257436E+01                   4
HNO3              121286H   1N   1O   3     G  0300.00   5000.00  1000.00     1
 0.07003845E+02 0.05811493E-01-0.02333789E-04 0.04288814E-08-0.02959385E-12    2
-0.01889952E+06-0.01047863E+03 0.01353185E+02 0.02220025E+00-0.01978812E-03    3
 0.08773908E-07-0.01658384E-10-0.01738563E+06 0.01851868E+03                   4
CH2               120186C   1H   2          G  0250.00   4000.00  1000.00     1
 0.03636408E+02 0.01933057E-01-0.01687016E-05-0.01009899E-08 0.01808256E-12    2
 0.04534134E+06 0.02156561E+02 0.03762237E+02 0.01159819E-01 0.02489585E-05    3
 0.08800836E-08-0.07332435E-11 0.04536791E+06 0.01712578E+02                   4
CH2(S)             31287C   1H   2          G  0300.00   4000.00  1000.00     1
 0.03552889E+02 0.02066788E-01-0.01914116E-05-0.01104673E-08 0.02021350E-12    2
 0.04984975E+06 0.01686570E+02 0.03971265E+02-0.01699089E-02 0.01025369E-04    3
 0.02492551E-07-0.01981266E-10 0.04989368E+06 0.05753207E+00                   4
CH3               121286C   1H   3          G  0300.00   5000.00  1000.00     1
 0.02844052E+02 0.06137974E-01-0.02230345E-04 0.03785161E-08-0.02452159E-12    2
 0.01643781E+06 0.05452697E+02 0.02430443E+02 0.01112410E+00-0.01680220E-03    3
 0.01621829E-06-0.05864953E-10 0.01642378E+06 0.06789794E+02                   4
CH2O              L 8/88H   2C   1O   1   00G   200.000  3500.000  1000.000    1
```

```
 1.76069008E+00 9.20000082E-03-4.42258813E-06 1.00641212E-09-8.83855640E-14    2
-1.39958323E+04 1.36563230E+01 4.79372315E+00-9.90833369E-03 3.73220008E-05    3
-3.79285261E-08 1.31772652E-11-1.43089567E+04 6.02812900E-01 1.00197170E+04    4
CH4                 121286C   1H   4          G  0300.00   5000.00  1000.00    1
 0.01683479E+02 0.01023724E+00-0.03875129E-04 0.06785585E-08-0.04503423E-12    2
-0.01008079E+06 0.09623395E+02 0.07787415E+01 0.01747668E+00-0.02783409E-03    3
 0.03049708E-06-0.01223931E-09-0.09825229E+05 0.01372219E+03                   4
CH2OH               120186H   3C   1O   1     G  0250.00   4000.00  1000.00    1
 0.06327520E+02 0.03608271E-01-0.03201547E-05-0.01938750E-08 0.03509705E-12    2
-0.04474509E+05-0.08329366E+02 0.02862628E+02 0.01001527E+00-0.05285436E-05    3
-0.05138540E-07 0.02246041E-10-0.03349679E+05 0.01039794E+03                   4
CH3O                121686C   1H   3O   1     G  0300.00   3000.00  1000.00    1
 0.03770800E+02 0.07871497E-01-0.02656384E-04 0.03944431E-08-0.02112616E-12    2
 0.01278325E+04 0.02929575E+02 0.02106204E+02 0.07216595E-01 0.05338472E-04    3
-0.07377636E-07 0.02075611E-10 0.09786011E+04 0.01315218E+03                   4
CH3OH               121686C   1H   4O   1     G  0300.00   5000.00  1000.00    1
 0.04029061E+02 0.09376593E-01-0.03050254E-04 0.04358793E-08-0.02224723E-12    2
-0.02615791E+06 0.02378196E+02 0.02660115E+02 0.07341508E-01 0.07170051E-04    3
-0.08793194E-07 0.02390570E-10-0.02535348E+06 0.01123263E+03                   4
C2H2                121386C   2H   2          G  0300.00   5000.00  1000.00    1
 0.04436770E+02 0.05376039E-01-0.01912817E-04 0.03286379E-08-0.02156710E-12    2
 0.02566766E+06-0.02800338E+02 0.02013562E+02 0.01519045E+00-0.01616319E-03    3
 0.09078992E-07-0.01912746E-10 0.02612444E+06 0.08805378E+02                   4
C2H5      12387         C   2H   5N   0O   0G   300.000  5000.000 1460.000    11
 5.57508447E+00 1.05558254E-02-3.55403212E-06 5.46155407E-10-3.14675617E-14    2
 1.10133650E+04-6.48758419E+00 1.60717554E+00 1.33592058E-02 1.85866156E-06    3
-5.67582851E-09 1.66338686E-12 1.30227172E+04 1.70908946E+01                   4
C2H6                121686C   2H   6          G  0300.00   4000.00  1000.00    1
 0.04825938E+02 0.01384043E+00-0.04557259E-04 0.06724967E-08-0.03598161E-12    2
-0.01271779E+06-0.05239507E+02 0.01462539E+02 0.01549467E+00 0.05780507E-04    3
-0.01257832E-06 0.04586267E-10-0.01123918E+06 0.01443229E+03                   4
CH2CO               121686C   2H   2O   1     G  0300.00   5000.00  1000.00    1
 0.06038817E+02 0.05804840E-01-0.01920954E-04 0.02794485E-08-0.01458868E-12    2
-0.08583402E+05-0.07657581E+02 0.02974971E+02 0.01211871E+00-0.02345046E-04    3
-0.06466685E-07 0.03905649E-10-0.07632637E+05 0.08673553E+02                   4
C2H3                12787C   2H   3          G  0300.00   5000.00  1000.00    1
 0.05933468E+02 0.04017746E-01-0.03966740E-05-0.01441267E-08 0.02378644E-12    2
 0.03185435E+06-0.08530313E+02 0.02459276E+02 0.07371476E-01 0.02109873E-04    3
-0.01321642E-07-0.01184784E-10 0.03335225E+06 0.01155620E+03                   4
C2H4                121286C   2H   4          G  0300.00   5000.00  1000.00    1
 0.03528419E+02 0.01148518E+00-0.04418385E-04 0.07844601E-08-0.05266848E-12    2
 0.04428289E+05 0.02230389E+02-0.08614880E+01 0.02796163E+00-0.03388677E-03    3
 0.02785152E-06-0.09737879E-10 0.05573046E+05 0.02421149E+03                   4
HCCOH                32387H   2C   2O   1     G  0300.00   4000.00  1000.00    1
 0.07328324E+02 0.03336416E-01-0.03024705E-05-0.01781106E-08 0.03245168E-12    2
 0.07598258E+05-0.01401214E+03 0.03899465E+02 0.09701075E-01-0.03119309E-05    3
-0.05537732E-07 0.02465732E-10 0.08701190E+05 0.04491875E+02                   4
HNO2      G2MP2//B3DP   C   0H   1N   1O   2G   300.000  5000.000 1432.000    11
 5.86536159E+00 3.31399617E-03-1.19686495E-06 1.92694936E-10-1.14665018E-14    2
-7.43588573E+03-7.16262271E+00 2.33853317E+00 7.87822298E-03-4.64351984E-07    3
-2.66198709E-09 9.09206462E-13-5.88999705E+03 1.30055842E+01                   4
HNOH        JWB/94      N   1H   2O   1    0G   300.000  5000.000 1375.000    11
 5.24159962E+00 3.64132385E-03-1.26199882E-06 1.97647403E-10-1.15363360E-14    2
 8.79675199E+03-2.52971854E+00 3.42226363E+00 6.62639079E-03-2.62136579E-06    3
 1.83974483E-10 7.81187077E-14 9.57854837E+03 7.72947399E+00                   4
NH2O        M/JB86      N   1H   2O   1    0G   300.000  5000.000 1398.000    01
 4.26222939E+00 4.60071183E-03-1.52686779E-06 2.32081624E-10-1.32607907E-14    2
 6.26937941E+03 1.89523882E+00 2.62132814E+00 8.05594293E-03-4.34199752E-06    3
 1.31067689E-09-1.79413169E-13 6.89825870E+03 1.08768221E+01                   4
C2H4O         Chase98   C   2H   4O   1    0G   300.000  5000.000 1400.000    01
 7.04272994E+00 1.00110676E-02-3.42398623E-06 5.31623557E-10-3.08469387E-14    2
-1.00228712E+04-1.61926118E+01-1.42915337E+00 2.91826985E-02-1.96414512E-05    3
 6.60926623E-09-8.79248471E-13-7.04124488E+03 2.94882584E+01                   4
CH2CHO              SAND86O   1H   3C   2     G   300.000  5000.000  1000.000   1
 0.05975670E+02 0.08130591E-01-0.02743624E-04 0.04070304E-08-0.02176017E-12    2
 0.04903218E+04-0.05045251E+02 0.03409062E+02 0.10738574E-01 0.01891492E-04    3
-0.07158583E-07 0.02867385E-10 0.15214766E+04 0.09558290E+02                   4
CH3CHO              L 8/88C   2H   4O   1     G   200.000  6000.000  1000.000   1
 0.54041108E+01 0.11723059E-01-0.42263137E-05 0.68372451E-09-0.40984863E-13    2
-0.22593122E+05-0.34807917E+01 0.47294595E+01-0.31932858E-02 0.47534921E-04    3
-0.57458611E-07 0.21931112E-10-0.21572878E+05 0.41030159E+01                   4
HOCN                110193H   1C   1N   1O   1G  0300.00   4000.00  1400.00    1
```

```
 0.06022112E+02 0.01929530E-01-0.01455029E-05-0.01045811E-08 0.01794814E-12    2
-0.04040321E+05-0.05866433E+02 0.03789424E+02 0.05387981E-01-0.06518270E-05    3
-0.01420164E-07 0.05367969E-11-0.03135335E+05 0.06667052E+02                   4
CH3NH          Burcat-03 C   1H   4N   1    0G   200.000  6000.000  1000.00    1
 0.43023153D+01 0.10277337D-01-0.36593760D-05 0.58702457D-09-0.34979453D-13    2
 0.20473126D+05 0.13025403D+00 0.47462749D+01-0.71705198D-02 0.50242579D-04    3
-0.58589231D-07 0.22243219D-10 0.21124201D+05 0.17162390D+01 0.22559203D+05    4
CH2NH       MELIUS 88   H   3C   1N   1    0G   300.000  5000.000 1577.000    01
 4.54737795E+00 7.17720948E-03-2.47935299E-06 3.87692351E-10-2.26113075E-14    2
 8.64056516E+03-1.16687427E+00 2.81849510E+00 5.11983235E-03 6.38887146E-06    3
-6.61374671E-09 1.65531940E-12 9.88442597E+03 1.03390629E+01 1.09953704E+04    4
N2O4               121286N   2O   4          G  0300.00   5000.00  1000.00    1
 0.01048220E+03 0.05972272E-01-0.02564044E-04 0.04916885E-08-0.03490969E-12    2
-0.02849989E+05-0.02612289E+03 0.03624593E+02 0.02474708E+00-0.02172875E-03    3
 0.09927104E-07-0.02222817E-10-0.09128241E+04 0.09457174E+02                   4
CH3NO2             103190C   1H   3N   1O   2G  0300.00   4000.00  1500.00    1
 0.01090158E+03 0.04326381E-01-0.04203548E-05-0.01893071E-08 0.03417444E-12    2
-0.01370862E+06-0.03073183E+03 0.03224717E+01 0.02665147E+00-0.01930574E-03    3
 0.07762620E-07-0.01398746E-10-0.09597527E+05 0.02726156E+03                   4
CH3NO              103190C   1H   3N   1O   1G  0300.00   4000.00  1500.00    1
 0.08820547E+02 0.03706233E-01-0.02894741E-05-0.01897910E-08 0.03237544E-12    2
 0.05362862E+05-0.02213220E+03 0.02109955E+02 0.01517822E+00-0.07071789E-04    3
 0.01510611E-07-0.01604204E-11 0.08293612E+05 0.01569702E+03                   4
H2CNO2             103190C   1H   2N   1O   2G  0300.00   4000.00  1500.00    1
 0.01127481E+03 0.02584711E-01-0.03934331E-05-0.05614969E-09 0.01392400E-12    2
 0.01360470E+06-0.03461951E+03 0.01165696E+02 0.02890490E+00-0.02817663E-03    3
 0.01387569E-06-0.02727595E-10 0.01694546E+06 0.01888293E+03                   4
CH3ONO             103190C   1H   3N   1O   2G  0300.00   4000.00  1500.00    1
 0.01136129E+03 0.04159349E-01-0.04145670E-05-0.01695140E-08 0.03028732E-12    2
-0.01281482E+06-0.03545435E+03 0.01490345E+02 0.02645433E+00-0.02112332E-03    3
 0.09414399E-07-0.01811205E-10-0.09125782E+05 0.01813766E+03                   4
C3H8               L 4/85C   3H   8          G   300.000  5000.000  1000.000   1
 0.75341368E+01 0.18872239E-01-0.62718491E-05 0.91475649E-09-0.47838069E-13    2
-0.16467516E+05-0.17892349E+02 0.93355381E+00 0.26424579E-01 0.61059727E-05    3
-0.21977499E-07 0.95149253E-11-0.13958520E+05 0.19201691E+02                   4
CH3ONO2   CH3ONO2_G3MP2BC   1H   3N   1O   3G   300.000  5000.000 1382.000    21
 1.13980493E+01 8.43730296E-03-2.97734215E-06 4.72072167E-10-2.77953870E-14    2
-1.99184963E+04-3.29755758E+01 2.00735388E+00 2.89172145E-02-1.93690231E-05    3
 6.14043414E-09-7.31614920E-13-1.65357106E+04 1.79360405E+01                   4
C2H5O     1/ 2/97 THERM C   2H   5N   0O   1G   300.000  5000.000 1397.000    11
 7.99494328E+00 1.16435818E-02-4.95527268E-06 9.40395740E-10-6.27179768E-14    2
-6.03840830E+03-1.80274987E+01-2.06105850E+00 3.90869199E-02-3.39343824E-05    3
 1.48663223E-08-2.60789426E-12-2.98499617E+03 3.45061278E+01                   4
CH3CO              120186C   2H   3O   1    G  0300.00   5000.00  1000.00    1
 0.05612279e+02 0.08449886e-01-0.02854147e-04 0.04238376e-08-0.02268404e-12    2
-0.05187863e+05-0.03274949e+02 0.03125278e+02 0.09778220e-01 0.04521448e-04    3
-0.09009462e-07 0.03193718e-10-0.04108508e+05 0.01122885e+03                   4
CNO2CDO   CNO2CDO_BH_B3GC   2H   3N   1O   3G   300.000  5000.000 1371.000    21
 1.32288746E+01 9.26849853E-03-3.22656841E-06 5.06934833E-10-2.96576108E-14    2
-2.46158782E+04-3.63830375E+01 7.03685016E+00 1.96126610E-02-7.54117304E-06    3
-1.86582837E-10 5.10199439E-13-2.20524759E+04-1.66421396E+00                   4
CDCJONO2  CDCJONO2_BH_M0C   2H   2N   1O   3G   300.000  5000.000 1402.000    11
 1.36529858E+01 6.71971893E-03-2.33498422E-06 3.66637602E-10-2.14480539E-14    2
 2.06425576E+04-4.21413165E+01 1.20749335E+00 4.09753525E-02-3.88019995E-05    3
 1.80063308E-08-3.25998536E-12 2.43932553E+04 2.27723030E+01                   4
CJCONO2                  C   2H   4N   1O   3G   300.000  5000.000 1399.000    01
 1.38517581E+01 1.18591964E-02-4.06013780E-06 6.30897516E-10-3.66300367E-14    2
 2.33167020E+02-4.36638294E+01 1.49800776E+00 4.26286420E-02-3.36922236E-05    3
 1.37060312E-08-2.25507906E-12 4.30675402E+03 2.19629786E+01                   4
COJCONO2  FREQ_COJCONO2_C   2H   4N   1O   4G   300.000  5000.000 1381.000    31
 1.67734530E+01 1.12681466E-02-3.99562895E-06 6.35582533E-10-3.75073915E-14    2
-1.64575681E+04-5.54185115E+01 3.05340507E+00 4.11055238E-02-2.75745073E-05    3
 8.54264158E-09-9.56389649E-13-1.15288168E+04 1.89578134E+01                   4
CDOCOJ    CDOCOJ_BK1_G3MC   2H   3N   0O   2G   300.000  5000.000 1400.000    11
 9.27571884E+00 7.75575520E-03-2.66050704E-06 4.13950919E-10-2.40557083E-14    2
-1.43202812E+04-2.15954698E+01 7.35801911E-01 2.94411702E-02-2.40116195E-05    3
 1.00523052E-08-1.69503344E-12-1.15462450E+04 2.36230662E+01                   4
C2H5OH     3/12/95 tHermC   2H   6O   1    0G   300.000  5000.000 1391.000    11
 7.95264841e+00 1.31574144e-02-4.43693359e-06 6.82201160e-10-3.93096335e-14    2
-3.23602958e+04-1.76537972e+01 4.23149045e-01 2.92858167e-02-1.73845099e-05    3
 5.33639892e-09-6.74917252e-13-2.95683054e+04 2.33538763e+01                   4
HOCHO     HCOOH   103190C   1H   2O   2    G  0300.00   4000.00  1500.00     1
```

```
 0.07959698E+02 0.03024532E-01-0.03434242E-05-0.01326767E-08 0.02520240E-12    2
-0.05027445E+06-0.01872208E+03 0.09326031E+01 0.01891002E+00-0.01554964E-03    3
 0.07290031E-07-0.01483695E-10-0.04760071E+06 0.01950653E+03                   4
OCHO       2/14/95 tHermC   1H   1O   2    0G   300.000  5000.000 1690.00     01
 6.12628782e+00 3.75602932e-03-1.42010352e-06 2.36429200e-10-1.44167651e-14    2
-2.17698466e+04-8.01574694e+00 1.35213452e+00 1.50082004e-02-1.09896141e-05    3
 3.73679840e-09-4.81014498e-13-2.02253647e+04 1.74373147e+01                   4
CH3CO2                   C   2H   3O   2    0G   300.000  5000.000 1402.000    01
 8.66668933E+00 8.12452077E-03-2.66950784E-06 4.03691210E-10-2.30057984E-14    2
-2.73530000E+04-1.77978225E+01 9.48577764E-01 2.69496305E-02-2.00635163E-05    3
 7.62275527E-09-1.15644350E-12-2.48005404E+04 2.32904248E+01                   4
PC2H4OH    3/12/95 tHermC   2H   5O   1     G  0300.00   5000.00  1391.00     1
 7.52241939e+00 1.10492715e-02-3.72576465e-06 5.72827397e-10-3.30061759e-14    2
-7.29333590e+03-1.24958732e+01 1.17714711e+00 2.48115685e-02-1.50299503e-05    3
 4.79006785e-09-6.40994211e-13-4.95369043e+03 2.20081586e+01                   4
C2H5ONO     b3lyp/6-31g*C   2H   5N   1O   2G   300.000  5000.000 1394.000    21
 1.17299657E+01 1.27562764E-02-4.35584164E-06 6.75510485E-10-3.91616614E-14    2
-1.71362413E+04-3.31116039E+01 1.84941267E+00 3.53907948E-02-2.41398149E-05    3
 8.54918027E-09-1.24564972E-12-1.36536655E+04 2.01222696E+01                   4
NH2NO     H2NNO_G4.out  H   2N   2O   1    0G   300.000  5000.000 1393.000    11
 5.58336257E+00 5.09204279E-03-1.73536968E-06 2.83666022E-10-1.73828574E-14    2
 9.12692776E+03-4.61046368E+00 1.64587862E+00 1.47076327E-02-1.09035730E-05    3
 4.33657169E-09-7.13659773E-13 1.04585192E+04 1.63982286E+01                   4
NH2OH     NH2OH_G4.out  H   3N   1O   1    0G   300.000  5000.000 1420.000    01
 4.63525852E+00 6.45493945E-03-2.08558973E-06 3.11059157E-10-1.75319478E-14    2
-7.64275787E+03-7.73608271E-01 2.09386013E+00 1.24417866E-02-7.51044198E-06    3
 2.55541054E-09-3.73533556E-13-6.76250551E+03 1.28607110E+01                   4
ONONO2    t_ONONO2_BHa_BN   2O   4    0    0G   300.000  5000.000 1394.000    01
 1.22043664E+01 3.45851420E-03-1.24871388E-06 2.01018965E-10-1.19612560E-14    2
-4.93024132E+02-3.16697375E+01 4.21575317E+00 2.46409530E-02-2.29584816E-05    3
 1.03444807E-08-1.82063749E-12 1.99316683E+03 1.02809212E+01                   4
HONNH     HONNH_G4      H   2N   2O   1    0G   300.000  5000.000 1410.000    01
 6.28422378E+00 5.37598499E-03-1.78502698E-06 2.71645903E-10-1.55420951E-14    2
 6.70148292E+03-8.61273360E+00 1.39096839E+00 1.79340781E-02-1.42097587E-05    3
 5.87052739E-09-9.78695345E-13 8.26845062E+03 1.72339344E+01                   4
ONOCHO                   C   1H   1N   1O   3G   300.000  5000.000 1410.000    21
 1.22840065E+01 2.54240817E-03-9.33422794E-07 1.51922313E-10-9.10868201E-15    2
-2.83490847E+04-3.52608565E+01 8.67680831E-01 3.59748223E-02-3.83580776E-05    3
 1.89460479E-08-3.55203605E-12-2.51378321E+04 2.35246630E+01                   4
NOHT                     H   1N   1O   1    0G   300.000  5000.000 1494.000    01
 4.15335857E+00 2.17576092E-03-6.98445456E-07 1.03709196E-10-5.82705329E-15    2
 2.36540099E+04 3.12788664E+00 2.97827839E+00 4.98521376E-03-3.18864388E-06    3
 1.06519801E-09-1.40366220E-13 2.40449163E+04 9.39740227E+00                   4
```

A.3 tran.dat

```
ETONO2          2      496.000     5.200     0.000     0.000     1.000    !
NO2             2      200.001     3.500     0.000     0.000     1.000    !
HONO            2      237.100     5.118     0.000     0.000     0.000    !
NO              1      139.320     3.339     0.200     1.760     4.000    !
O               0       80.000     2.750     0.000     0.000     0.000    !
N2O             1      232.400     3.828     0.200     0.000     1.000    !
H2O             2      572.400     2.605     1.844     0.000     4.000    !
N2              1       97.530     3.621     0.000     1.760     4.000    !
CO2             1      244.000     3.650     0.000     2.650     2.100    !
O2              1      107.400     3.458     0.000     1.600     3.800    !
H               0      145.000     2.050     0.000     0.000     0.000    !
HNO             2      170.000     3.430     1.620     0.000     1.000    !
OH              1       80.000     2.750     0.000     0.000     0.000    !
HCN             1      569.000     3.630     0.000     0.000     1.000    !
HNCO            2      232.401     3.828     0.000     0.000     1.000    !
NH              1       80.000     2.650     0.000     0.000     4.000    !
CO              1      260.690     4.433     0.000     0.000     0.000    !
H2CN            1      569.002     3.630     0.000     0.000     1.000    !
N               0       71.400     3.298     0.000     0.000     0.000    !
NO3             2      400.000     4.200     0.200     0.000     1.000    !
NH2             2       80.000     2.650     0.000     2.260     4.000    !
NH3             2      481.001     2.920     1.470     0.000    10.000    !
HCO             2      498.000     3.590     0.000     0.000     0.000    !
H2              1       38.000     2.920     0.000     0.790   280.000    !
HCCO            2      150.001     2.500     0.000     0.000     1.000    !
HCNO            2      237.100     5.118     0.000     0.000     0.000    !
NCO             1      232.401     3.828     0.000     0.000     1.000    !
NNH             2       71.400     3.798     0.000     0.000     1.000    !
HNC             2      110.700     4.443     0.000     0.000     0.000    !
HOCO            2      498.000     3.590     0.000     0.000     2.000    !
HNNO            2      232.401     3.828     0.000     0.000     1.000    !
HNO3            2      400.000     4.200     0.200     0.000     1.000    !
CH2             2      144.000     3.800     0.000     0.000     0.000    !
CH2(S)          2      144.000     3.800     0.000     0.000     0.000    !
CH3             2      144.000     3.800     0.000     0.000     0.000    !
CH2O            2      498.000     3.590     0.000     0.000     2.000    !
CH4             2      141.400     3.746     0.000     2.600    13.000    !
CH2OH           2      417.000     3.690     1.700     0.000     2.000    !
CH3O            2      417.000     3.690     1.700     0.000     2.000    !
CH3OH           2      481.800     3.626     0.000     0.000     1.000    !
C2H2            1      209.000     4.100     0.000     0.000     2.500    !
C2H5            2      252.300     4.302     0.000     0.000     1.500    !
C2H6            2      252.300     4.302     0.000     0.000     1.500    !
CH2CO           2      436.000     3.970     0.000     0.000     2.000    !
C2H3            2      209.000     4.100     0.000     0.000     1.000    !
C2H4            2      280.800     3.971     0.000     0.000     1.500    !
HCCOH           2      436.000     3.970     0.000     0.000     2.000    !
HNO2            2      350.000     3.950     1.639     0.000     1.000    !
HNOH            2      116.700     3.492     0.000     0.000     1.000    !
NH2O            2      116.700     3.492     0.000     0.000     1.000    !
C2H4O           2      436.000     3.970     0.000     0.000     2.000    !
CH2CHO          2      436.000     3.970     0.000     0.000     2.000    !
CH3CHO          2      436.000     3.970     0.000     0.000     2.000    !
HOCN            2      232.400     3.828     0.000     0.000     1.000    !
CH3NH           2      481.800     3.626     0.000     0.000     1.000    !
CH2NH           2      417.000     3.690     1.700     0.000     2.000    !
N2O4            2      399.300     5.949     0.000     0.000     0.000    !
CH3NO2          2      232.400     3.828     0.000     0.000     1.000    !
CH3NO           2      237.100     5.118     0.000     0.000     0.000    !
H2CNO2          2      232.400     3.828     0.000     0.000     1.000    !
CH3ONO          2      531.400     4.687     0.000     0.000     0.000    !
C3H8            2      266.801     4.982     0.000     0.000     1.000    !
CH3ONO2         2      459.500     5.036     1.700     0.000     1.000    !
C2H5O           2      362.600     4.530     0.000     0.000     1.500    !
CH3CO           2      436.000     3.970     0.000     0.000     2.000    !
CNO2CDO         2      399.300     5.949     0.000     0.000     0.000    !
CNO2CDJO        2      399.300     5.949     0.000     0.000     0.000    !
CJCONO2         2      399.300     5.949     0.000     0.000     0.000    !
COJCONO2        2      399.300     5.949     0.000     0.000     0.000    !
```

CDOCOJ	2	428.975	5.738	0.000	0.000	0.000	!
C2H5OH	2	362.600	4.530	0.000	0.000	1.500	!
HOCHO	2	481.800	3.626	1.700	0.000	1.000	!
OCHO	2	498.000	3.590	0.000	0.000	2.000	!
CH3CO2	2	452.392	5.643	0.000	0.000	0.000	!
PC2H4OH	2	362.600	4.530	0.000	0.000	1.500	!
C2H5ONO	2	503.072	5.340	1.670	8.800	1.000	!
NH2NO	2	237.100	5.118	0.000	0.000	0.000	!
NH2OH	2	116.700	3.492	0.000	0.000	1.000	!
ONONO2	2	399.300	5.949	0.000	0.000	0.000	!
HONNH	2	237.100	5.118	0.000	0.000	0.000	!
ONOCHO	2	341.100	5.784	0.000	0.000	0.000	!
NOHT	2	110.700	4.443	0.000	0.000	0.000	!

Appendix B. Representative Input File for Closed-System, Constant-Volume, Constant-Temperature (CNVT) Calculations

A customized precommercial version of SENKIN[1,2] was employed to set up and solve the homogeneous reactor (CNVT) problems discussed in the main body of this report. An input file (*senk.inp*) that is representative of the set is shown. Definitions for all the model parameters specified via this file (except CNVT and SFAC) are provided in a user's guide for our program.[2]

```
PREC
CNVT                ! closed, constant-volume, constant-temperature system
RTOL 1.E-8
ATOL 1.E-13
/PRES 0.0131579     ! atm (10 mm Hg)
PRES 0.0394737      ! atm (30 mm Hg)
/PRES 0.0657895     ! atm (50 mm Hg)
TEMP 434.15         ! K
TIME 52500.         ! sec
DELT 50.00          ! sec
REAC ETONO2  1.0    ! species, mole fraction
/SFAC  1.E0   2000. ! scaling factor = sfac(1)exp[sfac(2)/RT], where [R] = cal/mol-K
END
```

[1] Lutz AE, Kee RJ, Miller JA. SENKIN: a Fortran program for predicting homogeneous gas phase chemical kinetics with sensitivity analysis. Sandia National Laboratories (US); 1988 Feb. Report No.: SAND87-8248.

[2] McQuaid MJ. SENKIN3_PSB homogeneous reactor models: a primer. DEVCOM Army Research Laboratory (US); 2021 Mar. Report No.: ARL-TR-8921.

Appendix C. Representative Input Files for Gas- and Liquid-Phase PREMIX Problems

Customized precommercial versions of CHEMKIN III's PREMIX program[1,2,3] were employed to set up and solve the boundary value problems for the gas- and liquid-phase domains of the two-phase deflagration model summarized in the main body of this report. The solver in each case was TWOPNT.[4] This Appendix provides input files (*premix.inp* and *premix_lq.inp*) that are representative of those that were employed to parameterize the problems posed in the study. Inputs that were overwritten in the course of obtaining a solution in each domain are identified.

C.1 premix.inp

An input file named *premix.inp* was employed to parameterize problems in the gas-phase domain: $x > 0$. Starting with a template generated in the course of finding a solution that would serve as a good starting point for the problem of interest, the program would overwrite the mole fractions (X_k) of the species (k) at the liquid-phase side of the liquid–gas interface ($x = {}^{-}0$). Specified via the REAC keyword, for the first set of calculations in this domain, which corresponded to producing a solution based on the basic CYCLOPS framework, the value for ethyl nitrate (X_{ETONO2}^{-0}) was set equal to 1.0. Thereafter, all X_k^{-0} exceeding 10^{-10} in the solution for the liquid-phase domain were written into the file. (To reduce the file's size for presentation herein, only X_k^{-0} exceeding 1.0E-7 are shown.)

[1] Kee RJ et al. CHEMKIN collection. Release 3.6: PREMIX. Reaction Design, Inc.; 2000.
[2] Kee RJ, Rupley FM, Miller JA. CHEMKIN-II: a Fortran chemical kinetics package for the analysis of gas-phase chemical kinetics. Sandia National Laboratories (US); 1989 Sep. Report No.: SAND89-8009. https://doi.org/10.2172/5681118
[3] McQuaid MJ, Stone CP. CYCLOPS3 burning rate predictor: PREMIX3_WPSB version. DEVCOM Army Research Laboratory (US); 2024 Sep. Report No.: ARL-TR-9971.
[4] Grcar JF. The TWOPNT program for boundary value problems. Sandia National Laboratories (US); 1992 Apr. Report No.: SAND91-8230.

```
RSTR
PRES    3.0600000E+01
FLRT    7.2743436E-02           ! Value overwritten internally subsequent to initial guess.
XSTR    0.0000000E+00
XEND        1.2000E-01
GRID        0.0000E-00
GRID        0.1250E-04
GRID        0.5000E-04
GRID        0.7000E-03
GRID        0.3000E-02
GRID        0.3850E-01
GRID        0.7000E-01
GRID        1.2000E-01
GRID        2.4000E-01
TEMP        0.0000E+00    4.731233E+02    ! Corresponding to the temperature of the liquid-gas interface,
/                                         ! this parameter's value can be a variable or fixed after initial guess.
TEMP        0.1250E-04    5.542E+02
TEMP        0.5000E-04    5.580E+02
TEMP        0.7000E-03    6.409E+02
TEMP        0.3000E-02    9.900E+02
TEMP        0.3850E-01    1.406E+03
TEMP        0.7000E-01    1.601E+03
TEMP        0.1200E-00    1.850E+03
TEMP        0.2400E-00    1.850E+03
BURN
/REAC  ETONO2        1.000000E-00    ! Case A, C, or E
/ Inserted after a solution for the liquid-phase domain was obtained
REAC  ETONO2      9.999530E-01
REAC  NO2         2.143711E-06
REAC  CH2O        2.147102E-05
REAC  CH4         1.037735E-06
REAC  CH3CHO      1.076466E-06
REAC  CH3NO2      1.929985E-05
REAC  CH3ONO2     7.238945E-07
REAC  C2H5ONO     8.694675E-07
ENRG
MOLE
WDIF
PROD  CO2    3.65E-01
PROD  H2     3.33E-01
PROD  H2O    1.65E-01
PROD  N2     9.98E-02
PROD  CO2    3.49E-02
PROD  H      2.90E-03
GRAD  0.05
CURV  0.25
ATOL  1.E-10
RTOL  1.E-5
ATIM  1.E-9
RTIM  1.E-4
TIME   1000  1.00E-6
TIM2   1000  1.00E-6
DTMN  1.E-10
PRNT   1
END
```

C.2 premix_lq.inp

An input file named *premix_lq.inp* was employed to parameterize problems in the liquid-phase domain: $-d \geq x > 0$. Starting with a template that contained all the keywords and values for the parameters specified by them that were common to all calculations, the program wrote into the template the mass flow rate (via the keyword FLRT) and the temperature profile (via the keyword TEMP) generated internally by the program.

We note that the program's default specification (0.10) for the maximum allowed state-variable "gradient" in a solution (as defined in TWOPNT and specified via the keyword GRAD) was not adequate for the purposes of this study. Solutions for the temperature profile ($T(x)$) were observed to significantly change with a decrease in its value until the value was (approximately) 0.025. Therefore, that value was specified.

In contrast, the default specification (0.5) for maximum state variable "curvature" in a solution (as defined in TWOPNT and specified via the keyword CURV) proved to be problematic. For reasons we were unable to ascertain, calculations would often fail when 0.5 was specified, and relaxing it to somewhat higher values was not generally helpful. However, when this parameter was allowed to be the maximum it could be (1.0), the maximum actual value in converged solutions was typically less than 0.5, and usually much less. Therefore, we allowed it to be 1.0 and checked each solution to verify that its actual value did not exceed 0.5.

Similarly, we found that attempts to obtain solutions to problems in the liquid-phase domain that started from a heuristically generated $T(x)$ profile and with $X_{EthN}(x)$ = 1 for all x would invariably fail if the chemical production and consumption of species were allowed to any degree (by setting the parameter specified via GFAC to a value greater than 0). We found that this issue was addressed by first obtaining a solution for $T(x)$ with that parameter set equal to 0 and then setting it equal to 1.

```
/RSTR                    ! Inserted after the first problem in the domain is solved.
PRES  1.000000E+00       ! This is a dummy value. An effective pressure is calculated internally.
FLRT  7.717888E-02       ! Initial value set by preceding CYCLOPS calculation
/                        ! Subsequent values specified to produce target dT/dx at x=0
XSTR  0.000000E+00
XEND  1.034280E+00       ! Generated internally and written into this file
GRID  0.000000E+00       ! Grid generated internally and written into this file.
GRID  1.000000E+00
GRID  1.003428E+00
GRID  1.006856E+00
GRID  1.010284E+00
GRID  1.013712E+00
GRID  1.017140E+00
GRID  1.020568E+00
GRID  1.023996E+00
GRID  1.027424E+00
GRID  1.030852E+00
GRID  1.034280E+00
TEMP  0.000000E+00  2.981500E+02   ! Program generated T(x) written into this file.
TEMP  1.000000E+00  2.981500E+02
TEMP  1.003428E+00  3.156472E+02
TEMP  1.006856E+00  3.331445E+02
TEMP  1.010284E+00  3.506417E+02
TEMP  1.013712E+00  3.681389E+02
TEMP  1.017140E+00  3.856361E+02
TEMP  1.020568E+00  4.031334E+02
TEMP  1.023996E+00  4.206306E+02
TEMP  1.027424E+00  4.381278E+02
TEMP  1.030852E+00  4.556251E+02
TEMP  1.034280E+00  4.731223E+02
BURN
REAC  ETONO2  1.0
INTM  ETONO2  1.0
PROD  ETONO2  1.0
ENRG
MOLE
WDIF
GFAC  0.000000E+00    ! Turns off reaction chemistry. Specified until an FLRT that produces the
/                     ! targeted dT/dx is found.
/GFAC  1.000000E+00   ! Inserted after a converged solution for GFAC = 0 is obtained.
GRAD  0.025
CURV  1.00            ! Unconstrained. Check to see if the value in actual solution is reasonable.
ATOL  1.E-10
RTOL  1.E-5
ATIM  1.E-9
RTIM  1.E-4
TIME  100  1.00E-6
TIM2  100  1.00E-6
DTMN  1.E-10
PRNT  2
END
```

List of Symbols, Abbreviations, and Acronyms

1D/2D	One-/Two-Dimensional
A0	Cross-Sectional Area
A^{c-g}	Area of the Interface Between the Condensed and Gas Phases
amu	Atomic Mass Unit
AP	Ammonium Perchlorate
atm	Atmosphere
ATOL	Absolute Tolerance
B	Constant for a Given Liquid-Phase Chemical Composition
c	Condensed Phase
CNVT	Closed-System, Constant-Volume, Constant-Temperature
$c_{p,g}$	Gas-Phase Constant-Pressure Heat Capacity
$c_{p,l}$	Liquid-Phase Heat Capacity
d	Distance from the Interface
D	Deuterium
d_5-EthN	Perdeutero-Ethyl Nitrate
dT/dx	Temperature Gradient
DZ	Dark-Zone
Ea	Activation Energy
EM	Energetic Material
EthN	Ethyl Nitrate
$f_i(T)$	Liquid-Phase Scaling Factor
g	Gas Phase
$h_{k,g}$	Gas-Phase Mass-Specific Enthalpy
$h_{k,l}$	Liquid-Phase Mass-Specific Enthalpy
h_l	Liquid-Phase Enthalpy

HLK	Hertz–Langmuir–Knudsen
HR	Homogeneous Reactor
h_v	Enthalpy of Vaporization
IR	Infrared
k_g^i	Gas-Phase Reaction-Rate Coefficient
k_l^i	Liquid-Phase Reaction-Rate Coefficient
l	Liquid Phase
$\dot{M}$	Total Gasification Rate
MeN	Methyl Nitrate
MSP	Min-Smoke Propellant
NC	Nitrocellulose
NG	Nitroglycerine
NQ	Nitroguanidine
P	Pressure
Pr	Probability Factor
r	Effective Linear Regression Rate
R	Universal Gas Constant
s	Solid Phase
t	Temporal Instant
T	Temperature
T^0	Temperature at the Liquid-Gas Interface
T_b	Boiling Point
V_{hfv}	Free-Volume Hole
$V_{k,g}$	Gas-Phase Diffusion Velocity
W_k	Molecular Weight
X_k	Mole Fraction
Y_k	Mass Fraction

MATHEMATICAL SYMBOLS

λ_g	Gas-Phase Thermal Conductivity
λ_l	Liquid-Phase Thermal Conductivity
ρ_c	Condensed-Phase Density
ρ_g	Gas-Phase Density
ρ_l	Liquid-Phase Density
$\dot{\omega}_k$	Molar Production Rate per Unit Volume

1 (PDF)	DEFENSE TECHNICAL INFORMATION CTR DTIC OCA
1 (PDF)	DEVCOM ARL FCDD RLB CB TECH LIB